AD-A147 199 MECHANISTIC METHODOLOGY FOR AIRPORT PAVEMENT DESIGN WITH ENGINEERING FABR..(U) RESOURCE INTERNATIONAL INC COLUMBUS OH K MAJIDZADEH ET AL. AUG 84 1/2

UNCLASSIFIED DOT/FAA/PM-84/9-1 DTFA01-81-C-10043 F/G 13/2 NL

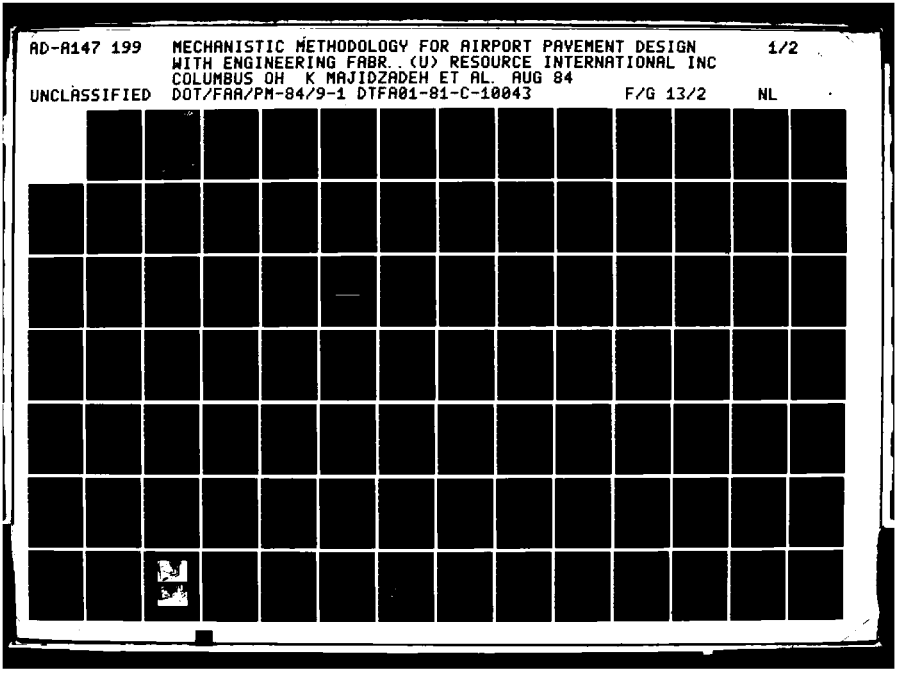

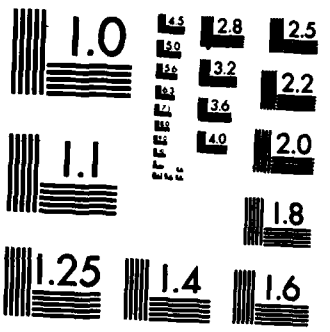
1.0
1.1
1.25
1.4
1.6
1.8
2.0
2.2
2.5
2.8
3.2
3.6
4.0
4.5
5.0
5.6

DOT/FAA/PM-84/9, I

Program Engineering &
Maintenance Service
Washington, D.C. 20591

Mechanistic Methodology for Airport Pavement Design with Engineering Fabrics

Vol. I: Theoretical and Experimental Bases

Kamran Majidadeh
George Ilves
Henry Sklyut
V.R. Kumar

Resource International Inc.
281 Enterprise Drive
Columbus, Ohio 43081

August 1984
Final Report

U.S. Department of Transportation
Federal Aviation Administration

NOTICE

This document is disseminated under the sponsorship of the Department of Transportation in the interest of information exchange. The United States Government assumes no liability for its contents or use thereof.

Technical Report Documentation Page

1. Report No.	2. Government Accession No.	3. Recipient's Catalog No.
DOT/FAA/PM-84/9,I		

4. Title and Subtitle	5. Report Date
Mechanistic Methodology for Airport Pavement Design with Engineering Fabrics Volume I: Theoretical and Experimental Base	August 1984
	6. Performing Organization Code
7. Author(s) Kamran Majidzadeh, George Ilves, Henry Sklyut and V.R. Kumar	8. Performing Organization Report No.
9. Performing Organization Name and Address Resource International Inc. 281 Enterprise Drive Columbus, OH 43081	10. Work Unit No. (TRAIS)
	11. Contract or Grant No. DTFA01-81-C-10043
12. Sponsoring Agency Name and Address U.S. Department of Transportation Federal Aviation Administration 800 Independence Avenue, S.W. Washington, D.C. 20591	13. Type of Report and Period Covered Final Report
	14. Sponsoring Agency Code FAA/APM-740

15. Supplementary Notes

16. Abstract

The rapid growth in air transportation volume with the associated increase in payload has led to faster rates of airport pavement deterioration. Overlays using engineering fabrics are often used as a rehabilitation technique. Although it is generally believed that the engineering fabrics will retard reflection cracking, no rational mechanistic design method is yet available that permits the effective use of these fabrics. In this report, a survey of available mechanistic models for reflection cracking as well as geotextile systems is reviewed. A first generation design program (EFRON) has been developed based upon a two-dimensional finite element program to determine the stress patterns in the overlay.

A three-dimensional computer program (RISC) is used to estimate existing pavement life. The fatigue cracking resistance of the fabric reinforced overlay system is evaluated by conducting laboratory beam fatigue testing on asphaltic overlays over concrete base. Three types of fabrics, as well as a control with no fabric, were used in the tests. Both thermal and loading fatigue cracking are simulated by applying external vertical and/or horizontal forces to produce joint movements equal to that of the full-scale pavements under field conditions.

The results of the laboratory fatigue testing demonstrated the effectiveness of the engineering fabrics in retarding the formation of reflective cracking. Furthermore, the comparison of these results with EFRON program analysis indicated the full capability of EFRON to model the laboratory performance and hence its potential to predict the performance of overlays of actual runway. The verification of the accuracy of the EFRON Program for runway overlays will be covered in Phase III of this study.

17. Key Words	18. Distribution Statement
Engineering Fabrics, Reflective Cracking, Overlay Design, Fatigue Cracking, Thermal Stresses Joint Movement	This document is available to the public through the National Technical Information Service, Springfield, VA 22161.

19. Security Classif. (of this report)	20. Security Classif. (of this page)	21. No. of Pages	22. Price
UNCLASSIFIED	UNCLASSIFIED	161	

Form DOT F 1700.7 (8-72) Reproduction of completed page authorized

PREFACE

This report reflects the part of the mission of the Federal Aviation Administration (FAA) to provide guidelines to airport owners and operators for cost effective rehabilitation techniques for airport pavements.

This research project entitled "Mechanistic Methodology For Airport Pavement Design With Engineering Fabrics", DTFA01-81-C-10043, was conducted by Resource International Inc., Worthington, Ohio. The project was sponsored by the Federal Aviation Administration (FAA).

During the preparation of this report, Dr. Aston McLaughlin was Technical Monitor for the Federal Aviation Administration.

LIST OF SYMBOLS

dc/dn	Rate of crack growth
E_A, E_{ov}	Overlay modulus of elasticity
E_i	Modulus of elasticity in the i-direction (for othotropic material)
EFF	Fabric effectiveness factor
G_{xy}	Shear modulus in the x-y plane
GEO	Geometry factor
h_{ov}, T_o	Overlay thickness
K1	Mode 1 (tensile opening mode) stress intensity factor
K2	Mode 2 (shear opening mode) stress intensity factor
K3	Mode 3 (tearing mode) stress intensity factor
K_n, K_s	Normal stiffness and shear stiffness of the joint element
K, K^1	Element global and local stiffness matrices.
K_F	Stiffness matrix of the foundation
ℓ	Length of the joint element
L	Amount of dowel bar looseness
N_f	Number of load applications to failure
T_R	Reference temperature of the overlay ("zero stress" temperature)
u, v	The global displacement components in the global x and y directions respectively.
u, v	Normal and rangential displacements of the joint element.
α_i	Coefficient of thermal expansion in the i-direction
η	Angle of rotation from the global x-y axes to the material principal x' - y' axes.

ΔT	Uniform change in slab temperature
$\underline{\phi}$	Interpolation functions for finite element formulation
ε_x, ε_y	Normal strains in the global x and y directions.
ε_{xy}	Shear strain in the x-y plane
$\underline{\varepsilon}_o$	Initial strain vector due to temperature change
σ_{ov}	Overlay stresses

TABLE OF CONTENTS

LIST OF FIGURES

LIST OF TABLES

CHAPTER I

INTRODUCTION

1.1 BACKGROUND

The rapid growth in air transportation over the last four decades and the increases in payload of commercial aircraft have led to severe deterioration of airport pavements. Invariably, these pavements are rehabilitated to preserve or increase load carrying capabilities or to maintain a smooth riding surface. Common practice is to overlay the cracked pavement with a matting of asphaltic material, or in some instances, with portland cement concrete. In any case, a new problem usually develops: the new overlay, after a short time, begins to crack in the same pattern as the pavement that was overlaid; this constitutes the phenomenon of reflection cracking.

Large sums of money are spent each year by pavement management groups to seal these cracks against the ingress of water and the growth of vegetation; other pavements that have been allowed to go unsealed have in a very short time necessitated complete reconstruction efforts. While many remedial measures have been taken to prevent or retard reflection cracking, no generally applicable method has been found that would apply to all pavement types. One of the most promising of those measures has emerged to be the addition of an engineering type of fabric to the cracked pavement before application of the bituminous overlay. Although many millions of dollars are expended annually in the certain belief that installation of fabric will retard cracking of airport pavements, much of this sum is wasted because of failure of the fabric to perform due to the lack of adequate construction controls and design criteria.

1.2 OBJECTIVE AND SCOPE

The objective of this research effort is the development of a mechanistic design methodology that permits the effective use of engineering fabrics on pavement overlay systems for the prevention of reflection cracking.

The scope of this research project includes literature search and review of analytical models related to the use of fabrics as crack arresting systems. Based on this review, functional criteria are established and existing analytical procedures modified or improved for the analysis and design of these systems. Prior results on the use of fabrics on pavements are augmented by additional laboratory work and theoretical studies. A modular computer program is also developed and acceptance tested and documented in the form of a User's Manual

and an Operations Manual. The scope of this development effort also includes sufficient laboratory testing of small scale models for representative types of pavements with varying characteristics of engineering fabrics included. Field verification of the structural model will be performed before a design manual is formulated from the total results of this effort.

1.3 OUTLINE OF STUDY

This study is divided into two volumes. Volume I describes the development of the design method including an appendix containing the user guide which also includes guidelines for development of the input parameter required by the method.

Volume I is divided into the following sections:

CHAPTER II: Review of Literature
CHAPTER III: Mechanistic Models for Geotextile Systems
CHAPTER IV: Design Methods
CHAPTER V: Laboratory Testing
CHAPTER VI: Data Analysis
CHAPTER VII: Conclusion and Recommendations
APPENDIX: User Guide

Volume I documents the research efforts of the first phase of this study.

Volume II will include activities of Phase III, "Field Verification", which is currently underway. The design model presented in this report may require modification and/or calibration as a result of the field studies. It should be noted that since the field phase is still under investigation, Volume I is limited at this stage to a computer program input guide rather than a full design model. The final design model will be presented at the conclusion of all activities.

CHAPTER II

REVIEW OF LITERATURE

2.1. INTRODUCTION

Reflection cracking is the cracking of a resurface or overlay above underlying cracks or joints. This cracking occurs in overlays of both flexible and rigid pavements and is a major cause of future pavement distress including spalling, surface water infiltration to underlying base and subgrade layers, and a general reduction in the stiffness of the pavement structure. Reflective cracks require labor intensive operations for crack sealing and patching, thus becoming a significant maintenance expense item.

The problem of reflection cracking is not a new one to the pavement engineer. Since the early 1950's many different materials, methods and techniques have been tried to prevent or at least delay reflection cracking. Most of these efforts have been concerned with asphalt concrete overlays over existing Portland Cement Concrete pavements, where existing cracks or joints are usually reflected through the asphalt overlay within a 1 year period (1). Early research recognized that the probable cause of reflection cracking was movement of some form in the underlying pavement at existing cracks and joints. This movement can result from both traffic and environmentally induced forces. The movement includes differential vertical movement and thermal or moisture induced expansion, contraction or distortion (curling) at underlying joints and cracks. Because the overlay is bonded to the existing pavement, movement at underlying joints or cracks induces stresses in the overlay. If sufficiently high, these stresses cause fracturing or cracking of the overlay. If the induced stresses do not exceed the yield strength of the overlay material, cracking could still develop as the result of cyclic load applications which produce fatigue fracturing of the asphalt concrete. Techniques or measures which have been used to delay reflection cracking are: (i) Bond Breakers; (ii) Cushions; (iii) Rubber - Asphalt Interlayer (SAMI); (iv) Fabrics; (v) Modifying Existing Pavement; (vi) Stronger Overlays.

Currently the technique subjected to the most extensive field testing to determine its effectiveness in delaying reflection cracking is the placement of engineering fabrics over cracks or joints prior to overlay. There are numerous experimental projects of this type throughout the country. Reference (1) contains a tabulation of experimental projects using "Petromat" fabric including location, test features, evaluation procedures, and observations to date. "Petromat" is a nonwoven polypropylene fabric produced by Phillips Petroleum and

has been the most widely used fabric to date. There are at least 6 other major U.S. Corporations manufacturing fabrics from such materials as nylon, polyester, polypropylene, polyvinylidene chloride, or fiberglass.

Fabrics are available in rolls and are placed as sheets tack coated to the existing pavement prior to overlay. Recently manufacturers have started producing 2 to 3 foot (3/4 to 1m) wide rolls so that the fabric can be placed as strips over joints or cracks. These narrow rolls sometimes have an adhesive (usually rubberized asphalt) on one side so they can be placed without tack coating the existing surface. The strip type fabrics are usually used on rigid pavements while sheet fabrics which cover the entire area are used on flexible pavements. In a Virginia project 3 foot (0.91m) wide strips of non-woven polypropylene fabrics were placed over a composite pavement at existing transverse reflection cracks (2). Joint spacing of the PCC base was 30 feet (9.1m). An emulsion tack coat was applied under the fabric and overlaid with 1 1/4 inches (32mm) of asphalt concrete. After three months under traffic many of the joints were reflected through the second overlay although there was somewhat more cracking in an adjacent section where no fabric has been used. Virginia constructed other projects with fabric placed directly on PCC slabs at joints and cracks prior to overlay and attempted to correlate the fabric's crack prevention performance with differential vertical movement or load transfer under 18 kip axle loads at the joints. The Virginia study found a significant correlation between fabric performance and joint load transfer. The researchers stated that "... it is likely that many of the 20 fabric-treated joints that were uncracked and had a differential deflection of 0 (100% load transfer) were working joints where the fabric served its intended purpose of reducing overlay stresses to the point that no cracking occurred. Conversely, it is likely that, for those joints that had higher differential deflections, the fabric, a thin sheet, could not sufficiently distribute the shear stresses and was thus unable to reduce reflection cracking significantly." The study also concluded that at differential deflections greater than .002 in (.05mm) reflection cracks form very early. Lower differential deflections delay cracking, but cracks will occur as the magnitude and frequency of wheel loads increase.

The Virginia study appears to validate the fatigue fracture mechanism for reflection cracking under traffic load first presented by Majidzadeh, et al, (3). The Virginia results are very important and may explain why other states have had difficulty in assessing fabric reflection crack prevention performance. A recent State of Art review conducted by FAA summarizing highway experience with fabrics stated that no definite conclusions could be drawn from the collective results (4). In some instances apparently the fabric (Petromat and others) appeared to be effective, but in apparently similar situations at other locations, results would contradict previous conclusions. Based upon Army Corps of Engineers experience,

there is some evidence that fabrics are more effective on asphalt over asphalt than on asphalt over jointed concrete in retarding reflection cracking (5). However, fabric placed beneath a 1 3/4 in (44mm) overlay over an existing flexible pavement in an Arizona study did not perform favorably. This technique was not among the five most successful methods for reducing reflection cracking at the Arizona site (6).

The reflection cracking studies and field experimental projects to date have generally been of an empirical nature with little control or even identification of the parameters known to affect cracking. Characterization of the existing pavement in terms of joint width, load transfer, crack spacing, crack and joint opening under known temperature conditions, and deflection under load has usually not been part of these studies. Obviously, certain crack prevention treatments are sensitive to some of these factors as shown in the Virginia study where fabric performance was related to load transfer. Unfortunately, past research has not established the quantitative relationship between these factors and success or failure of the preventative techniques.

2.2 Evaluation of Existing Reflection Cracking Models

Within the last 10 years, several theoretical (mathematical) models have been developed to analyze and predict the occurrence of reflection cracking. All of the models consider the same mechanisms as previously noted (e.g., reflection cracking is caused by differential horizontal or vertical movements in the underlying layer). The models differ in the methods for predicting the magnitude of underlying layer movements, on the magnitude of stresses induced into the overlay by the movements, and in the response of the overlay to stress state (sudden fracture vs. fatigue fracture). The following discussions summarize some of the reflection cracking models which currently exist and present an evaluation of each model's limitations.

2.2.1 Ohio State University (OSU) - Ultimate Strength Model

This model, developed by researchers at Ohio State University (OSU) (7), is a nomograph procedure for predicting Asphalt Conrete (A.C.) overlay stresses over joints or cracks, resulting from thermally induced movements in underlying portland cement concrete (PCC) slabs. Separate stress analyses are performed for horizontal slab movements, due to seasonal changes in average slab temperature, and vertical slab movements (curling) which occur due to differential vertical temperature of the slabs. Curling is the response state where the top of the PCC slab is colder than the bottom of the slab.

The horizontal movement of the PCC slab as a function of the change in slab temperature is calculated using an average value for the friction coefficient, similar to the calculation for

determining temperature reinforcement in jointed reinforced concrete pavements. This model neglects the resistance to joint movement provided by the uncracked overlay which is bonded by a tack coat to the underlying slab. The OSU model assumes that this resistance is small and that thin overlays do not affect the movement of the joint due to temperature change. The joint dimension, the thickness, and the modulus of elasticity of the overlay and the slabs are input into a finite element model to determine the overlay stresses.

The effect of vertical movements on the overlay due to slab curling, similar to the horizontal joint movement, is also based upon the premise that the thin overlays do not affect the curling of slabs significantly. Thus the restraint against curling of the slabs provided by the uncracked overlay is again neglected. This important assumption permits the curved shapes of slabs to be predicted utilizing a computer simulation (program called "PLATES") of the Westergaard solution for temperature differentials between top and bottom of the slab. Curling induced overlay stresses are estimated on the assumption that the overlay takes the slope illustrated in Figure 1. The radius of curvature of the overlay, R, can be estimated from the joint width, j, and edge slope, θ, calculated from the "PLATES" program:

$$R = \frac{j}{2\theta} \qquad (1)$$

In turn, overlay stresses can be calculated from the expression:

$$\sigma_{ov} = \frac{Eov\ hov}{j} \qquad (2)$$

where

Eov = overlay stiffness

hov = overlay thickness

Equation (2) is derived from the basic strength of materials for pure bending:

$\epsilon(u) = u/R$
$\epsilon(u)$ = axial strain at distance u from the neutral axis

where

R = radius of curvature

Since equation (2) is derived from pure bending, symmetric bending of the overlay with tension at the top and compression at the bottom is implied.

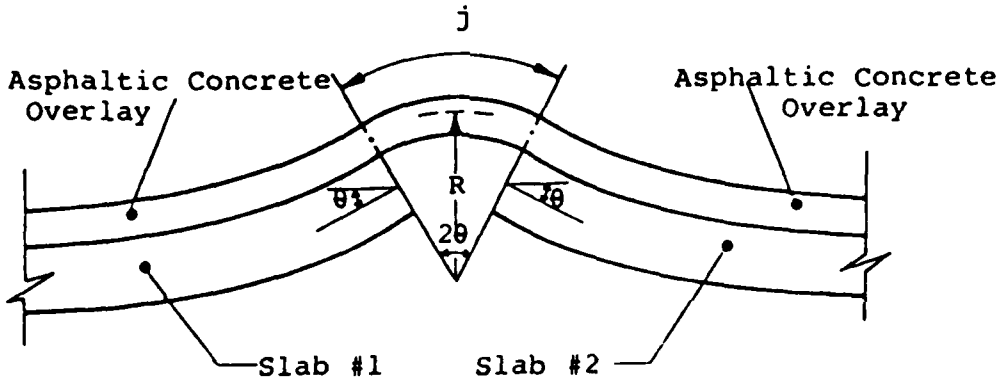

Figure 1. Bending of Overlay by Joint Vertical Movement

The OSU-Ultimate Strength Model presents an easy nomograph procedure for determining overlay stresses from thermal movements of underlying PCC slabs. However, the accuracy of the stress computation is suspect for the following reasons:

a) Restraint imposed by the uncracked overlay against slab movements (both horizontal and curling) is not considered. Thus, the calculated force in the overlay at the time of cracking is probably incorrect.

b) The overlay stresses due to horizontal joint movement appear low and should be validated by additional finite element investigation.

c) The tack coat bonding stress values also seem low and should be established by a laboratory investigation which considers temperature, tack coat type and amount, and roughness of the PCC slab.

d) The Westergaard analysis used to predict slab curling neglects the weight of slab and overlay which would tend to reduce the curl.

e) The simplified analysis of overlay stresses due to curling should be verified by finite element analysis. The fact that curling introduces a horizontal joint opening is neglected; this horizontal movement could be significant and thus change the stress state considerably.

f) The model is not capable of assessing the effects of crack prevention measures upon stresses in the overlay.

g) The model does not present recommendations for selecting design parameters such as seasonal temperature change T, vertical temperature gradient T, asphalt concrete modulus, and asphalt concrete strength.

2.2.2 ARE - Ultimate Strength Model

Austin Research Engineers (8) have developed a procedure for reflection crack stress or strain analysis. Two different failure modes are considered. The first is an opening mode (Figure 2) due to horizontal movements of the underlying PCC slab, resulting from a seasonal temperature change. Both joints or cracks without steel reinforcement, or cracks with steel reinforcement (such as CRCP), can be analyzed for horizontal

movement. The second is a shearing mode (Figure 2) resulting from a differential deflection across the joint or crack as the traffic load moves across the discontinuity.

A number of assumptions have been made in developing the model, including: the materials are elastic in response; temperature variations are uniformly distributed in the existing concrete slab (no curling); concrete movement is continuous with slab length; and movement is uniform with depth in a particular layer.

The ARE-Ultimate Strength Model has been computerized (program called RFLCR1) which minimizes difficulties in using the model. The model is the most versatile procedure currently available in that it can consider slab or overlay reinforcement, bond breakers, and granular cushions (shear failure analysis only). However, the simplifications in the model, which permit strain calculation without the use of analytical computations of stress distribution, have not been validated.

Although the force magnitudes may be reasonable, the assumed simplified distribution of stresses within the overlay for both opening and shear failure modes is very suspect since no concentration of stresses at the joint tip is considered. Other less significant questions regarding the ARE model include:

a) Characterization of the existing pavement by joint opening measurements over a certain temperature range cannot necessarily be extrapolated to a different design temperature range. For example, restraint exhibited between 70 and 50 degrees F (21 and 10 degrees C) may not identify the restraint between 70 and 20 degrees F (21 and -7 degrees C).

b) The assumed value for bonding stress between overlay and slab is very important to the anslysis since it establishes the gage length over which the overlay force at the joint is distributed. The suggested values need to be validated experimentally.

c) The concept that a bond breaker reduces overlay strain by merely increasing the gage length for force transfer should be validated by analytical investigation of stress distribution.

d) Load transfer is determined from preoverlay measurements without any adjustment for the effect of the overlay. This effect may not be negligible. Also load transfer is probably load and temperature dependent.

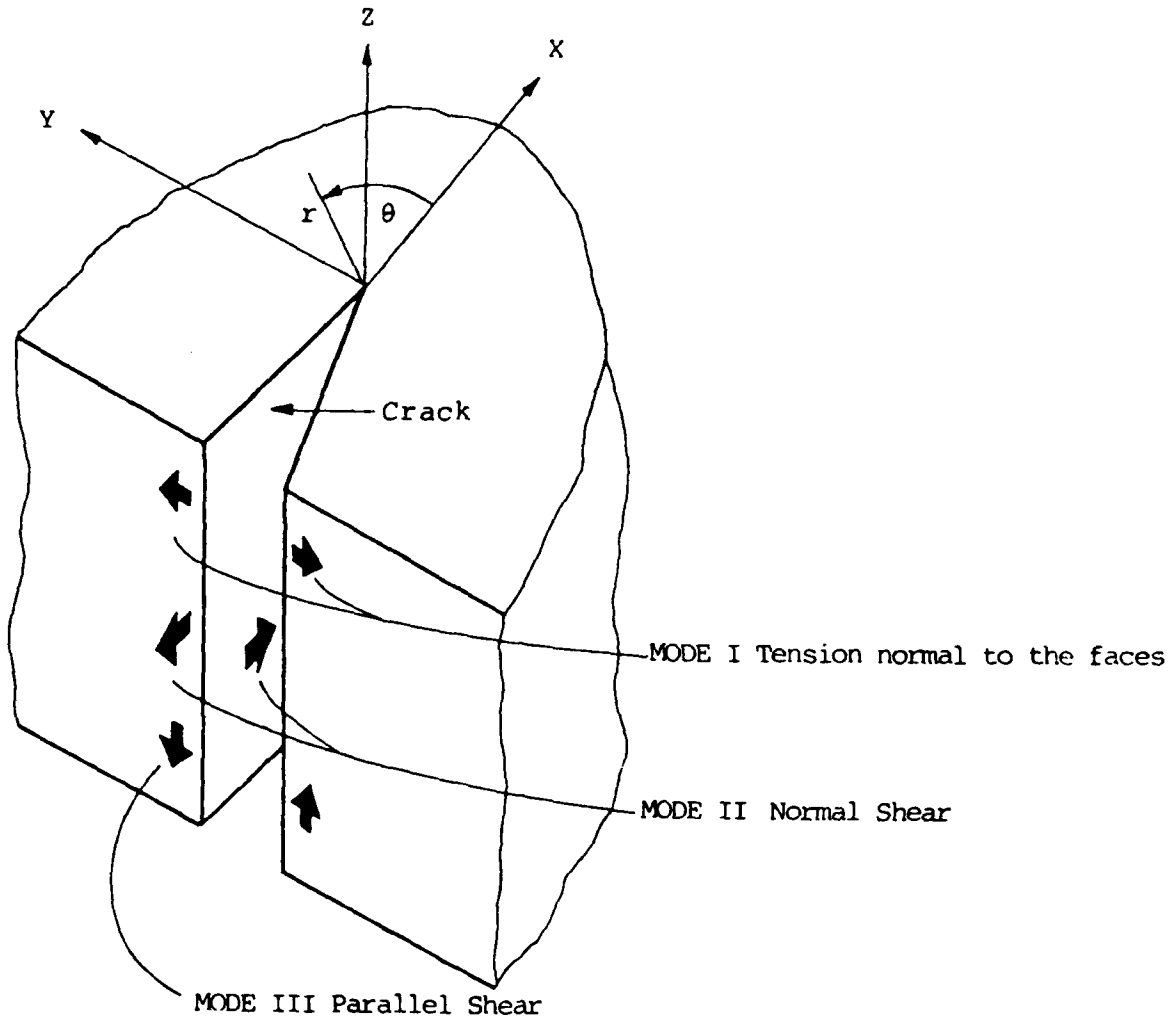

Figure 2. Modes of Deformation of a Crack

(e) The temperature for determination of dynamic modulus in the shear model is not specified. By the model, a high temperature would be critical, since larger strains would result. However, the allowable strain is likely to be temperature dependent.

2.2.3 Ohio State University (OSU) - Fracture Mechanics Model

Fracture mechanics has been utilized to develop a reflection crack propagation model for asphalt overlays over PCC slabs (3, 9). The model considers only traffic induced fatigue cracking resulting from differential deflection at slab joints or cracks.

The first step in applying fracture mechanics principles was to identify the fracture mode or modes associated with crack initiation and extension (Figure 2). A finite element analysis of full scale pavements predictd the asphaltic concrete overlay to be in compression, thus leading to the conclusion that the opening mode (Mode I) type fracture does not occur. Additionally, the computer analysis predicted that there would be significant relative vertical displacement (Mode II) across the joint when the load edge is placed over the joint. These conclusions led to the hypothesis that load induced reflection cracking is a result of general or mixed mode fracture of the bituminous material occurring under the simultaneous interaction of -K1 (negative σx), K2 and K3. Laboratory testing of 2 and 3 dimensional model overlay pavements supported this hypothesis.

Sih's theory of fracture (10) based on the field strength of the local strain-energy-density was utilized to analyze mixed mode crack propagation. The two fundamental hypotheses of crack extension in Sih's theory are:

1. The crack will spread in the direction of maximum potential engergy density or minimum strain energy density

2. The critical intensity Scr of this potential field governs the onset of rapid or brittle crack propagation

In those cases where a fracture is not a rapid, unstable process (i.e., the stress intensity factor under the applied load condition does not exceed the critical stress intensity factor, or the strain-energy-density factor Smin is less than the critical value Scr), slow stable fatigue crack growth is presumed. Typically, crack growth laws relate the rate of change of crack length to the stress level or stress intensity factor such as:

$$\frac{dc}{dn} = A(\Delta K)^n \qquad (3)$$

where

dc/dn = rate of crack growth
ΔK = stress intensity factor
A,n = material constents

For mixed mode fracture, the OSU model utilizes the crack growth law in terms of the strain-energy-density factor along the direction of fracture (Smin):

$$\frac{dc}{dn} = B(\Delta Smin)^{n} \qquad (4)$$

The fatigue life, or number of load applications to produce a crack through the overlay, is given by:

$$Nf = \int_{co}^{cf} \frac{dc}{B\,(\Delta Smin)^{n}} \qquad (5)$$

where

co = initial starter flaw length

cf = crack length at which the overlay is considered failed (either its thickness or the length at which the critical Smin = Scr, is reached, whichever is less)

and Scr, B, and n are material constants derived from fatigue tests on asphaltic concrete beams.

The OSU-Fracture Mechanics model is not a complete method for predicting the occurrence of reflection cracking. An analytical method for computing stress intensity factors and Smin (such as a finite element model) must be coupled to a program to calculate the fatigue life in an incremental fashion using the growth law shown in equation (4). It is likely that a nomograph procedure could be developed from this model similar to that of Majidzadeh, et al (11) for fracture mechanics prediction of load associated fatigue cracking in flexible pavements. Thus, further development of the OSU-Fracture Mechanics model is necessary before it could be implemented by pavement engineers.

2.2.4 TEXAS TRANSPORTATION INSTITUTE - Fracture Mechanics Model

The TTI model (12) also uses fracture mechanics crack propagation theory to predict cracking. Only Mode I fracture, and therefore the KI stress-intensity factor, induced by

Schapery's theory on crack growth in viscoelastic materials to develop the following growth law (12):

$$\frac{dc}{dn} = B_t (\Delta K)^{2(1+1/m)} \quad (6)$$

where

$$B_t = \frac{\pi}{6\sigma_m^2 I_1^2} \left[\frac{(1-\nu^2)D_2}{2\Gamma}\right]^{1/m} \left[\int_0^{\Delta t} W(t)^{2(1+1/m)}\, dt\right] \quad (7)$$

and

ν = Poisson's ratio

σ_m = maximum tensile stress the asphalt concrete mixture can sustain

I_1 = a dimensionless integral between 0 and 2

Δt = the period of the load cycle

$W(t)$ = wave shape of the stress intensity factor

m = slope of the straight line portion of the tension creep compliance curve for the asphalt cement binder

$D2$ = intercept of straight line with log t = 0 on creep compliance curve

Γ = fracture energy density (force times displacement) to produce a unit area of crack surface.

The TTI model is also not a complete procedure for predicting the occurrence of reflection cracking. It is merely a technique for obtaining crack growth laws without having to perform fatigue tests. Fatigue life is then obtained by integrating equation (6) from the limits of Co to Cf, similar to that of equation (5) in the OSU fracture mechanics model. The limitations discussed for the OSU fracture mechanics model also apply to TTI model.

2.2.5 RII - Phenomenological Model

Resource International engineers have developed a phenomenological model for crack prediction in overlaid flexible pavement structures which are reinforced by placement of engineering fabrics on the existing surface prior to overlay (13). The model considers only traffic load stresses in

predicting the fatigue life of the overlayed pavement; it has been converted into a computerized design program called HWYPAV.

This model was formulated after extensive laboratory testing had been conducted which established the relationship between the fatigue life of reinforced and normal or unreinforced asphalt concrete beams. All fatigue tests were with beams on an elastic foundation tested at a temperature of 70 degrees F (21 degrees C). The performance factor of the fabric in enhancing fatigue life and/or delaying reflective cracking is called fabric effectiveness factor (FEF), shown schematically in Figure 3:

$$FEF = \frac{Nf \text{ reinforced}}{Nf \text{ unreinforced}} \quad (8)$$

i.e., FEF is simply the ratio of fatigue lives as obtained from the beam tests. FEF generally ranges from 4 to 8 depending on strain level, placement depth within the beam, and fabric type.

The FEF function is expressed as

$$FEF = a1 \, (\epsilon h)^{a2} \, .GEO \quad (9)$$

where

a1 and a2 = constants depending upon fabric type

ϵh = horizontal strain at the bottom of the existing asphalt bound layer.

GEO = geometry factor which considers depth, as shown in Figure 4.

The fatigue life of the pavement in the HWYPAV program is:

$$Nf = Nf'u \; (FEF) \quad (10)$$

where Nf'u is a strain dependent distress function for asphalt concrete developed from AASHO Road Test Data

Cracking of the existing pavement is accounted for by reducing the elastic modulus of this layer. The design program uses the elastic multilayer program ELSYM-5 (14) to calculate pavement strains. The layers used in the strain analyses are shown in Figure 5. As can be seen from this figure, the fabric has not been included as a separate layer. Although the presence of fabric has a significant effect on the allowable strains, its inclusion in layer theory analysis is of no practical significance since the fabric is very thin in comparison with other layers in the system.

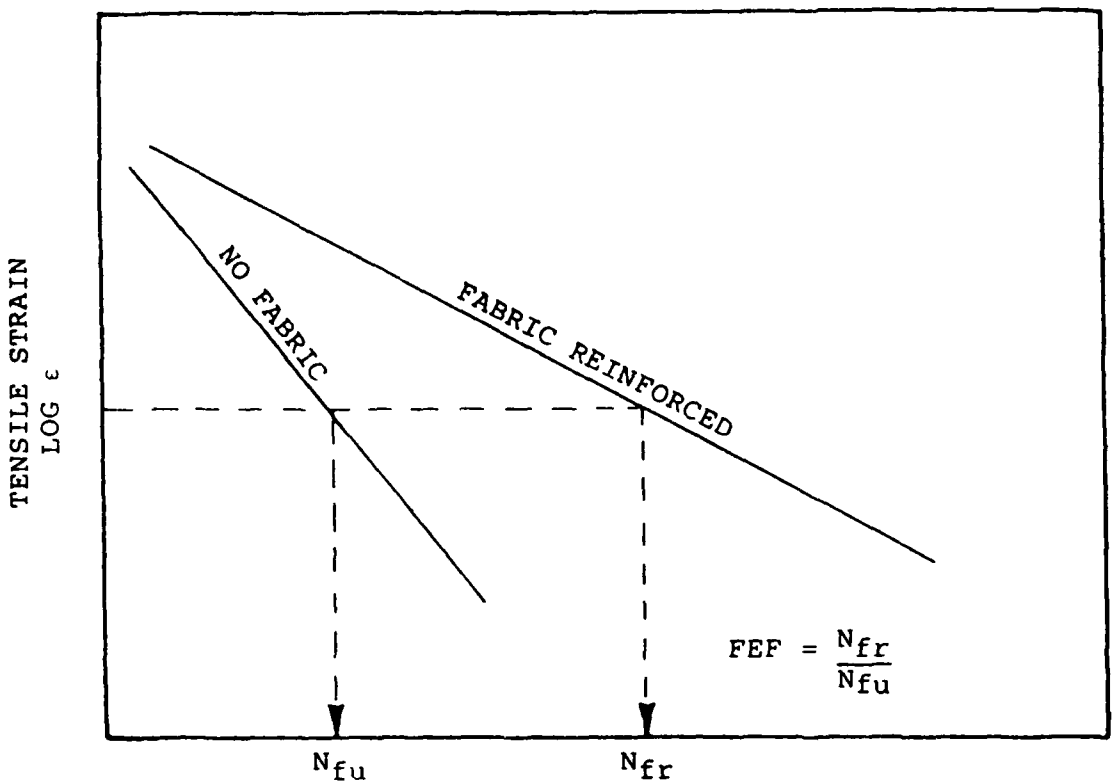

Figure 3. Calculation of FEF

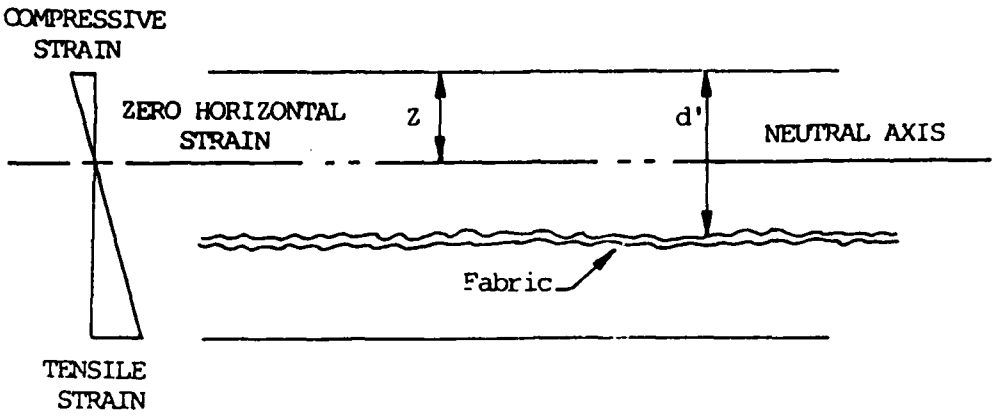

GEOMETRY ADJUSTMENT FOR DEPTH
OF FABRIC PLACEMENT IN ASPHALT
LAYER

Note: For overlay design d' equals the overlay thickness.

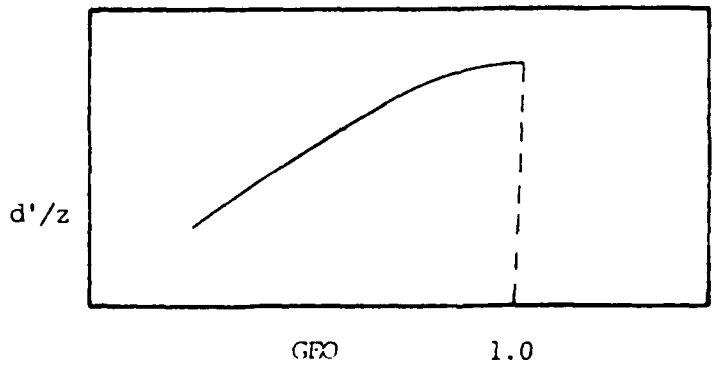

Figure 4. Definition of Geometry Factor GEO

The RII model has the following limitations:

(a) Since the model is phenomenological, the mechanics of crack propagation and crack arrest are not identified.

(b) FEF parameters are established from small beam tests and do not necessarily represent those of full slab conditions.

CHAPTER III

MECHANISTIC MODELS FOR GEOTEXTILE SYSTEMS

3.1 Introduction

Field and laboratory data have indicated that fabrics imbedded in pavement structures enhance the fatigue life and retard reflection cracking. To support these significant experimental data, various mechanistic models have been postulated which present a theoretical basis for the observed phenomena. The so-called "fabric effectiveness" is attributed to three mechanisms which might act singly or simultaneously to effectively retard crack growth in pavements.

3.1.1 Crack Tip Blunting

To explain the blunting mechanism of geotextiles, one should consider the current state of practice in which bitumen-saturated geotextile is laid on the top of an existing pavement surface or is imbedded within an asphaltic layered system.

In the case of rehabilitation of an existing pavement, as shown in Figure 5, the tips of all existing cracks and discontinuities in the old pavement lie directly beneath the bitumen-saturated fabric. In the case of a new pavement, where the geotextile is imbedded in the lower third of the structure, a propagating fatigue crack tip encounters the bitumen-saturated layer. From the fracture mechanics viewpoint, it is postulated that the crack growth is a consequence of the changing of the crack tip profile. During a cyclic deformation of a pavement under many loads, a crack tip undergoes the phenomenon of blunting and resharpening. The formation of a plastic zone, and its spread ahead of a crack tip during tensile loading cycles, blunts the propagating crack. Conversely, during unloading cycles, elastic contraction of the material surrounding the crack imposes a residual stress which resharpens the crack tip, aiding its growth. The rate at which a crack may propagate, and the path it follows, depends entirely on the energy balance at the crack tip. The presence of a viscous layer of finite thickness ("bitumen-saturated geotextile") produces a large amount of plastic deformation which could blunt the tip and thus retard crack propagation. It is postulated that bitumen-impregnated geotextiles, of finite thickness, could alter the energy balance at the crack tip:

$$\dot{U} = \dot{V} + \dot{T} + \dot{D} \qquad (11)$$

where

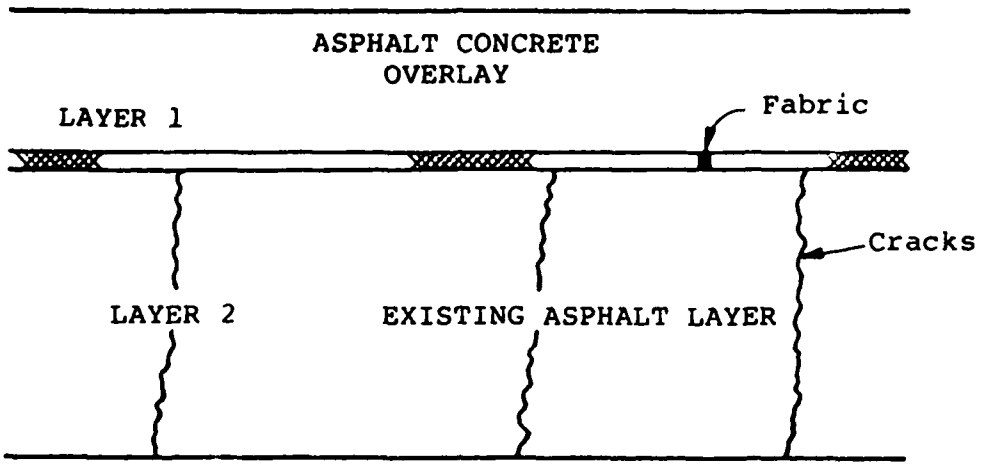

Figure 5. Fabric-Reinforced Asphalt Overlay

U = the work done by the external loads
V = the elastic stored energy
T = the kinetic energy, and
D = irreversible energy, viscous dissipation, plastic work and surface energy.

The dot in the above quotation indicates the rate of change or differentiation with time. Obviously, the viscous dissipation rate of fabric-reinforced systems is dependent on the thickness of the tack coat as well as the viscoelastic nature of the fabric itself. A soft non-woven fabric, with intermediate modulus, when saturated with sufficient quantity of viscoelastic tack coat, could enhance the blunting mechanism as discussed previously.

A double layer system, as shown in Figure 6, could be formed to sandwich the viscous material to form a viscoelastic constraint.

3.1.2 Strain Reduction

It has also been hypothesized that the addition of geotextiles reinforces the pavement structure by increasing relative stiffness and subsequently reducing the local strains and stresses responsible for fatigue crack propagation. It could be argued from the fracture mechanics point of view that a low stress intensity factor is achieved by lowering stresses and strains at localized crack tip regions, which subsequently reduces the crack growth rate. Both theoretical and experimental data suggests that in soft ground reinforcement application, the fabric stiffness may play a significant role. However, unpublished proprietary work recently done by the authors has shown that for moduli values in excess of 50,000 psi (345 MPa) the stress intensity factor is not sensitive to the stiffness or modulus of the bitumen-impregnated geotextile. Therefore, the significance of geotextile stiffness, when imbedded in a flexible pavement and saturated with asphalt cement, is questionable. In a soft ground reinforcement application, however, the geotextile responds as a tensile membrane with substantial elastic-plastic yielding and shear distortion occurring in the soil beneath it. Theoretical elastic-plastic analysis of the soft ground support condition was utilized to formulate Figure 7. This figure shows that the deflection under load is significantly reduced as the fabric modulus increases.

3.1.3 Buffer Zone Debonding

According to the Buffer Zone concept, as a propagating crack in a rather stiff medium reaches a relatively softer zone, the crack tip blunts and may turn its direction by 90 degrees, growing horizontally along the soft zone. A crack running along the interface would result in the debonding of the

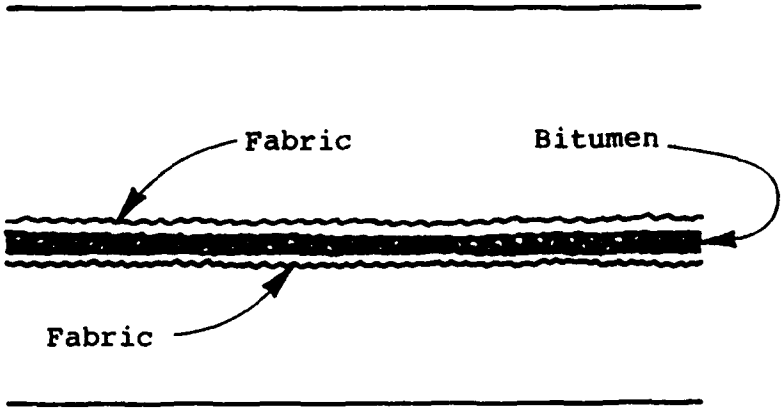

Figure 6. Double "Sandwich" Fabric Layer

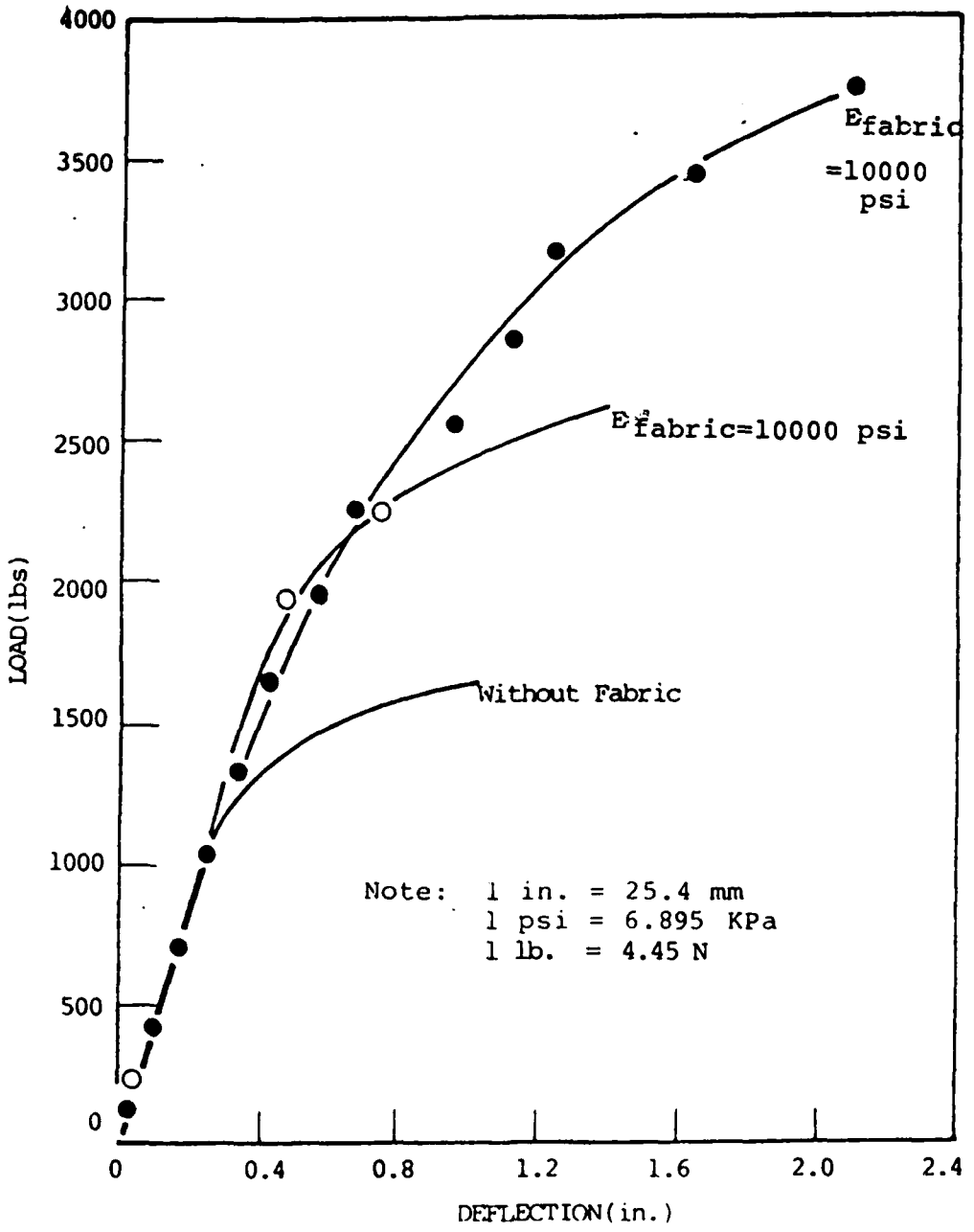

Figure 7. Load Deflection for System with/without fabric.

asphalt-impregnated geotextile from the existing pavement surface. Recent field data from South Africa, using sand as a bondbreaker as well as theoretical analysis of reflection cracking, confirms that the debonding mechanism retards crack growth in overlay pavements, thus indicating a reduction in the stress intensity factor. Factors affecting debonding mechanisms are fabric thickness, saturated geotextile modulus, and required modulus ratio between the asphalt mixture and the saturated geotextile.

3.2 Thermal Forces in Overlaid PCC Pavement Structures

It is generally agreed that the most serious reflection cracking problem occurs in bituminous overlays of PCC pavements. It is also generally agreed that the primary cause of the cracking is thermally induced movement of the concrete slab. The literature review of theoretical models has recently disclosed much disparity regarding the stress state in the overlay under thermal loading.

Thermal stresses result from both seasonal and daily changes in slab temperature. The thermal loading can be represented by the superposition of two different thermal conditions:

A. Uniform change (T) in slab temperature. This condition represents seasonal changes in average slab temperature which can occur over long time periods.

B. "Pure" curling. This condition represents the daily or short time period temperature variation within the slab. For pure curling the average slab temperature has not changed; however, the top of the slab is colder than the bottom of the slab with the temperature assumed linearly related to slab depth. The curling gradient (CG) is given in degrees F/in (degrees C/mm) of slab depth. Figure 8 shows the representation of thermal loading using these two definitions. The reference temperature (TR) is the "zero-stress" temperature for the overlay; slab temperatures below TR will transfer tensile stresses to the overlay. Figure 9 shows the expected monthly average slab temperature and curling gradient for overlaid concrete slabs in Ohio. This figure is based upon computer prediction of pavements in the central Ohio area. Slab thickness varied from 8 to 10 inches (203 to 254mm) and asphalt overlay thickness from 2.5 to 5.0 inches (64 to 127mm) for the pavements used in the Ohio study. Figure 9 provides an estimate of the thermal load magnitudes. Expected curling gradients (CG) varies from .5 degree F/in (.011 degree C/mm) in the spring and fall to about 1 degree F/in (.022 degree C/mm) in the winter months. Mean slab temperature changes by about 40 degrees F (22 degrees C) from summer to winter, dropping at a rate of about 8 degrees F (4.4 degrees C) per month during the fall.

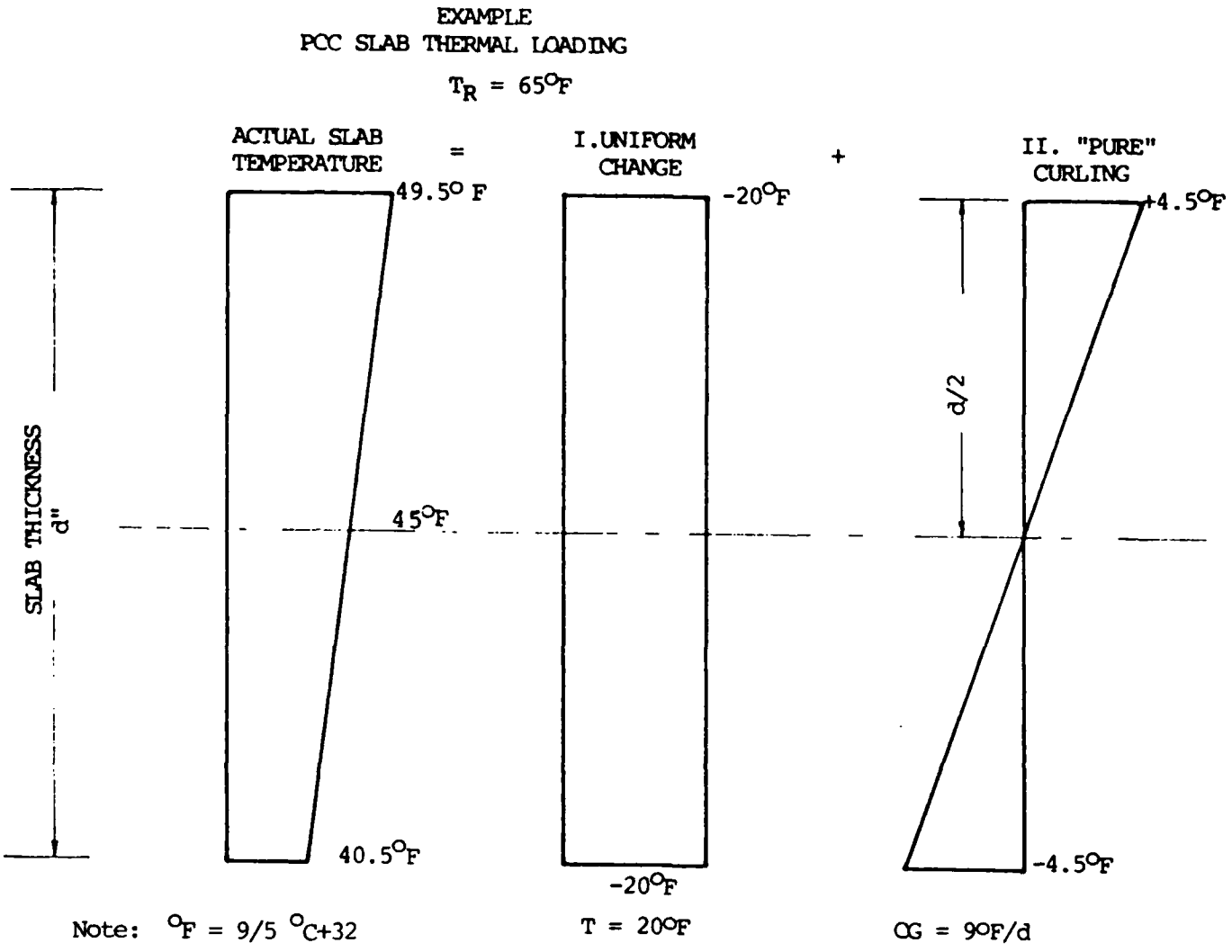

Figure 8. Loading Components of Thermal Loading.

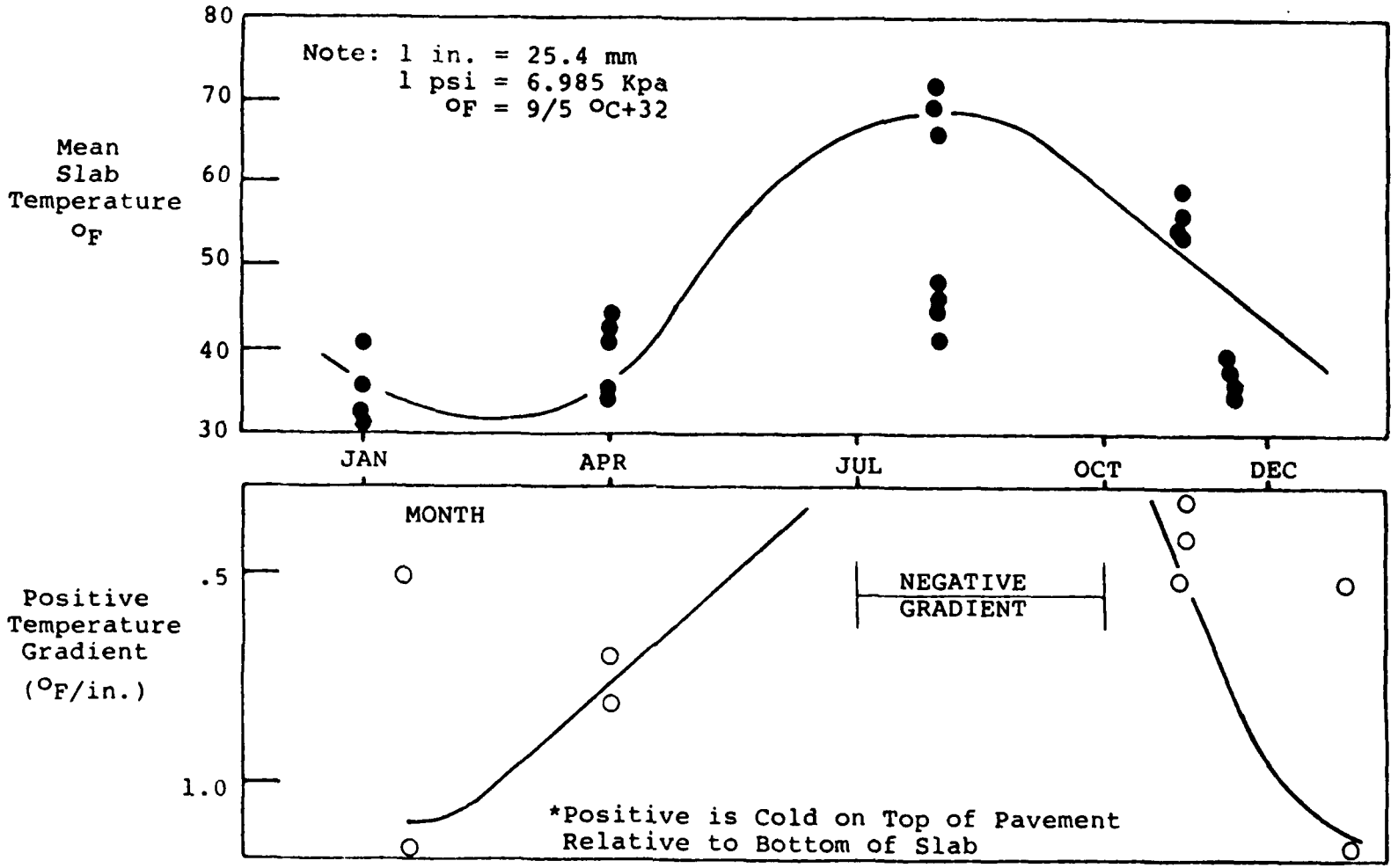

Figure 9. Expected Seasonal Pavement Temperature and Curling Temperature Gradient.

The 2-D finite element analysis of the full scale pavement shown in Figure 10 was conducted using the SAP IV program. As shown in Figure 10, only asphalt overlay modulus and overlay thickness were varied in these analyses. Slab length was 20 feet (6.1m) in all cases. Two separate thermal loading conditions were analyzed: (1) a uniform reduction (T) of 30 degrees F (16.7 degrees C) in slab temperature, and (2) "pure" curling with gradient (CG) of .5 degree F/in (.011 degree C/mm). For constant overlay thickness and modulus, overlay stresses and joint opening were found to be linearly related to T and CG. Both full friction (no slip) and no friction (slip) between PCC slab and aggregate base were investigated. Full friction reduced overlay maximum stress by less than 6% for uniform temperature change and 4% for curling as compared to the no friction condition. Full bond between asphalt overlay and PCC slabs was assumed in all cases.

Figures 11 through 14 show computed stresses in the overlay at the center of the joint as a function of depth (Z). In all cases for both curling load and uniform temperature change, maximum stress occurs at the bottom of the overlay. The stress distributions are very similar for the uniform temperature change and curling loading conditions. The similarities occur throughout the range of overlay thickness and overlay moduli investigated. Figures 15a and b show the computed shear stress at the overlay/slab interface. Again the stress distributions are similar for the two loading conditions. These shear stresses would have to exceed the tack coat bonding stress to cause slippage between the two layers. The maximum shear stresses are below the bonding stresses given by ARE (8). Figure 16 shows the effect of breaking the bond (either by slippage or introduction of a bond breaker) upon maximum overlay stress. A dramatic reduction in stress is predicted for bond breaker lengths as short as 1 in (25mm).

The high sensitivity of overlay stress to overlay stiffness is clearly demonstrated. As noted earlier, ARE (8) suggests that the creep modulus, Ec, be utilized for stress calculations. However, Ec is both temperature and time of loading dependent. Figure 17 presents this dependency for a typical dense-graded asphalt concrete with Ec calculated by the Heukelom and Klomp (15) (or Shell) procedure. This procedure determines the compressive creep modulus. The tensile creep modulus is actually needed for reflection cracking analysis. However, no procedure for predicting tensile creep modulus has been published. If creep modulus curves in tension are similar to those of Figure 17, then the implications to thermal reflection cracking analysis and modeling are very significant. An incremental analysis which utilizes the loading time and temperature dependent creep modulus

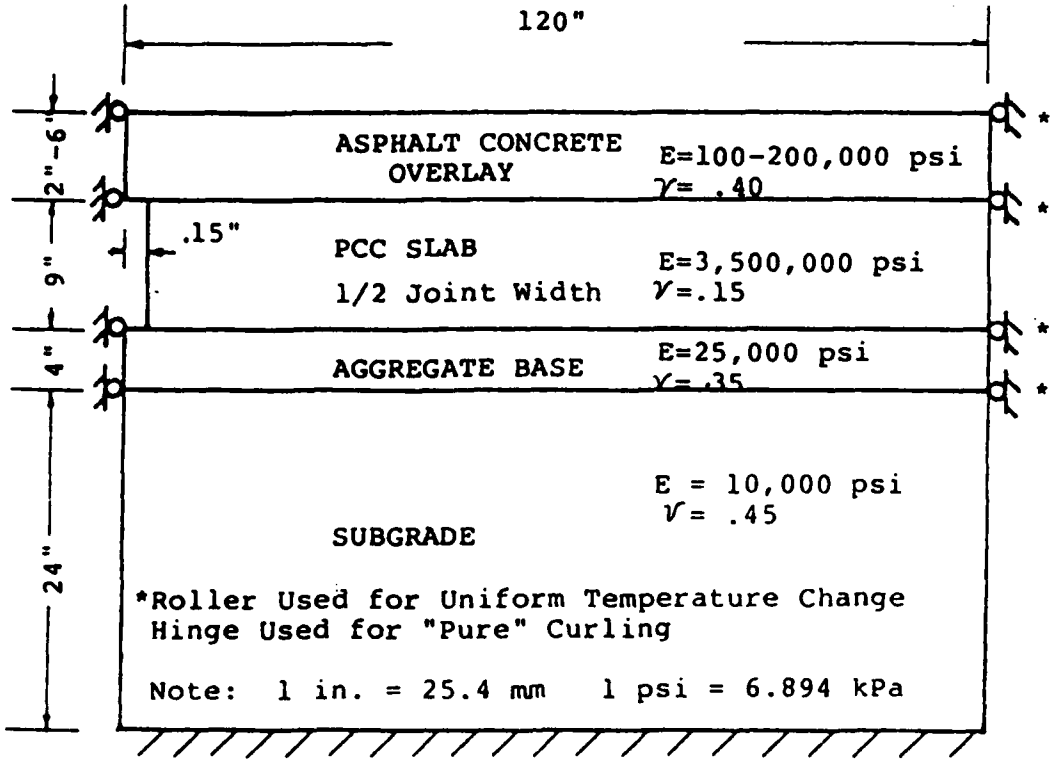

Figure 10. Schematic 2-D Finite Element Model

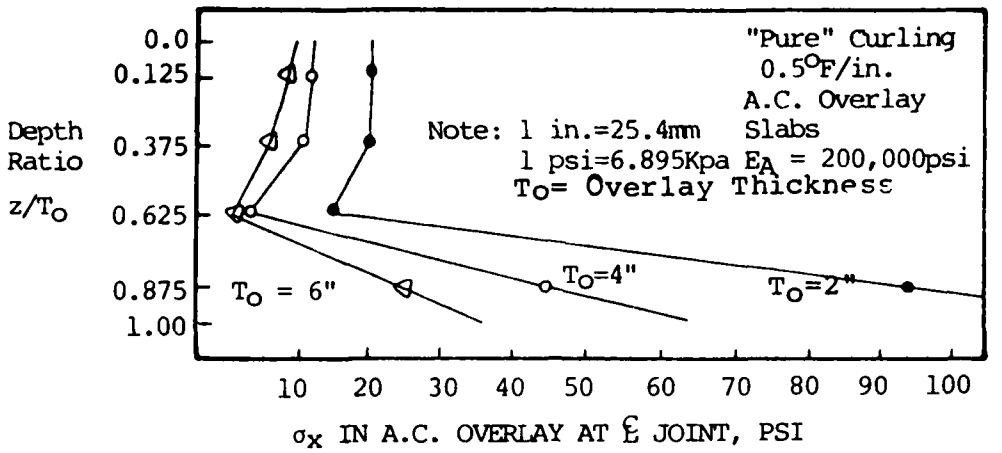

Figure 11. Stress Distribution in Overlay Due to "Pure" Curling

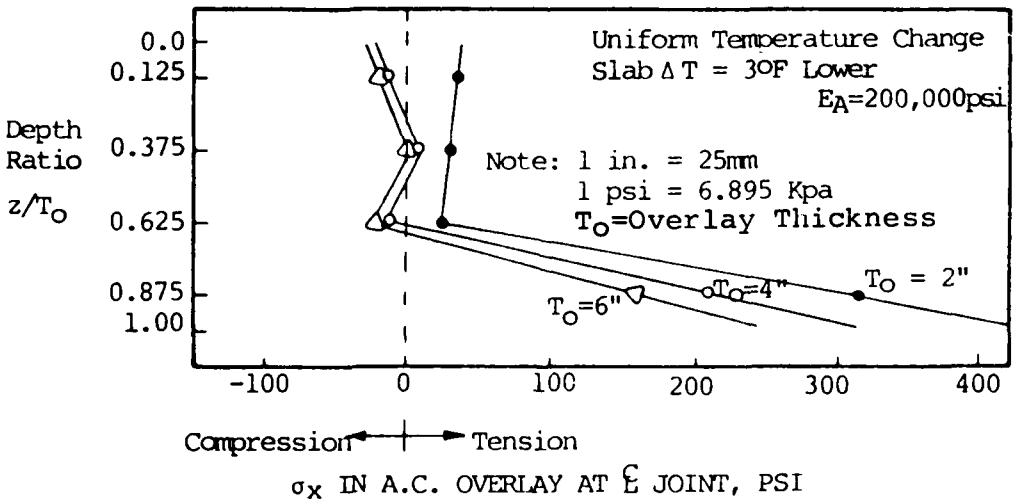

Figure 12. Stress Distribution Overlay Due to Uniform Temperature Change.

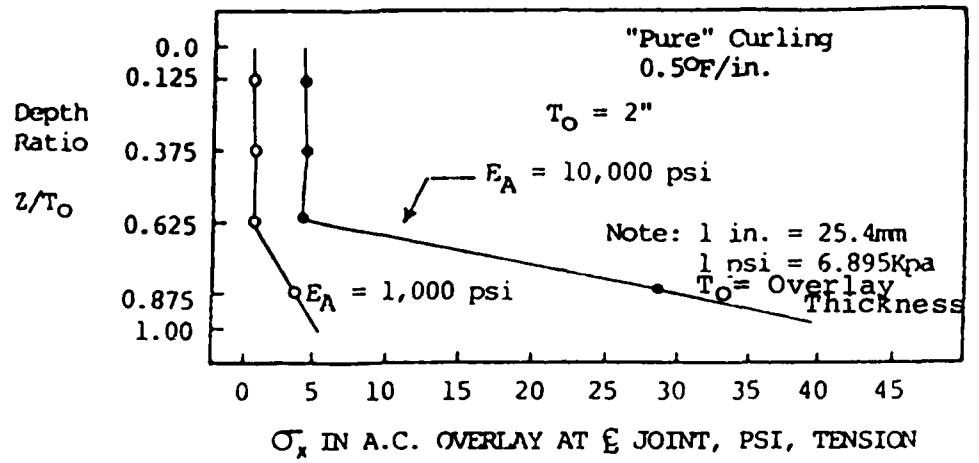

Figure 13. Stress Distribution in Overlay Due to "Pure" Curling

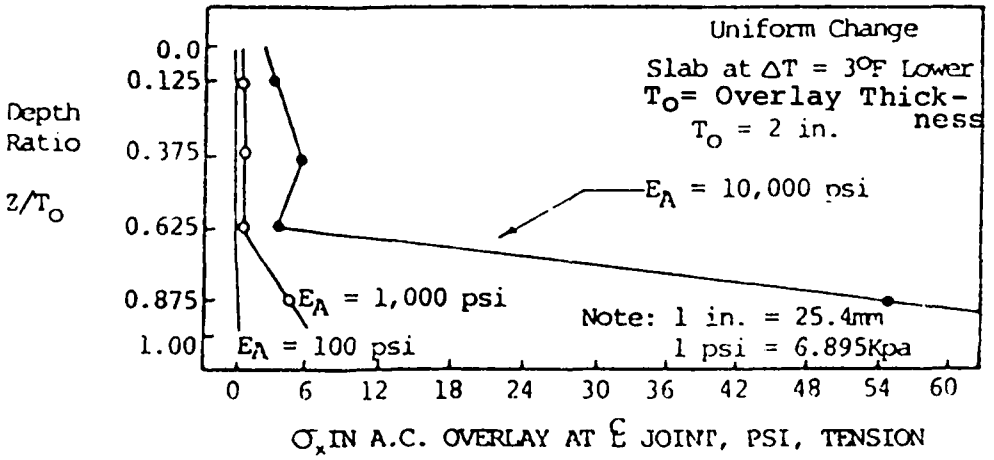

Figure 14. Stress Distribution Overlay Due to Uniform Temperature Change

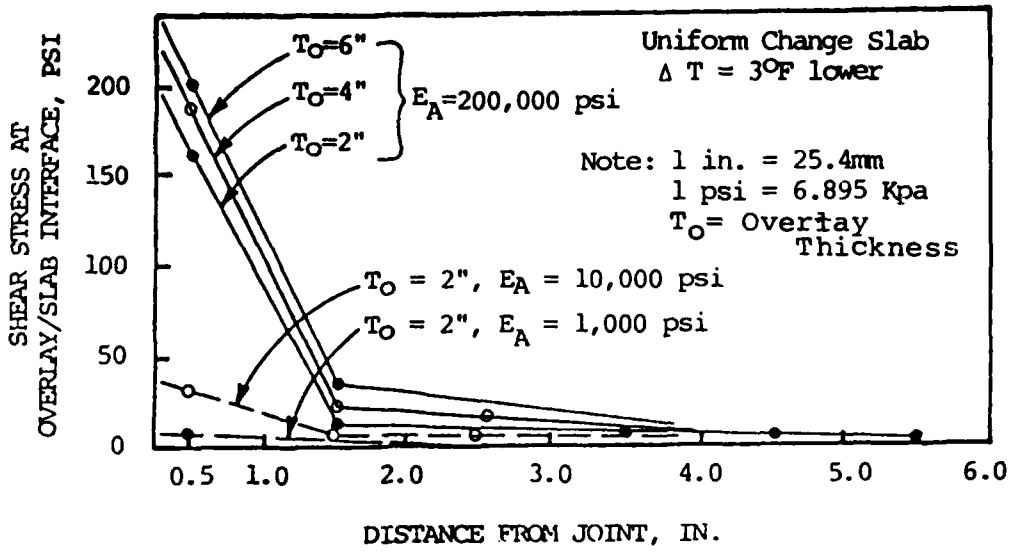

Figure 15a. Shear Stress Overlay Due to Uniform Change in Slab Temperature

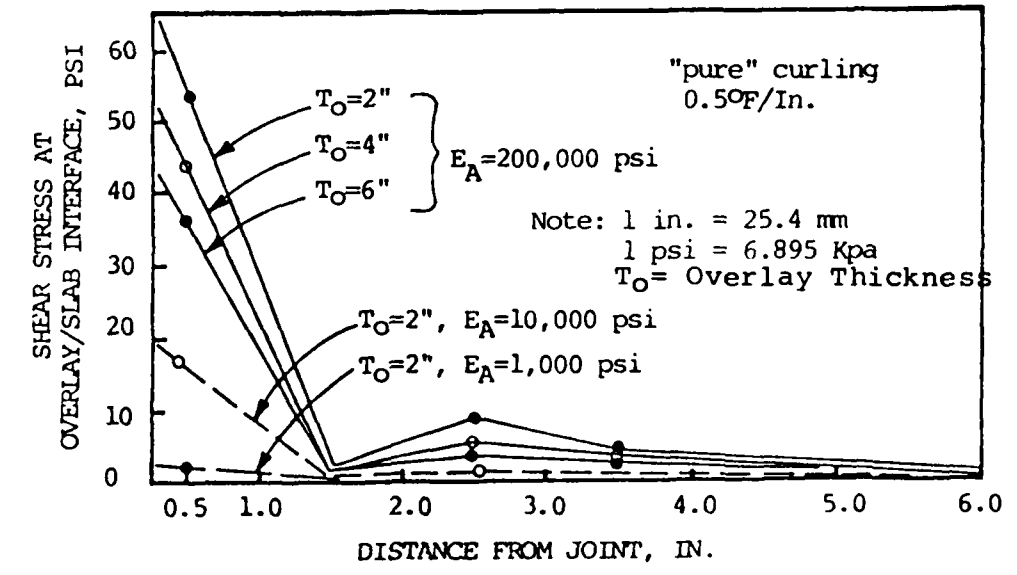

Figure 15b. Shear Stress Distributions Overlay Due to "Pure" Curling

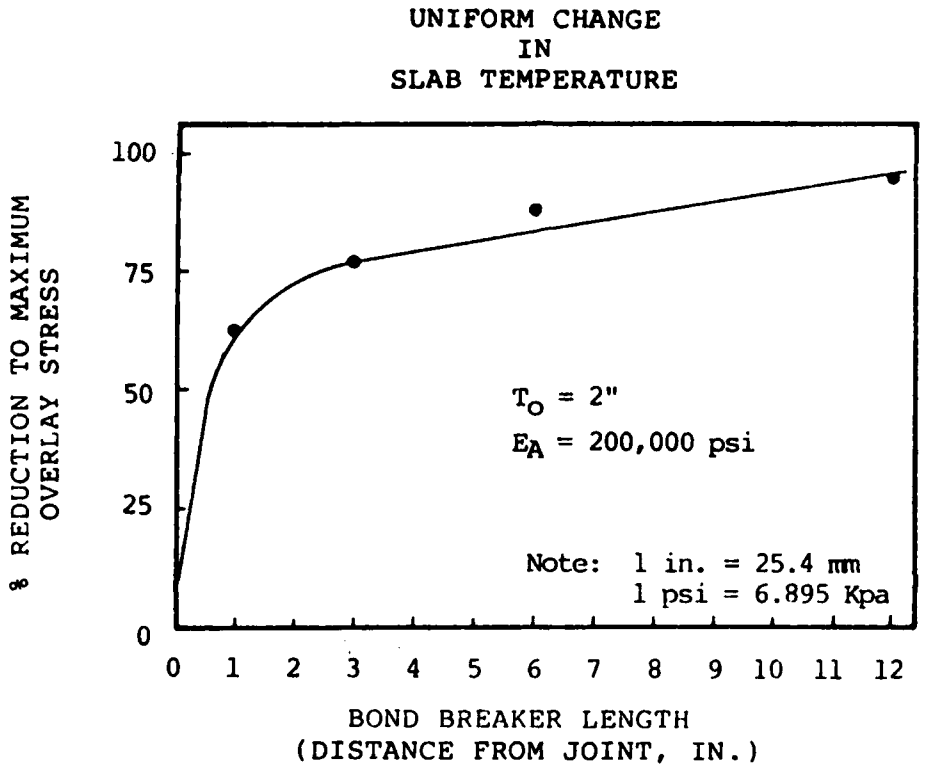

Figure 16. Effect of bond breaker length or stresses.

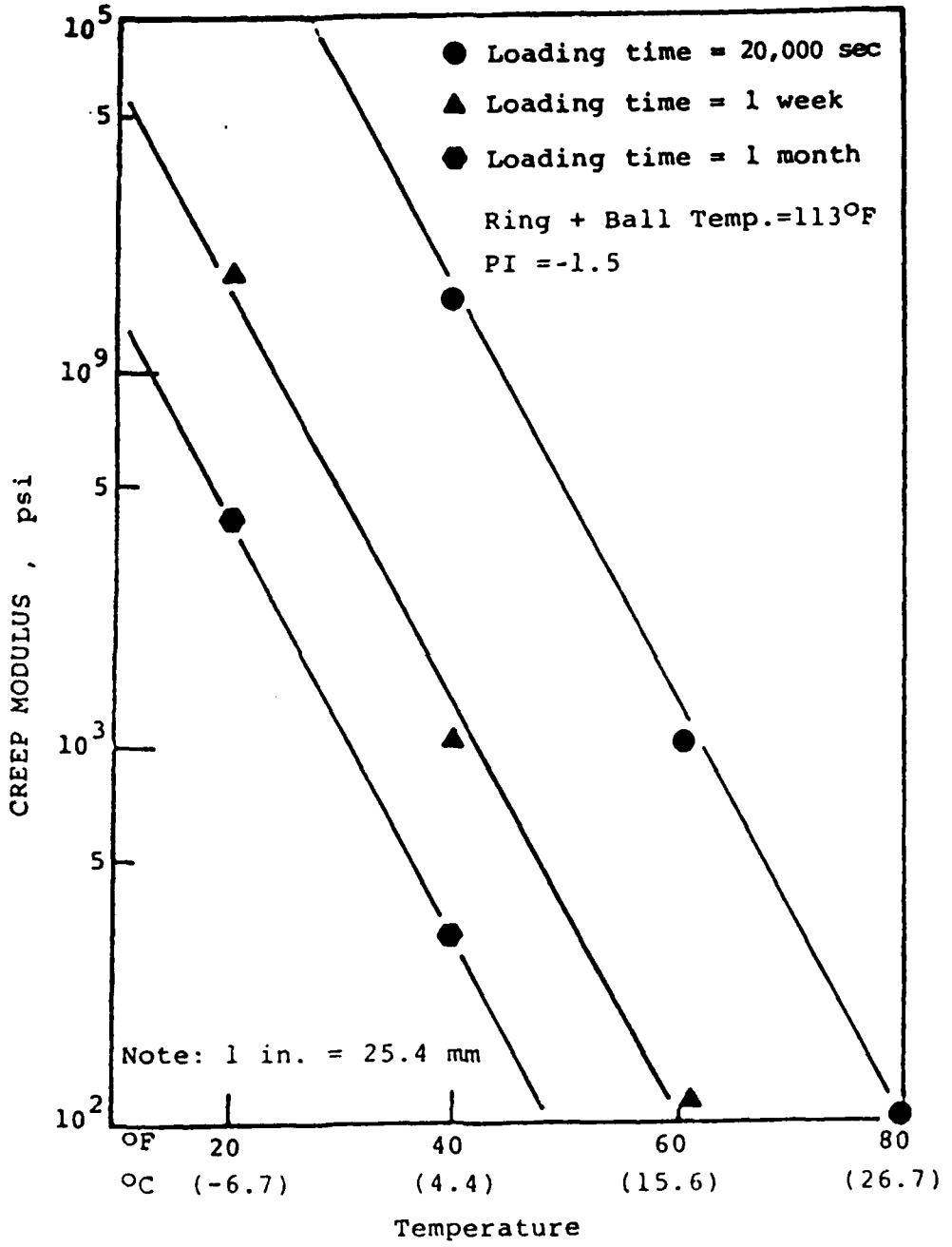

Figure 17. CREEP MODULUS VS. TEMPERATURE

would be necessary to calculate overlay stress and joint opening. Seasonal changes occur over long periods of time (time required to drop from TR to T amount) while curling can occur over relatively short periods (less than 1/2 day) and at all temperatures. The fact that curling occurs over shorter loading times than seasonal uniform temperature change means that a higher Ec should be used for curling load than for uniform temperature change stress calculations. The higher Ec will result in higher overlay stresses which should be considered when comparing seasonal and curling induced loading conditions.

Since both curling and seasonal change produce joint openings which induce similar overlay stress distributions, it is believed that it is possible to equate the two loading conditions. Figure 18 shows that overlay stress is linearly related to displacement at the top of the joint. The slope of the stress-joint displacement line is a function of overlay modulus. The overlay stresses are independent of the type of thermal load. At constant overlay modulus, a horizontal displacement of x will produce the same overlay stress regardless of whether this displacement was produced by slab curling or uniform temperature change. This is further evidence that curling can be equated to seasonal temperature change.

Figure 19 shows the relationship between overlay modulus and predicted joint displacement for the finite element model. For Ec below 1500 psi (10.3 MPa), movement nearly equals that for free unrestrained thermal movement (TL/2). From Figure 17 the expected modulus is below 1500 psi (10.3 MPa) for long loading times (greater than 1 month) for temperature greater than 25 degrees F(-4 degrees C). Subsequent design of fabric reinforced overlay should consider that the modulus of the overlay will be less than 1500 psi (10.3 MPa). The joint opening can then be calculated using the $\alpha \Delta T$ L/2 expression. This will simulate joint openings which occur in real pavements at temperatures above about 25 degrees F (-4 degree C).

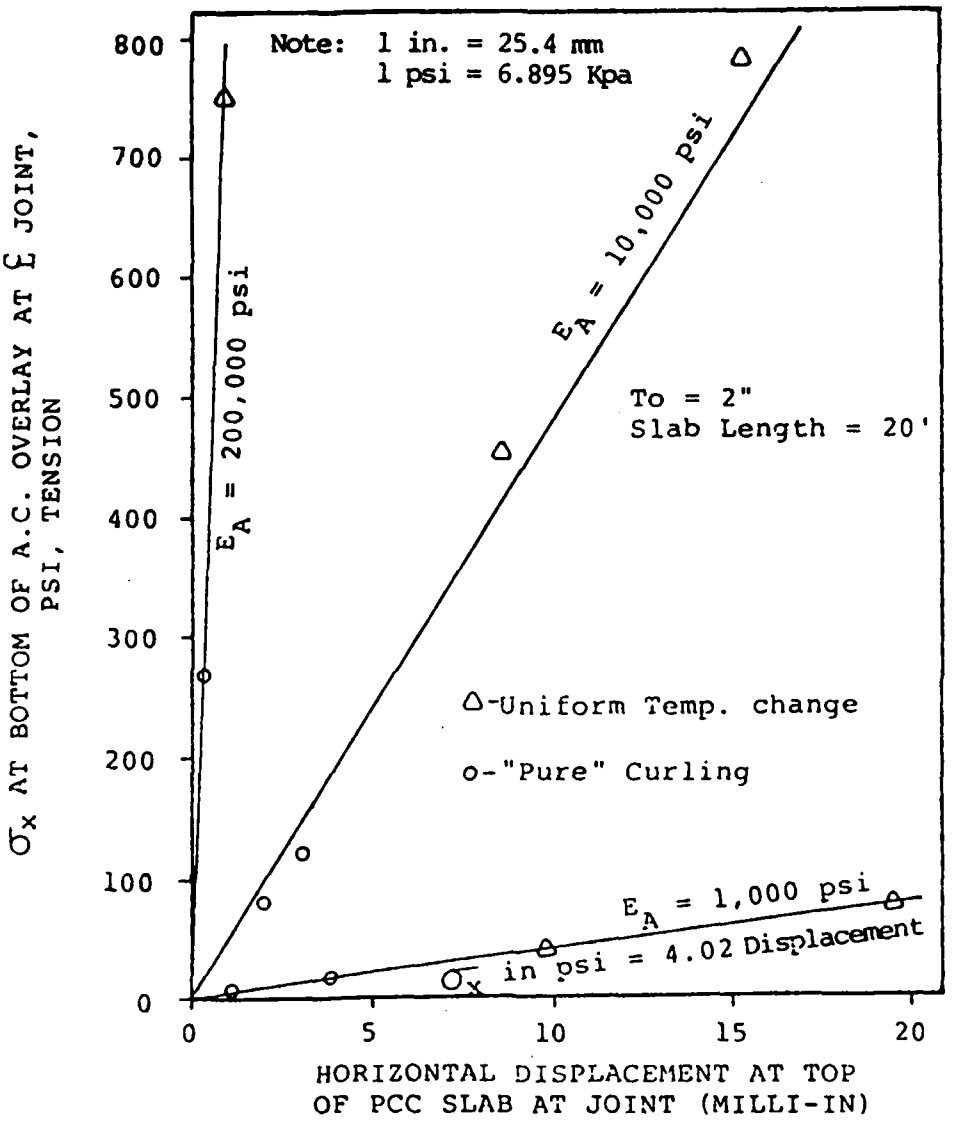

Figure 18. Overlay stress as a function of joint movement.

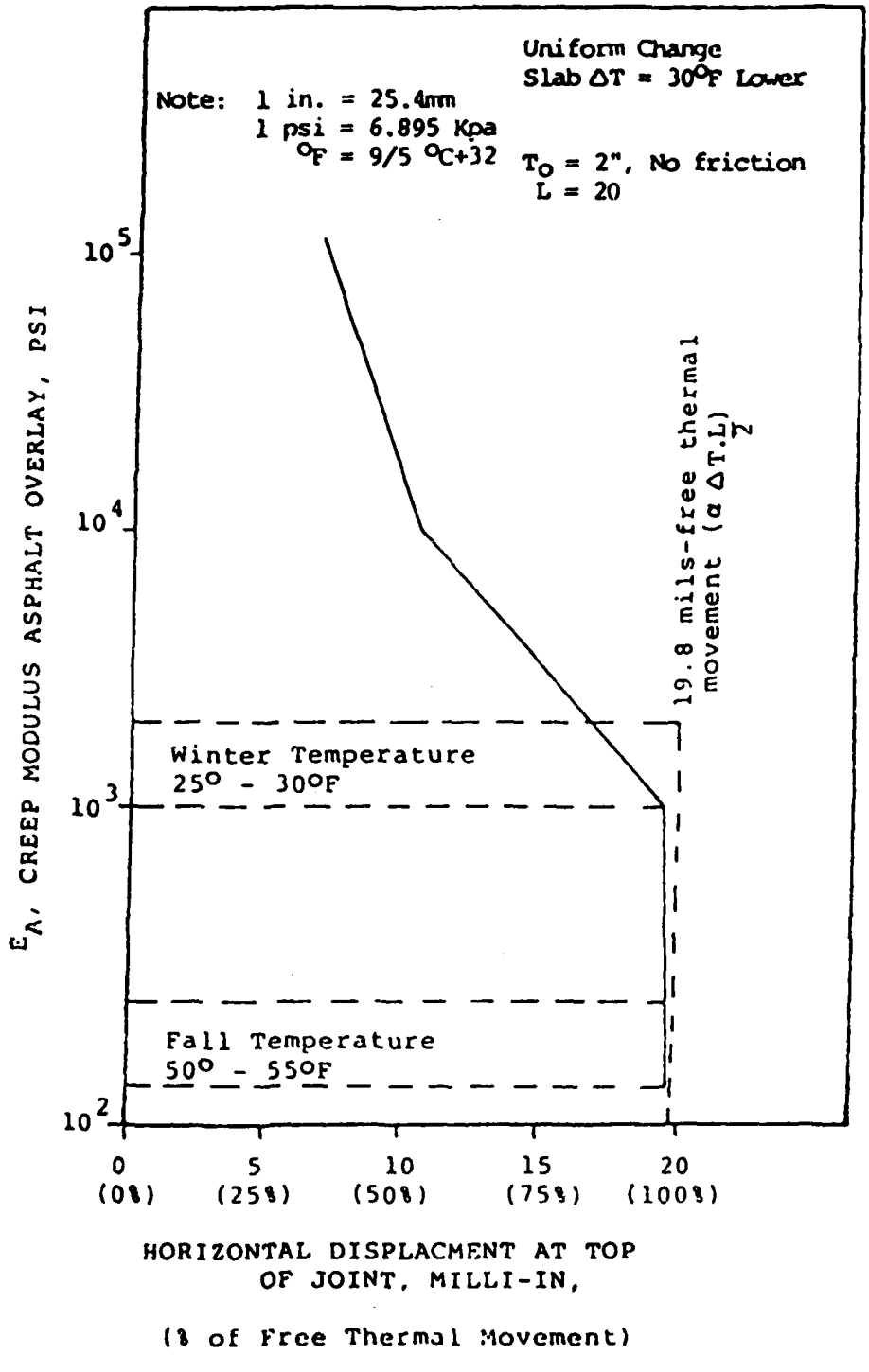

Figure 19. Thermal Movement of slab as a function of asphalt creep modulus.

CHAPTER IV. DESIGN PROGRAM

4.1 Scope and Outline of Research

The primary objective of this study is to develop a procedure for the design of flexible overlays for existing rigid pavements based upon mechanistic concepts of the "Overlay Pavement Foundation" (OPF) structure, including the use of engineering fabrics as a reflective crack arrest phenomenon.

The program can also be used to design rigid overlays of rigid or flexible pavements, as well as flexible overlays of flexible pavements, if appropriate material properties are input.

A three-dimensional finite element approximation would probably be most rational representation of the OPF system. However, the amount of linear equations involved in the solution of any non-academic problem is so large that it makes this approximation economically unreasonable and very sensitive to a numerical error. Therefore, in this study a two-dimensional model is used to determine the stress patterns in the overlay structure and a three-dimensional model (RISC*) computer program (16)) can be used to estimate the existing pavement life.

4.1.1 Model Description and Program Capacity

For finite element modeling the OPF structure is divided into the following structural elements (see Figure 20):

a. Overlay
b. Fabric
c. Existing slabs
d. Slab-foundation contact zone
e. Elastic foundation
f. Joint structure
g. Crack

Each of these structural elements has its own finite element type, mesh and materials properties, which are described in the following sections.

---

* RISC - Finite element computer program developed by Resource International Inc. for the analysis of rigid pavements using the coupling of a finite element plate with a multilayer elastic solid foundation.

4.1.2 Overlay Structure

For finite element approximation of the overlay structure a two- dimensional isoparametric element with incompatible mode (Wilson element) are used (see Figure 21). The local and global coordinates are related by the transformation

$$x = \phi^T \underset{\sim}{x} \tag{12}$$

$$y = \phi^T \underset{\sim}{y} \tag{13}$$

where

$$\underset{\sim}{x}^T = [x_1, x_2, x_3, x_4] \tag{14}$$

$$\underset{\sim}{y}^T = [y_1, y_2, y_3, y_4] \tag{15}$$

$$\phi = 1/4 \begin{Bmatrix} (1-s)\ (1-t) \\ (1+s)\ (1-t) \\ (1+s)\ (1+t) \\ (1-s)\ (1+t) \end{Bmatrix} \tag{16}$$

In order to insure rigid-body displacement modes, the same interpolation functions, ϕ , are used in the displacement approximation for a compatible element, i.e.,

$$u = \phi^T \underset{\sim}{u} \tag{17.a}$$

$$v = \phi^T \underset{\sim}{v} \tag{17.b}$$

where

$$\underset{\sim}{u}^T = [u_1, u_2, u_3, u_4] \tag{18.a}$$

$$\underset{\sim}{v}^T = [v_1, v_2, v_3, v_4] \tag{18.b}$$

Here u_i, v_i, i=1, 2, 3, 4, are the global displacement components at node i in the global x and y directions respectively.

To account for the errors in bending deformation, Wilson (17) suggested that the following form of displacement approximation be used if higher accuracy is desired.

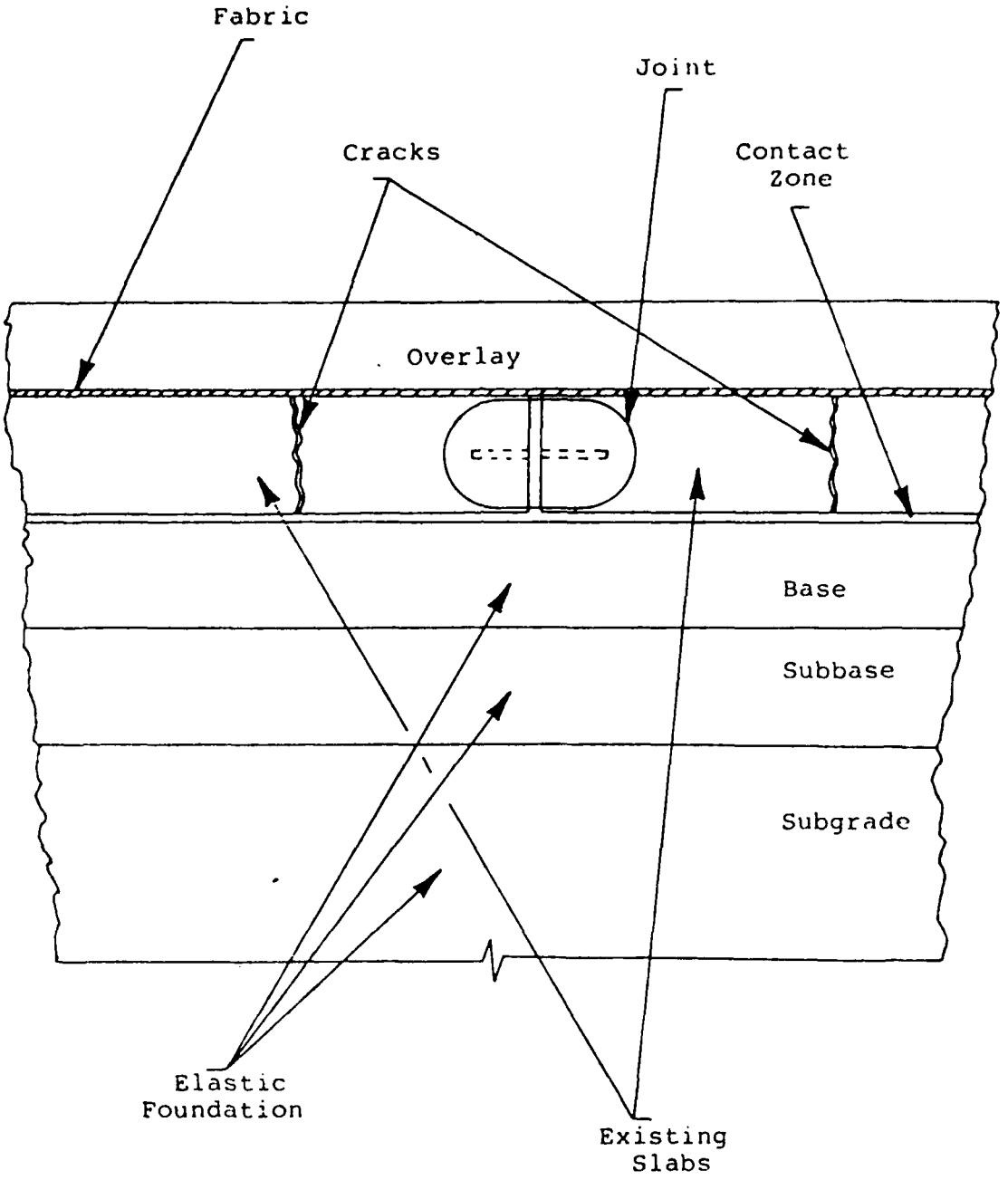

Figure 20. Structural eleminates of the pavement.

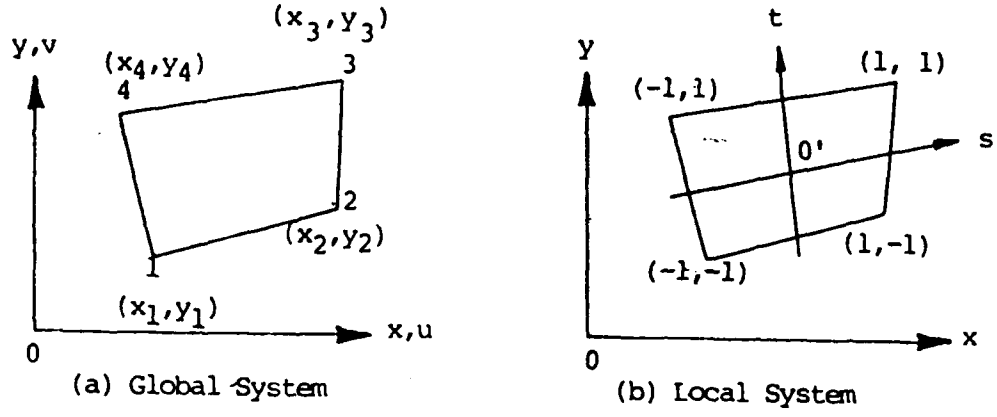

Figure 21. Two-Dimensional Isoparametric Elements

$$u = \psi^T \underset{\sim}{u} \tag{19.a}$$

$$v = \psi^T \underset{\sim}{v} \tag{19.b}$$

where

$$\underset{\sim}{u}^T = [u_1, u_2, u_3, u_4, a_1, a_2] \tag{20.a}$$

$$\underset{\sim}{v}^T = [v_1, v_2, v_3, v_4, a_3, a_4] \tag{20.b}$$

$$\psi = 1/4 \begin{Bmatrix} (1-s)\ (1-t) \\ (1+s)\ (1-t) \\ (1+s)\ (1+t) \\ (1-s)\ (1+t) \\ \hline 4\ (1-s\ ) \\ 4\ (1-t\ ) \end{Bmatrix} = \begin{pmatrix} \phi \\ \hline \lambda \end{pmatrix} \tag{21}$$

$$\lambda = \begin{Bmatrix} (1-s\ ) \\ (1-t\ ) \end{Bmatrix} \tag{22}$$

Here the a's are arbitary constants representing internal degrees of freedom within the element. Hence the displacement matrix can be written as

$$\begin{Bmatrix} u \\ v \end{Bmatrix} = \left[\begin{array}{cc|cc} \phi^T & \{0\}^T & \lambda^T & \{0\}^T \\ \{0\}^T & \phi^T & \{0\}^T & \lambda^T \end{array}\right] \begin{pmatrix} q \\ \hline r \end{pmatrix} \tag{23}$$

where $$\underset{\sim}{q}^T = [u_1, u_2, u_3, u_4, v_1, v_2, v_3, v_4] \tag{24.a}$$

$$\underset{\sim}{r}^T = [a_1, a_2, a_3, a_4] \tag{24.b}$$

$$\{0\}^T = [0, 0, 0, 0] \tag{25.a}$$

$$\{\bar{0}\}^T = [0,\ 0] \tag{25.b}$$

or

$$\phi_q = \begin{bmatrix} \phi^T & \{d\}^T \\ \{d\}^T & \phi^T \end{bmatrix} \tag{26}$$

$$\phi_r = \begin{bmatrix} \lambda^T & \{\bar{0}\}^T \\ \{\bar{0}\}^T & \lambda^T \end{bmatrix} \tag{27}$$

where the matrices ϕ and λ are given by Equations (16) and (22).

4.1.3 Strain-Displacement Equations

For a two-dimensional analysis, the strain-displacement equations are given by:

$$\begin{Bmatrix} \epsilon_x \\ \epsilon_y \\ \epsilon_{xy} \end{Bmatrix} = \begin{Bmatrix} \frac{\delta u}{\delta x} \\ \frac{\delta v}{\delta y} \\ \frac{\delta u}{\delta y} + \frac{\delta v}{\delta x} \end{Bmatrix} \tag{28}$$

In view of Equations (19), (20) and (21), Equation (28) becomes

$$\begin{Bmatrix} \epsilon_x \\ \epsilon_y \\ \epsilon_{xy} \end{Bmatrix} = \begin{vmatrix} \psi^T_{,x} & \begin{Bmatrix} 0 \\ - \\ \bar{0} \end{Bmatrix}^T \\ \begin{Bmatrix} 0 \\ - \\ \bar{0} \end{Bmatrix}^T & \psi^T_{,x} \\ \psi^T_{,y} & \psi^T_{,x} \end{vmatrix} \begin{Bmatrix} \underset{\sim}{u} \\ \underset{\sim}{v} \end{Bmatrix} \tag{29}$$

where ψ^T is the transpose of ψ and $\psi^T_{,x}$, $\psi^T_{,y}$ are partial derivatives of ψ^T with respect to x and y, respectively. With the chain rule it can be verified that

$$\begin{Bmatrix} \frac{\delta}{\delta x} \\ \frac{\delta}{\delta y} \end{Bmatrix} = \frac{1}{|J|} \begin{vmatrix} \frac{\delta y}{\delta t} & -\frac{\delta y}{\delta s} \\ -\frac{\delta x}{\delta t} & \frac{\delta x}{\delta s} \end{vmatrix} \begin{Bmatrix} \frac{\delta}{\delta s} \\ \frac{\delta}{\delta t} \end{Bmatrix} \tag{30}$$

where the Jacobian determinant $|J|$ is given by

$$|J| = \begin{vmatrix} \frac{\delta x}{\delta s} & \frac{\delta y}{\delta s} \\ \frac{\delta x}{\delta t} & \frac{\delta y}{\delta t} \end{vmatrix} \tag{31}$$

Substituting Equations (12) and (13)in Equation (30) and (31) results in

$$\begin{Bmatrix} \frac{\delta}{\delta x} \\ \\ \frac{\delta}{\delta y} \end{Bmatrix} = \frac{1}{|J|} \begin{vmatrix} \phi_{,t}^T \underset{\sim}{y} & -\phi_{,s}^T \underset{\sim}{y} \\ \\ -\phi_{,t}^T \underset{\sim}{x} & \phi_{,s}^T \underset{\sim}{x} \end{vmatrix} \begin{Bmatrix} \frac{\delta}{\delta s} \\ \\ \frac{\delta}{\delta t} \end{Bmatrix} \tag{32}$$

$$|J| = \underset{\sim}{x}^T \begin{bmatrix} \phi_{,s} \phi_{,t}^T & -\phi_{,t} \phi_{,s}^T \end{bmatrix} \underset{\sim}{y} \tag{33}$$

where

$$\phi_{,s} = \frac{1}{4} \begin{Bmatrix} -1+t \\ 1-t \\ 1+t \\ -1-t \end{Bmatrix}; \phi_{,t} = \frac{1}{4} \begin{Bmatrix} -1+s \\ -1-s \\ 1+s \\ 1-s \end{Bmatrix} \tag{34}$$

Using Equations (21) and (32), Equation (29) can be written:

$$\underset{\sim}{\epsilon} = \left[\begin{array}{c|c} B_q & B_r \end{array}\right] \begin{Bmatrix} \underset{\sim}{q} \\ \hline \underset{\sim}{r} \end{Bmatrix} \tag{29.a}$$

where $\underset{\sim}{\epsilon}$ is the vector of physical strain components, and

$$B_q = \begin{bmatrix} \phi^T_{y,\tilde{t}} & \phi^T_{,s} & -\phi^T_{y,\tilde{s}} & \phi^T_{,t} & \{0\}^T \\ \{0\}^T & \phi^T_{x,\tilde{s}} & \phi^T_{,t} & -\phi^T_{x,\tilde{t}} & \phi^T_{,s} \\ \phi^T_{x,\tilde{s}} & \phi^T_{,t} & -\phi^T_{x,\tilde{t}} & \phi^T_{,s} & \phi^T_{y,\tilde{t}} \quad \phi^T_{,s} \quad \phi^T_{y,\tilde{s}} \quad \phi^T_{,t} \end{bmatrix} \tag{35}$$

$$B_r = \begin{bmatrix} \phi^T_{y,\tilde{t}} & \lambda^T_{,s} & -\phi^T_{y,\tilde{s}} & \lambda^T_{,t} & \{\bar{0}\}^T \\ \{\bar{0}\}^T & \phi^T_{x,\tilde{s}} & \lambda^T_{,t} & -\phi^T_{x,\tilde{t}} & \lambda^T_{,s} \\ \phi^T_{x,\tilde{s}} & \lambda^T_{,t} & -\phi^T_{x,\tilde{t}} & \lambda^T_{,s} & \phi^T_{y,\tilde{t}} \quad \lambda^T_{,s} \quad \phi^T_{y,\tilde{s}} \quad \lambda^T_{,t} \end{bmatrix} \tag{36}$$

$$\lambda^T_{,s} = [-2s, 0] \quad ; \quad \lambda^T_{,t} = [0, -2t] \tag{37}$$

4.1.4 Element Stiffness Matrix

Referring to the local s-t coordinates, the element stiffness matrix can be written as:

$$K = b \int_{-1}^{1} \int_{-1}^{1} |J| \, B^T E B \, ds \, dt \tag{38}$$

where b is the constant thickness of the element. The elasticity matrix E for a general orthotropic material is the inverse of the compliance matriX C given by:

$$C = \begin{bmatrix} (1 - \nu_{zx}\nu_{zx})/E_x & -(\nu_{xy} + \nu_{xy}\nu_{zy})/E_y & 0 \\ \text{symmetric} & (1 - \nu_{zy}\nu_{yz})/E_y & 0 \\ & & 1/G_{xy} \end{bmatrix} \tag{39}$$

for the plane strain condition, and for the plane stress condition

$$C = \begin{bmatrix} 1/E_x & -\nu_{xy}/E_y & 0 \\ & 1/E_y & 0 \\ \text{symmetric} & & 1/G_{xy} \end{bmatrix} \qquad (40)$$

where E_i = modulus of elasticity in the i direction

ν_{ij} = Poisson coefficient which characterizes the decrease in the j direction for tension in i direction

G_{xy} = shear modulus in the x-y plane.

Here it is assumed that the principal axes for the orthotropic material coincide with the global axes. If this is not the case, the following transformation has to be made. Let be the angle of rotation from the global x-y axes to the material principal x'-y' axes. Let C be the compliance matrix with respect to the material principal axes and C be the corresponding compliance matrix with respect to the global x-y axes; the third material principal axis (normal to the x'-y' plane) being coincided with the global z axis. Then the two matrices are related by:

$$C = T_\eta C' \qquad (41)$$

where

$$T = \begin{bmatrix} \cos^2\eta & \sin^2\eta & \sin 2\eta \\ \sin^2\eta & \cos^2\eta & -\sin 2\eta \\ -1/2 \sin 2\eta & 1/2 \sin 2\eta & \cos^2\eta - \sin^2\eta \end{bmatrix} \qquad (42)$$

Having obtained C in the global coordinate system, the matrix E can be computed as the inverse of the C matrix and substituted in Equation (38). The integrals in (38) are carried out by the direct application of one-dimensional numerical integration using the two-point Legendre integration formula. For example,

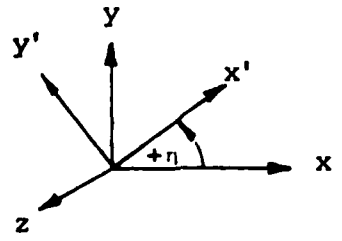

Figure 22. Principal Axes of Material Properties and Global Axes

$$K = b \sum_{j=1}^{2} \sum_{i=1}^{2} W_i W_j \left| J(s_j, t_j) \right| B^T(s_j, t_i)\, E\, B(s_j, t_i) \quad (43)$$

where the integration points sj, ti, and the corresponding weight functions are given by

$$\begin{aligned} s_1 &= t_1 = + 0.57735026918963 \\ s_2 &= t_2 = - 0.57735026918963 \\ W_1 &= W_2 = 1.0 \end{aligned} \quad (44)$$

4.1.5 Element Equivalent Nodal Load Vector

(a) Due to the Body Force

Since the body force considered here is due to gravity, it is assumed to be constant throughout the element. Let fx and fy be the components of gravity force in the global x and y directions respectively, i.e.,

$$\{f\} = \begin{Bmatrix} f_x \\ f_y \end{Bmatrix} \quad (45)$$

$$\underset{\sim}{P}_{qf} = b \int_{-1}^{1} \int_{-1}^{1} |J|\, \Phi_q^T \, ds \, dt \, \{f\} \quad (46)$$

and

$$\underset{\sim}{P}_{rf} = b \int_{-1}^{1} \int_{-1}^{1} |J| \, \Phi_r^T \, ds \, dt \, \{f\} \tag{47}$$

(b) Due to Temperature

The temperature variation within the element is assumed to be related to the temperatures at the nodes of the element by the interpolation functions ϕ, i.e.,

$$T = \phi^T \underset{\sim}{T} \tag{48}$$

where

$$\underset{\sim}{T} = \begin{bmatrix} T_1, T_2, T_3, T_4 \end{bmatrix} \tag{49}$$

T_i = temperature at node i

ϕ is given by Equation (16). The temperature rise at any point within the element is assumed to be

$$\Delta T = T - T_r \tag{50}$$

T = temperature rise at any point (s,t)

T_r = reference temperature for the temperature stress free state within the element

For an orthotropic material, it can be shown that the initial strains due to temperature change ΔT is given by:

$$\underset{\sim}{\epsilon}_0 = \begin{Bmatrix} \epsilon_{x0} \\ \epsilon_{y0} \\ 0 \end{Bmatrix} = \Delta T \begin{Bmatrix} \alpha_x + \nu_{zx}\alpha_z \\ \alpha_y + \nu_{zy}\alpha_z \\ 0 \end{Bmatrix} \tag{51}$$

for plane strain condition, and for plane stress condition, by:

$$\underset{\sim}{\epsilon}_0 = \Delta T \begin{Bmatrix} \alpha_x \\ \alpha_y \\ 0 \end{Bmatrix} \tag{52}$$

where

α_i = coefficient of thermal expansion in the i direction.

If the principal axes of the material do not coincide with the

global axes, the strain transformation has to be performed, using the transformation matrix T_η given in Equation (41), in the same manner as the compliance matrix transformation (40). The equivalent nodal load vectors due to temperature change are:

$$\underset{\sim}{P}_q = b \int_{-1}^{1} \int_{-1}^{1} |J| \, B_q^T \, E \, \underset{\sim}{\epsilon}_0 \, ds \, dt \tag{53}$$

$$\underset{\sim}{P}_r = b \int_{-1}^{1} \int_{-1}^{1} |J| \, B_r^T \, E \, \underset{\sim}{\epsilon}_0 \, ds \, dt \tag{54}$$

The integrations are carried out, as before, by the two-point Legendre integration formula.

(c) Due to Boundary Surface Tractions

For an element which has a boundary face subjected to a distributed external load, the equivalent nodal loads due to this surface load have to be considered. For illustration purposes, it is assumed that the boundary 1-2 of the element is subjected to the prescribed linearly distributed load per unit area as shown below.

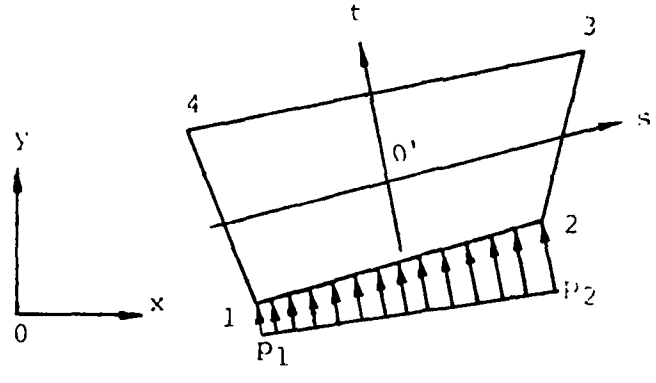

Figure 23. An Element Subjected to Surface Pressure on 1-2 Side

Let px1, py1 be the components of the load intensity p1 at node 1 and px2, py2 be the components of the load intensity p2 at node 2. Since along 1-2 edge the local t ordinate is constant (= -1), hence it can be shown that the components px and py of the distributed load along this surface are described as:

$$\{p\} = \begin{Bmatrix} p_x \\ p_y \end{Bmatrix} = \frac{1}{2}\begin{bmatrix} (1-s) & (1+s) & 0 & 0 \\ 0 & 0 & (1-s) & (1+s) \end{bmatrix} \begin{Bmatrix} p_{x1} \\ p_{x2} \\ p_{y1} \\ p_{y2} \end{Bmatrix} \quad (55)$$

Along the 1-2 side, the matrix of displacement interpolation functions Φ_q and Φ_r are given by

$$\Phi_q\Big|_{t=-1} = \bar{\Phi}_q = \begin{bmatrix} (1-s) & (1+s) & 0 & 0 & 0 & 0 & 0 & 0 \\ 0 & 0 & 0 & 0 & (1-s) & (1+s) & 0 & 0 \end{bmatrix} \quad (56)$$

$$\Phi_r\Big|_{t=-1} = \bar{\Phi}_r = \begin{bmatrix} (1-s^2) & 0 & 0 & 0 \\ 0 & 0 & (1-s^2) & 0 \end{bmatrix} \quad (57)$$

The differential surface dS along the side 1-2 is given by:

$$dS = b\sqrt{\left(\frac{dx}{ds}\right)^2 + \left(\frac{dy}{ds}\right)^2}\, ds = b\ell_{12}\, ds \quad (58)$$

where ℓ_{12} is the length of side 1-2 and b is the element constant thickness.

The reduced equivalent nodal load vector is

$$\underset{\sim}{P} = \underset{\sim}{P}_q - K_{rq}^T K_{rr}^{-1} \underset{\sim}{P}_r \quad (59)$$

In the case when the incompatible modes of displacements are not used,

$$\underset{\sim}{P} = \underset{\sim}{P}_q \quad (60)$$

If, in addition, a set of concentrated loads are applied at the nodes, the final element load vector will be of the form:

$$\underset{\sim}{P} = \underset{q}{\underset{\sim}{P}} - K_{rq}^{T} K_{rr}^{-1} \underset{\sim}{P}_r + \underset{\sim}{P}_N \tag{61}$$

where $\underset{\sim}{P}_N$ is the vector of concentrated load at the nodes (or the static equivalent of a simple beam reactions of a distributed load between the nodes).

4.1.6 Element Stress Output

The element output stress vector is given by:

$$\underset{\sim}{\sigma} = E\,(\underset{\sim}{\epsilon} - \underset{\sim}{\epsilon}_0) \tag{62}$$

$$\underset{\sim}{\sigma}^T = \left[\sigma_x, \sigma_y, \tau_{xy}\right] \tag{63}$$

$\underset{\sim}{\epsilon}$ can be expressed as:

$$\underset{\sim}{\epsilon} = (B_q - K_{rr}^{-1} K_{rq})\,\underset{\sim}{q} + B_r K_{rr}^{-1} \underset{\sim}{P}_r \tag{64}$$

Hence, Equation (62) can be written as:

$$\underset{\sim}{\sigma} = E\,(B_q - K_{rr}^{-1} K_{rq})\,\underset{\sim}{q} + E(B_r K_{rr}^{-1} \underset{\sim}{P}_r - \underset{\sim}{\epsilon}_0) \tag{65}$$

Once the solution for the compatible nodal displacement vector q is obtained, the element stresses at some specified points in the element can be computed from Equation (65). Obviously, if the incompatible modes of displacement are not used, Equation (65) reduces simply to

$$\underset{\sim}{\sigma} = EB_q \underset{\sim}{q} - E\,\underset{\sim}{\epsilon}_0 \tag{66}$$

Here, $\underset{\sim}{\epsilon}_0$ is the initial strain vector which, if due to temperature changes, is given by either Equation (51) or (52).

4.1.7 Material Properties

The overlay structure is assumed to be a homogeneous and isotropic matrix; therefore, the elasticity matrix for plane stress condition is given by:

$$E = \frac{E_x}{1-\nu^2}\begin{bmatrix} 1 & \nu & 0 \\ & 1 & 0 \\ \text{symmetric} & & \frac{1-\nu}{2} \end{bmatrix} \tag{67}$$

and for plane strain condition is given by:

$$E = \frac{E_x(1-\nu)}{(1+\nu)(1-2\nu)}\begin{bmatrix} 1 & \frac{\nu}{1-\nu} & 0 \\ & 1 & 0 \\ \text{symmetric} & & \frac{1-2\nu}{2(1-\nu)} \end{bmatrix} \tag{68}$$

4.2 Fabric

The fabric in this computer model has been represented as a N-layered stripe (N = 0,1,...,4). Each layer could have individualorthotropic material properties, thicknesses and fabric lengths (see Figure 24).

With this model it is possible:

(1) To investigate the Fabric Effectiveness Factor (FEF) of the composite fabric structure.

(2) To model bond conditions between fabric and overlay or fabric and existing slab.

(3) To establish a necessary fabric length in the case of horizontal temperature change when fabric must act as a bond breaker to prevent thermal cracking of the overlay.

Finite elements used to approximate the fabric absolutely are identical to "overlay elements" with the exceptions that Equations (39) and (40) are applicable.

4.3 Existing Slabs

Existing slabs generally have the same finite element type as the overlay structure described above except for the elements used for modeling cracks. These elements have a very small elastic modulus in x,y,z directions and Poissons' ratio $\nu x = \nu y = \nu z = .47$. In other words they represent a crack(s) with no shear resistance.

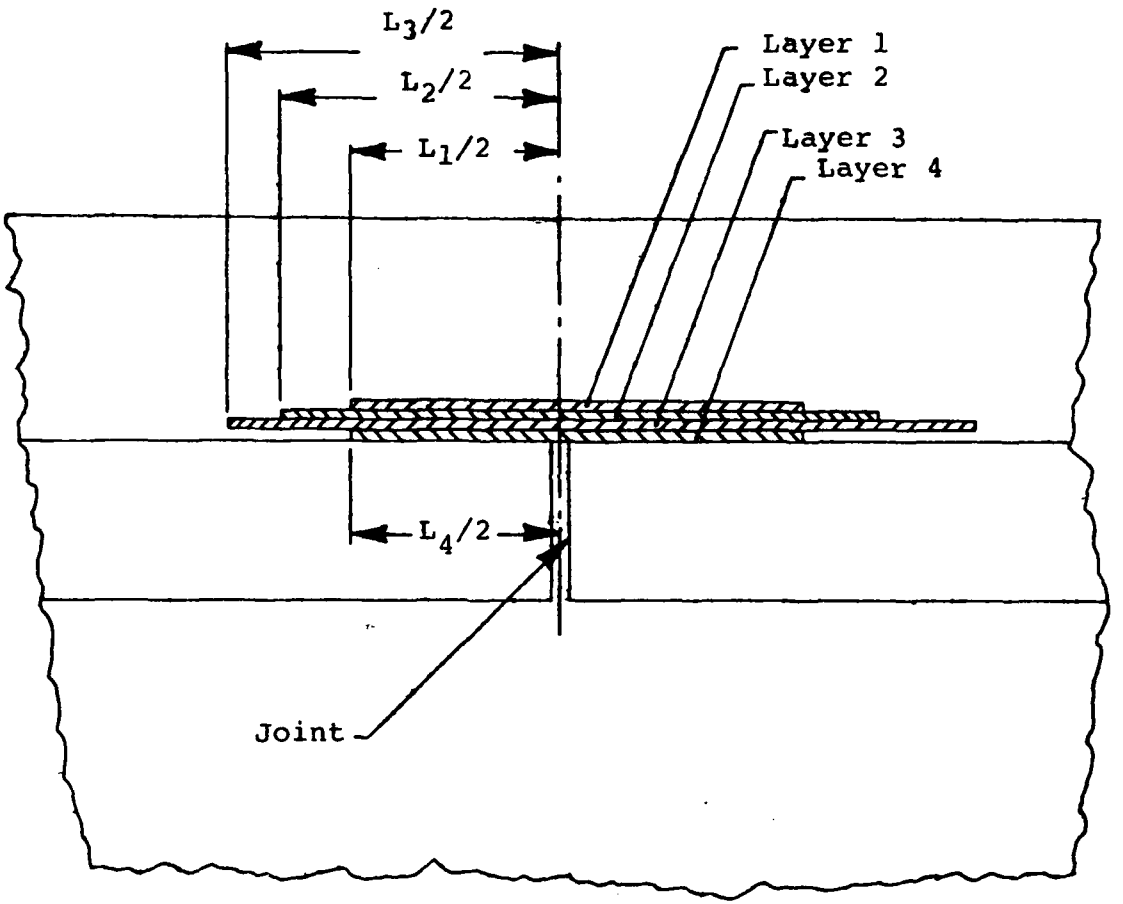

Figure 24. N-Layer Fabric Model

4.4 Slab-Foundation Contact Zone

The correct finite element model of this part of the OPF is extremely important in the case of a temperature load or a vertical mechanical load which can produce either a partial contact of the slab or a large horizontal displacement. Partial contact due to a void formation will be discussed later. Special "joint" elements are used in this model to achieve more realistic finite element approximation of the contact zone..

The joint element was first introduced by Goodman (18) as a finite element model representing joints and seams in the analysis of rock mass structures. The configuration of the joint element is as shown in Figure 25. It consists of a pair of straight lines with four nodal points. The element has zero width, a unit length, and a thickness b in the direction normal to the plane of the element (x-y plane). The nodal point pairs (1, 4) and (2,3) initially have identical coordinates.

The joint element is assumed to have essentially no resistance to a net tension in the direction normal to the sides 1-2 and 3-4, i.e., in the y' direction. It offers high resistance to compression in the y' direction and may deform somewhat under normal pressures, particularly if there are crushable irregularities or compressible filling materials. It also offers shear resistance in the x' direction under normal pressures. However, at no point within the element can the shear stresses exceed shear strength of the joint.

Linear displacements are assumed for the element. Let v' and u' be the displacements in the normal and the tangential directions of the element, respectively. Then the displacements along the top of the element can be expressed in terms of the local nodal displacements as:

$$\begin{Bmatrix} (u')_{top} \\ (v')_{top} \end{Bmatrix} = \frac{1}{2} \begin{bmatrix} t & s & 0 & 0 \\ 0 & 0 & t & s \end{bmatrix} \begin{Bmatrix} u'_3 \\ u'_4 \\ v'_3 \\ v'_4 \end{Bmatrix} \quad (69)$$

where $s = 1 - \frac{2x'}{\ell}$; $t = 1 + \frac{2x'}{\ell}$ (70)

Similarly, along the bottom of the element

$$\begin{Bmatrix} u' \\ \text{bottom} \\ v' \\ \text{bottom} \end{Bmatrix} = \frac{1}{2} \begin{bmatrix} s & t & 0 & 0 \\ 0 & 0 & s & t \end{bmatrix} \begin{Bmatrix} u'_1 \\ u'_2 \\ v'_1 \\ v'_2 \end{Bmatrix}$$

Next let Wn and Ws be the relative displacements between the top and bottom of the element in the normal and tangential directions. Hence, in view of Equations (69) and (71), the relative displacements are given by:

$$\underset{\sim}{w} = B\underset{\sim}{q}' \tag{72}$$

where

$$\underset{\sim}{w}^T = \begin{Bmatrix} w_s, w_n \end{Bmatrix} \tag{73}$$

$$\underset{\sim}{q}'^T = \begin{Bmatrix} u'_1, u'_2, u'_3, u'_4, v'_1, v'_2, v'_3, v'_4 \end{Bmatrix} \tag{74}$$

$$B = \frac{1}{2} \begin{bmatrix} -s & -t & t & s & 0 & 0 & 0 & 0 \\ 0 & 0 & 0 & 0 & -s & -t & t & s \end{bmatrix} \tag{75}$$

The local nodal displacements are related to the global nodal displacements by the transformation

$$\underset{\sim}{q}' = T_c \underset{\sim}{q} \tag{76}$$

where

$$\underset{\sim}{q}^T = \begin{Bmatrix} u_1, u_2, u_3, u_4, v_1, v_2, v_3, v_4 \end{Bmatrix} \tag{77}$$

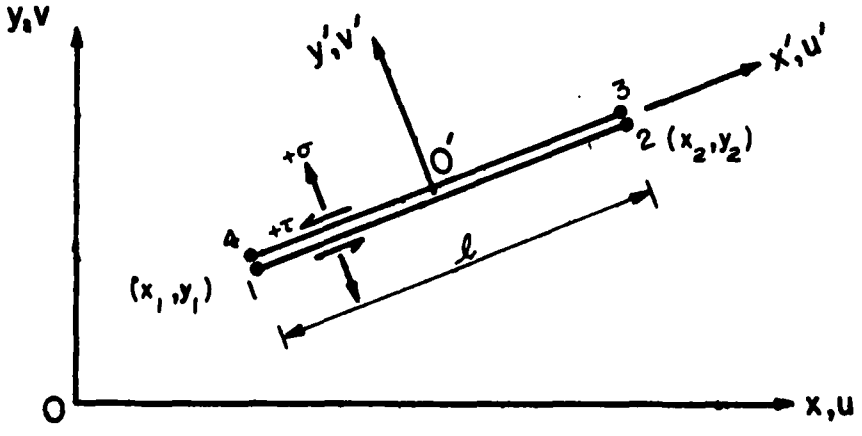

Fig. 25 A Joint Element in Local and Global Coordinates

$$T_c = \left[\begin{array}{c|c} T_{c_1} & T_{c_2} \\ \hline T_{c_3} & T_{c_4} \end{array}\right] \tag{78}$$

$$T_{c_1} = T_{c_4} = \begin{bmatrix} n_x & 0 & 0 & 0 \\ 0 & n_x & 0 & 0 \\ 0 & 0 & n_x & 0 \\ 0 & 0 & 0 & n_x \end{bmatrix} \tag{79}$$

$$T_{c_2} = T_{c_3} = \begin{bmatrix} n_y & 0 & 0 & 0 \\ 0 & n_y & 0 & 0 \\ 0 & 0 & n_y & 0 \\ 0 & 0 & 0 & n_y \end{bmatrix} \tag{80}$$

$$n_x = (x_2 - x_1)/\ell$$

$$n_y = (y_2 - y_1)/\ell \tag{81}$$

$$\ell = \sqrt{(x_2 - x_1)^2 + (y_2 - y_1)^2}$$

The element has a normal stiffness K_n and a shear stiffness K_S (both in F/L^3 units). The stresses at any point within the element are proportional to the relative displacements between the top and bottom of the element, i.e.,

$$\begin{Bmatrix} \tau \\ \sigma \end{Bmatrix} = \begin{bmatrix} k_s & 0 \\ 0 & k_n \end{bmatrix} \begin{Bmatrix} w_s \\ w_n \end{Bmatrix} \tag{82}$$

The element stiffness matrix in the global coordinate system is given by

$$k = b\, T_c^T \left(\int_{-\ell/2}^{\ell/2} B^T k\, B\, dx' \right) T_c \qquad (83)$$

with the displacement interpolation matrix B given by Equation (75) and the coordinate transformation matrix T_c given by Equation (78). The axial stiffness k in Equation (83) is replaced in this case by:

$$k = \begin{bmatrix} k_s & 0 \\ 0 & k_n \end{bmatrix} \qquad (84)$$

Substituting Equations (75) and (84) into Equation (83) and integrating over the element leads to

$$K = T_c^T\, K'\, T_c \qquad (85)$$

where K, is the global element stiffness matrix, and K' is the local element stiffness matrix given by:

$$K' = \frac{b\ell}{6} \left[\begin{array}{c|c} K'_{11} & 0 \\ \hline 0 & K'_{22} \end{array} \right] \qquad (86)$$

with

$$K'_{11} = k_s \begin{bmatrix} 2 & 1 & -1 & -2 \\ & 2 & -2 & -1 \\ & & 2 & 1 \\ \text{symetric} & & & 2 \end{bmatrix} \qquad (87)$$

$$K'_{22} = k_n \begin{bmatrix} 2 & 1 & -1 & -2 \\ & 2 & -2 & -1 \\ & & 2 & 1 \\ \text{symmetric} & & & 2 \end{bmatrix} \qquad (88)$$

The stress output can be computed from Equation (88) which, in view of Equation (84) and (85) can be written as:

$$\underline{\sigma} = k\, T_c\, \underline{q} \qquad (89)$$

where $$\underline{\sigma}^T = [\sigma, \tau] \qquad (90)$$

The corresponding equivalent nodal load vector is calculated from:

$$\underset{\sim}{P} = K \underset{\sim}{q} \tag{91}$$

where

$$\underset{\sim}{P}^T = \begin{bmatrix} P_{x1} & P_{x2} & P_{x3} & P_{x4} & P_{y1} & P_{y2} & P_{y3} & P_{y4} \end{bmatrix} \tag{92}$$

P_{x_i} and P_{y_i} are, respectively, the equivalent nodal load components in the x and y directions at node i.

The resulting shear stresses must be compared with the shear strength of the element. The shear strength at any point within the element is assumed to be of the form:

$$\tau_s = c + \sigma \tan\phi \tag{93}$$

where τ_s is the shear strength, c is the cohesion and ϕ is the angle of friction of the material, σ is the normal compressive stress at that particular point. The shear stresses at the nodal points are checked with the corresponding shear strength. If at any node the stress exceeds the shear strength, it is reduced to the shear strength value. The excess shear stress is used to compute the corresponding equivalent nodal loads and are applied back as a new load vector in the iteration procedure.

The element normal stresses are also checked for tension. If any nodal normal stress is tensile, the normal and shear stresses at that particular node are reduced to zero and the corresponding nodal loads are applied back as a new set of load vectors in the iteration procedure. The iteration process is repeated until all of the nodal normal stresses are essentially compressive and the nodal shear stresses do not exceed the nodal shear strength. The iteration scheme used is based upon the initial stress concept proposed by Zienkiewicz (19).

4.5 Elastic Foundation

A complete review of the State-of-the Art of existing models of the pavement foundations couple is presented in Chapter II of Reference [16]; Chapter III of the same reference discusses the model used in the RISC computer program development.

An identical procedure has been incorporated in this study, with corrections for a 2-dimensional space, i.e., all integrations by area in 3-dimensional case have been replaced by integration by line. In addition to elastic foundation support, the EFRON computer program provides, as an option, Winkler or rigid type of support. This option is provided so that the user can compare the results from the two different methods. It

should be emphasized that Winkler foundation is not a reasonable representation of a real foundation and should not be used in general.

An initial void could be assumed under existing slab, as shown in Figure 26. In a finite element model, a void is reflected by replacing with zero all diagonal and off-diagonal terms of the fully populated stiffness matrix of the foundation which correspond to the nodal points out of contact, eg. (94).

$$K_F = \begin{bmatrix} k_{11} & \cdots & \cdots & \cdots & 0 & 0 & 0 & \cdots & k_{1N} \\ \cdots & \cdots & \cdots & \cdots & 0 & 0 & 0 & \cdots & k_{2N} \\ & & \cdots & \cdots & 0 & 0 & 0 & \cdots & \cdots \\ & & & k_{\ell\ell} & 0 & 0 & 0 & \cdots & k_{\ell N} \\ & & & & 0 & 0 & 0 & 0 & 0 \\ & & & & & 0 & 0 & 0 & 0 \\ & & & & & & 0 & 0 & 0 \\ & & & & & & & k_{mm} & k_{mN} \\ & & & & & & & & k_{NN} \end{bmatrix}$$

where K = stiffness matrix of the foundation
N = number of nodal points along the slab(s)

4.6 Joint Structure

Doweled or plain joints can be presented in finite element model, as shown in Figure 27.

Joint space is represented in the model by a set of rectangular elements with very low elastic moduli in all directions. The dowel bar, if it exists, is approximated by one of the three types of elements indicated below:

1. Type 1 elements correspond to an actual body of the dowel bar and is represented by element type described in Section 2.1 with elastic modulus E_e computed from:

$$E_{D.B.}\frac{\pi^4 D_{D.B}}{64} = E_e \frac{b_e h_e^3}{12}$$

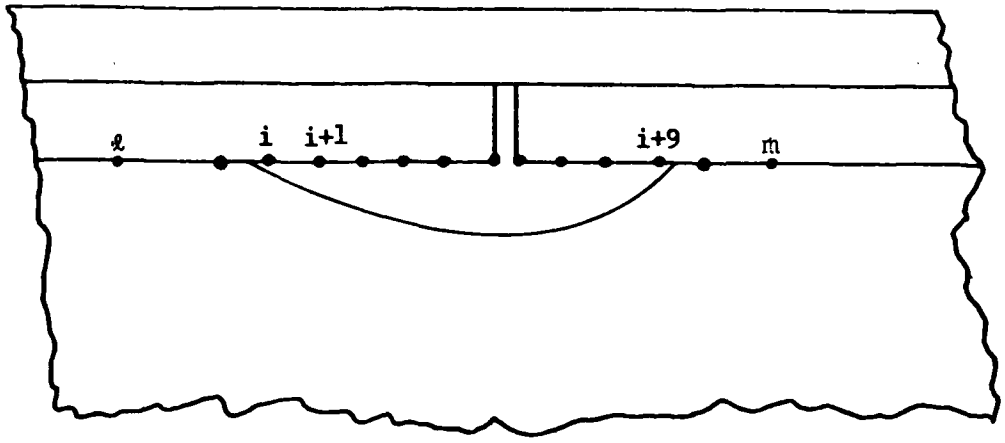

Figure 26. Void Under Existing Slab

$$D_{D.B.} = h_e$$

where

$E_{D.B.}$ = Elastic modulus of the dowel bar
$D_{D.B.}$ = Dowel bar diameter
h_e = Elements height
b_e = Elements width

2. Type 2 and 3 elements actually model the horizontal degrees of freedom of the dowel bar. These elements have a very low horizontal elastic modulus E . In addition to that, the type 2 element has a very low shear modulus G.

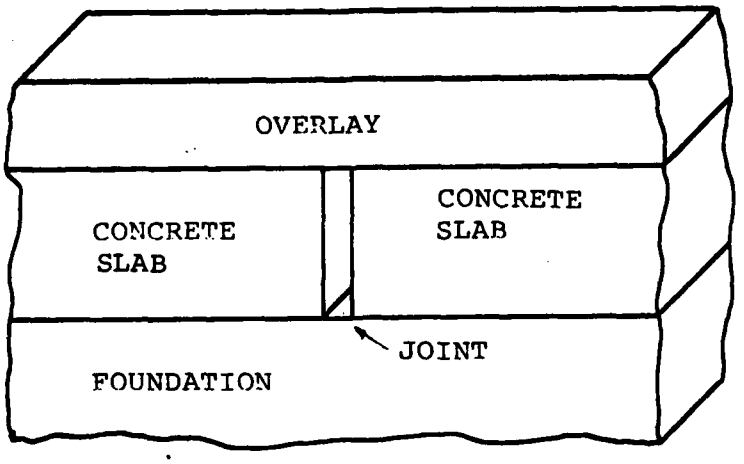

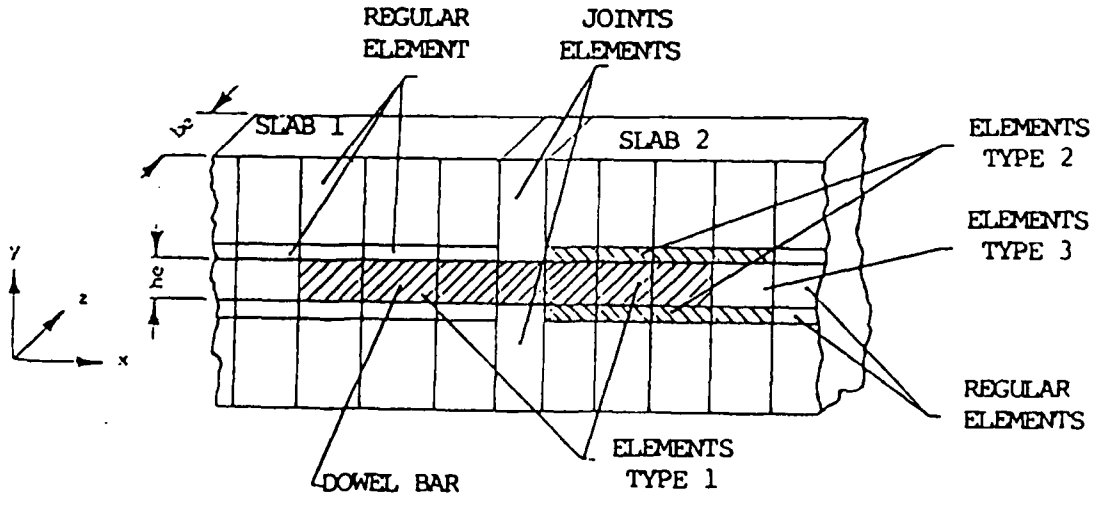

Figure 27. Finite element representation of plain and doweled joints.

The major reason for such a complicated model of the dowel bar is to transfer bending moment from slab to slab. This would not be possible in any other finite element model using bar or beam types of elements because of the existence of only two degrees of freedom in each nodal point of the 2-dimensional element.

To incorporate dowel bar looseness, an effective (reduced) dowel bar diameter is used, which can be calculated from

$$D' = D_{D.B.} [1-10.5L-12.58L^{.7} \log(E_s/1000)] \quad (97)$$

where

D' = Effective dowel bar diameter
$D_{D.B.}$ = Actual dowel bar diameter
L = Amount of looseness (inches)
E_S = Subgrade modulus (PSI)

This equation is a result of the parametric study described in Chapter III of Reference (16).

4.7 Cracks

A finite element model of the crack(s) is absolutely identical to a plain joint model described above. Up to ten different cracks could be included in a single problem. The crack pattern is not necessary nor does it have to be identical for both slabs if vertical load is present. However for a horizontal temperature load an identical crack pattern must be used if cracks are present.

CHAPTER V. LABORATORY TESTING

5.1. Types of Testing

This study is concerned with the evaluation of the cracking resistance of the fabric reinforced asphalt concrete overlays of rigid (portland cement concrete) pavement. In order to evaluate the cracking resistance of the fabric reinforced system, tests were conducted under the following conditions at two temperatures:

1. Fatigue resistance under load of asphalt overlays over concrete bases for both control and fabric reinforced conditions. Control conditions are conventional overlays without fabric reinforcement.

2. Horizontal and vertical temperature induced stresses: test condition for both control and fabric reinforced overlays.

The beam testing simulates full scale flexible pavement overlay behavior under aircraft load as experienced in runways and taxiways. Figure 28 illustrates the concept for an overlay condition. Fabric reinforcement involves placement of an engineering fabric or geotextile underneath the asphalt overlay. The purpose of fabric reinforcement is to enhance the fatigue crack resistance of the bound layer. Simulation of reflective cracking of rigid pavement overlays requires modeling of both thermal and traffic loading conditions. Thermal stresses result from both seasonal and daily changes in slab temperature. The thermal loading can be represented by the superposition of two different thermal conditions as was discussed in Section 3.2.

a. Uniform change in slab temperature: this condition represents the seasonal changes in average slab temperature which occur over long periods of time.

b. Pure curling condition: daily, or short time period, temperature variation within the slab. For pure curling the average slab temperature remains unchanged but the upper surface of the slab is at a different temperature from the lower surface, with the temperature assumed to be linearly related to the slab depth.

Manufacturing full scale pavement models and subjecting them to actual thermal loads experienced in the field is neither economically feasible nor possible given the time constraints of this study. Therefore model pavements with external forces applied to produce joint movements equal to those of full scale pavements under field thermal loading were designed. Uniform

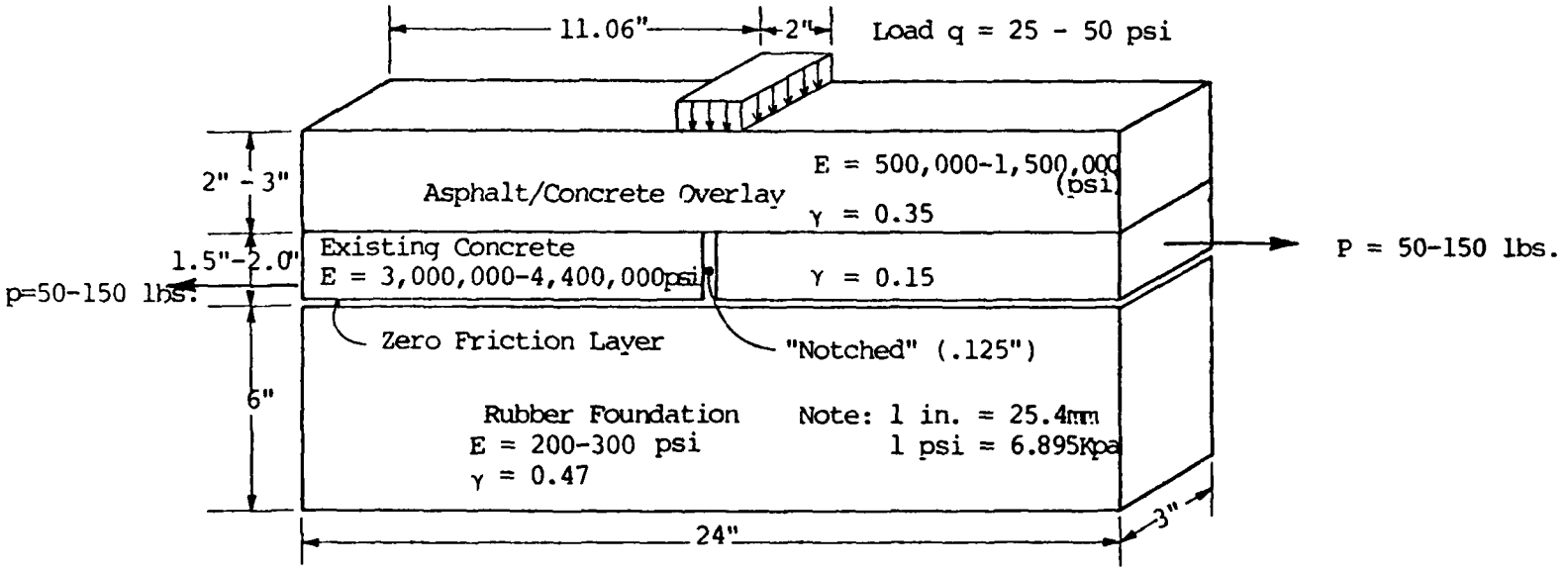

Figure 28. Laboratory Simulation of Overlaid Concrete Pavement.

seasonal reduction in slab temperature was simulated by applying horizontal tensile forces to the PCC slab pavements. Traffic forces were simulated by applying dynamic vertical loads to the model which was a beam supported on an elastic foundation.

5.2 Fabric Selection

Three types of engineering fabric membranes were selected for this study and a fourth type of membrane is currently being evaluated. The test results of this material will be included in the final report at the end of all work. The three fabrics were selected to represent typical fabrics with low, medium, and high tensile moduli. The pertinent fabric properties are listed in Table 1.

5.3 Mix Design

A brief report on the mix design of concrete used for rigid base, and mix design used for asphalt overlays are detailed in the following sections:

5.3.1 Cement Concrete Beams

Two different sizes of aggregates from the local American Aggregate Company were utilized for the manufacture of cement concrete beam specimens. The aggregates used were #57 crushed gravel as coarse aggregate and natural sand as fine aggregate. The aggregate gradation limits were in accordance with FAA specifications (401), actual gradation chosen for preparing the mix design is shown in Figure 29. The quantities of the constituents of concrete, namely coarse and fine aggregate, cement and water, were chosen as per FAA specifications for Class C concrete after making necessary adjustments for water absorbed by the dry aggregate, and for the net water requirement of concrete due to presence of water in the polymer additive. The polymer additive used was supplied by Dow Chemical Company and the quantity used was 10 gallons of additive per cubic yard of concrete. The calculated mixture preparations were checked by means of trial batches. The quantities by weight of the several constituents of regular concrete are indicated in Table 2. The slump selected was three inches, entrained air 4.5% and water cement ratio of 0.45. The procedures delineated in ASTM C-192 were strictly followed for making and curing beam specimens of concrete in the laboratory. Molds used for casting beam specimens were made out of sawed wood. Molds were water-tight during use, as judged by their ability to hold water. Beam molds were rectangular in shape and of the dimensions required to produce the stipulated specimens. Curing of concrete specimens was performed as per ASTM C-192. After the required period of curing, the beam specimens were sawed with a diamond blade saw to get specimens of the following sizes:

(1) 1.5 x 3 x 12 in (38 x 76 x 305 mm)

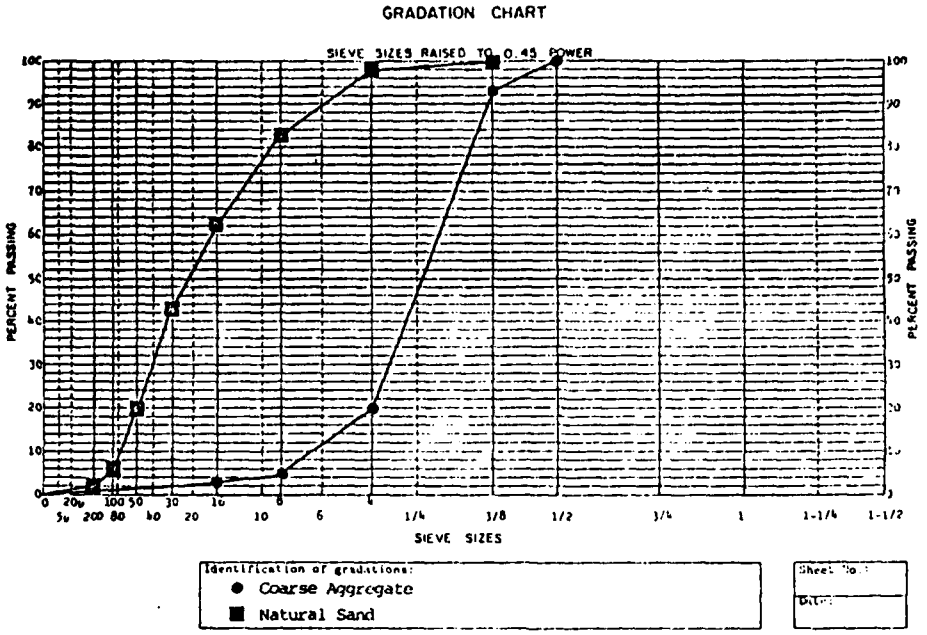

Figure 29A. Gradation of Concrete Aggregate

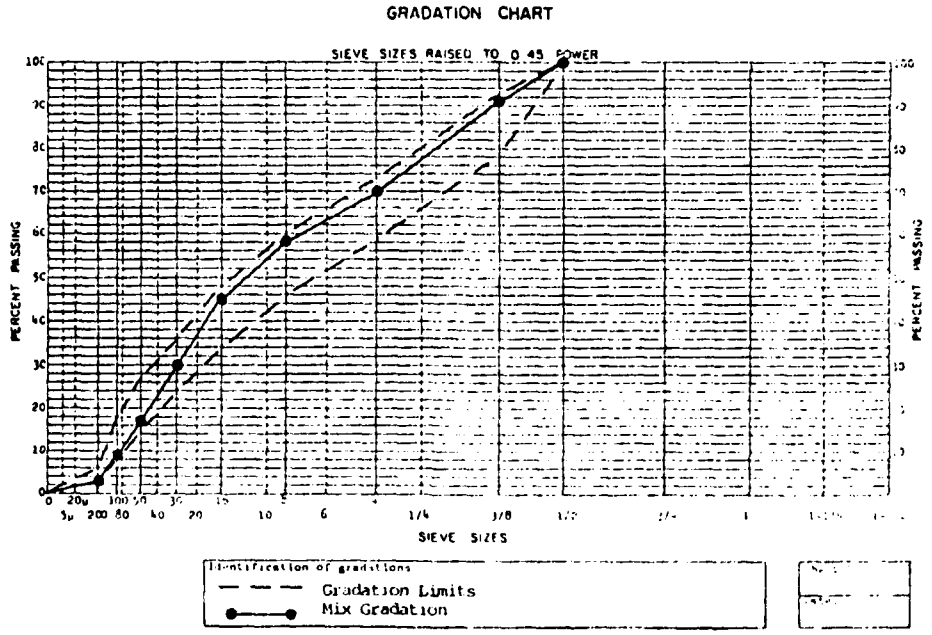

Figure 29B. Gradation of P-401 Asphalt Concrete Mix

TABLE 1

FABRIC PROPERTIES

PROPERTY	FABRIC B	FABRIC C	FABRIC D	TEST METHOD
Weight (oz)	3.8	5.4	3	
Modulus (psi)	NA	NA	850	ASTM D 1682
Tensile Strength (lbs)	90	90	90	ASTM D 1682
Elongation (percent)	55	55	55	ASTM D 1682
Burst Strength (psi)	NA	230	NA	Mullen Burst Test
Asphalt Retention (gsy)	0.20	0.18	0.07	Texas DOT-3099
Shrinkage	NA	<2	.3	Texas DOT-3099

@ Furnished by manufacturer

NA = Not available from manufacturer
1 oz = 0.028 kg
1 lb = 0.454 kg
1 psi = 6.894 kPa

1 gsy = 4.527 lit./m^2

TABLE 2

POLYMER CONCRETE MIX DATA

Cement Content	= 658 lb/C.Y.	
Coarse Aggregate	= 1737 lb/C.Y.	(#57 Gravel)
Absorption	= 1.2%	
Specific Gravity	= 2.64	
Fine Aggregate	= 1107 lb/C.Y.	(natural sand)
Absorption	= 2.7%	
Specific Gravity	= 2.50	
Water/Cement Ratio	= .40	
Polymer Additive	= 10 gal./C.Y.	(manufactured by Dow Chemical Co.)
Percent Entrained Air	= 4.0	
Slump	= 3"	
Compressive Strength (28 days)	= 4800 psi	

TABLE 2A

AGGREGATE GRADATION LIMITS			
#57 Lime Stone		Natural Sand	
Sieve Size	% Passing	Sieve Size	% Passing
1/2"	100	3/8"	100
1"	95-100	#4	95-100
1/2"	25-60	#8	70-100
#4	0-10	#16	45-80
#8	0-5	#30	25-60
		#50	5-30
		#100	1-10
		#200	0-4

(2) 2 x 3 x 12 in (51 x 76 x 305 mm)

5.3.2 Asphalt Concrete

Two different sizes of crushed limestone aggregates from the local American Aggregate Company were utilized for the manufacture of asphalt concrete specimens. The aggregates used were #8 crushed limestone as coarse aggregate, and limestone dust as fine aggregate. The #8 crushed aggregate generally showed sharp, angular, and gritty particles, and, for the most part, contained at least one fractured face in the particles, and were reasonably free from excessive dust or other deleterious coatings, weathered pieces, or excessive flaky and/or elongated pieces. Measured water absorption of particle size ranged from between 2.9% and 3.2%. Aggregate gradation conformed to FAA specifications for asphalt concrete surface course. Gradation ranges of the #8 crushed aggregate, based on frequent samplings, are shown in Table 3. Asphalt cement (AC-20) used in this investigation was obtained from Chevron Asphalt Company. Table 2A gives details about the aggregate gradation of #57 limestone aggregate and natural sand, used in development of P-401 mix. Design of aggregate blends for this investigations is based on:

i) Raw material aggregates and their individual gradings

ii) General conformance with FAA specifications for P-401 mix

For mix design and investigation, five levels of binder were used, namely: 5.5, 6, 6.5, 7, and 7.5% by weight of total mix.

The optimum asphalt content for the selected aggregate gradation was determined using Marshall design procedures and 75 blows/face compaction efforts. Optimum asphalt content was determined as the average of asphalt content for optimum stability, density, and 4% air voids. Figure 30 shows the Marshall mix design properties for this mix.

5.4 Sample Preparation

The test specimens for testing were of the following types:

(1) 1.5 in (38 mm) thick base cement concrete beam, notched with teflon strip in the notch and overlaid with 2 in (51 mm) thick asphalt concrete. The concrete beam had tack coat with SS-1h at the rate of 0.15 gallons per squre yard. (0.68 liters per square meter)

(2) Same as above with three types of engineering fabric membrane placed on the tack coat, before the AC overlay

(3) Same as (1) but using 2 in (51 mm) thick cement concrete base

TABLE 3

GRADATION OF P-401 ASPHALTIC CONCRETE

Sieve Size	Percent Passing	FAA Gradation Limits
1/2"	100	100
3/8"	91	79-93
#4	70	59-73
#8	58	46-60
#16	45	34-48
#30	30	24-38
#50	17	15-27
#100	9	8-18
#200	3	3-6

Note: 1 in. = 25.4mm

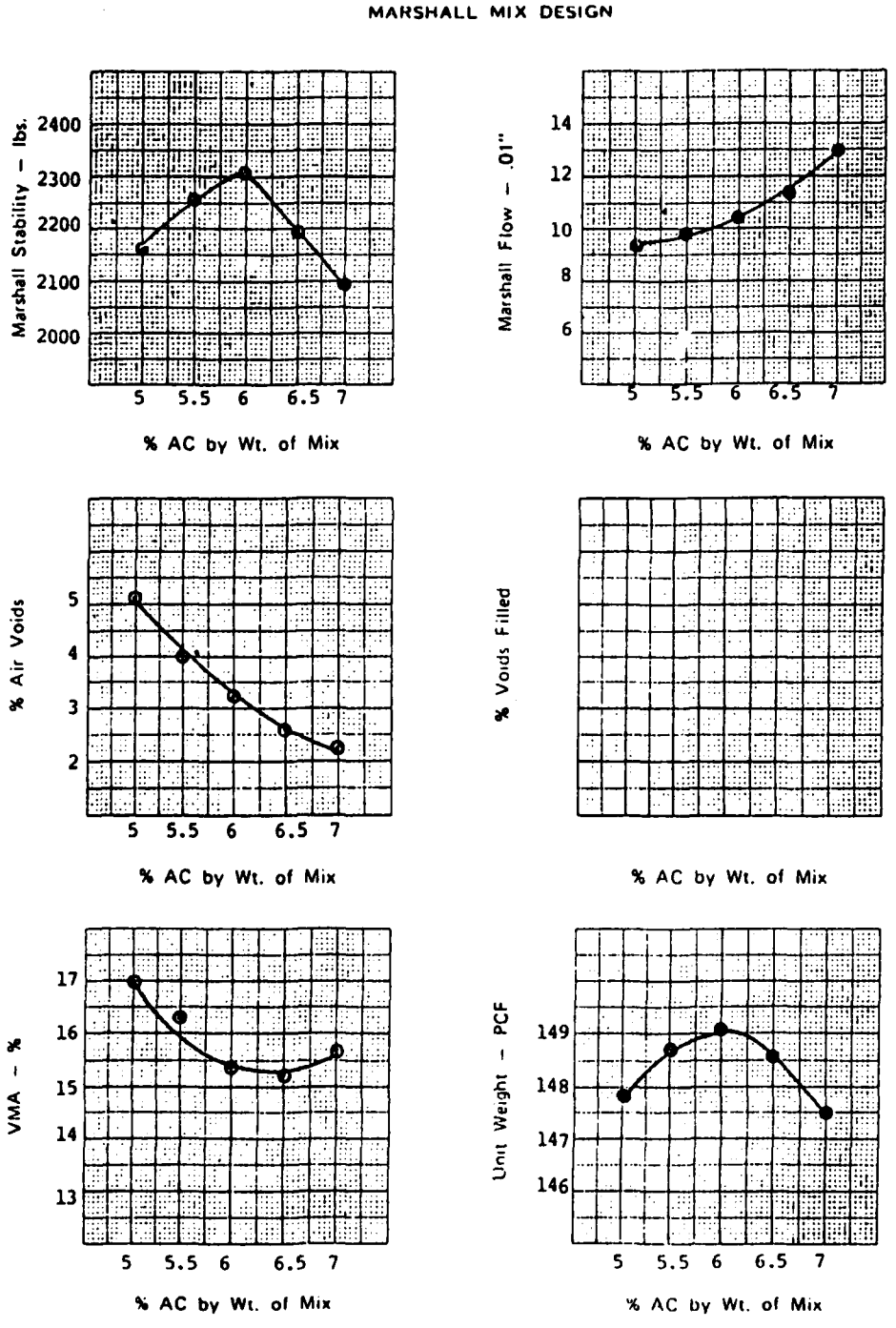

Figure 30. Marshall mix design data for P-401

(4) Same as (2) above but using 3 in (76 mm) thick overlay

(5) Same as (1) and (3) above but with 3 in (76 mm) thick overlay

(6) Same as (1) but with 1 in (75 mm) A.C. base instead of cement concrete

(7) Same as (6) above, but with a 3 in (76 mm) overlay

For the fabric reinforced beams, the lower part of the specimen was first manufactured with concrete as a beam of size 1.5 x 3 x 2 in (38 x 76 x 610 mm) and then sawed into two parts. Tack coat with SS-1h was applied over the concrete beam and then the fabric membrane was placed over the sticky tack coat material. Care was taken to maintain a 1/8 in (3 mm) separation between the saw-cut pieces during fabric placement.

After the placement of fabric on the top of tack coated base beam the fabric surface was smoothly brushed to bring it into complete contact with the binder. The base beam with tack coat and the fabric thus prepared was placed in a beam mold and a weighed quantity of hot mix poured over the beam. A wire comb was passed through the loose material back and forth for even distribution of the mixture in the mold. The mixture in the mold was pressed under steadily increasing load until the asphaltic mixture was compacted to desired thickness rather than specific load to insure that desired density would be achieved. The mold was then dismantled and the specimen was placed on a stiff support, such as a piece of wood or steel, to await testing. All precautions were taken to prevent bending and any possible damage to the beam sample prior to the testing. The compacted test specimen was allowed to cool at room temperature for a minimum of 24 hours prior to testing.

5.5 Laboratory Testing

5.5.1 Fatigue Testing

The fatigue experiments were conducted using a beam on elastic foundation with geometry as shown in Figure 28. The selection of this experimental set-up was based on a two-dimensional modeling of pavement structure in which a beam representing the pavement is supported on an elastic foundation representing the subgrade. The dimensions of the beam and foundation, as well as the stiffness of foundation, are selected with consideration to simulating the stress and strain at the bottom of a pavement structure subjected to traffic loading. The test set-up is the same as previously used by Resource International Inc. and researchers at Ohio State University to study the fatigue properties of asphaltic mixtures. The fatigue tests were performed using a dynamic load function of haversine shape. An MTS electro-hydraulic testing system was used to

generate the load factor. To insure complete recovery of the sample before the next load cycle, a rest period of 0.4 seconds was allowed between each load application. The duration of load application in all tests was kept constant at 0.1 seconds. Fatigue test data of samples tested at 40 and 72 degrees F (4 and 22 degrees C) and at different stress levels are presented in Appendix A.

5.5.2 Horizontal and Vertical Stresses

The test set up is shown schematically in Figure 28 and pictorially in Figure 31. A constant horizontal pull was applied and the crack development in the asphalt overlay was measured with a micrometer guage. Tests were conducted until the crack developed fully in the asphalt overlay. Test temperatures were 40 and 72 degrees F (4 and 22 degrees C). Test results are shown in Appendix B.

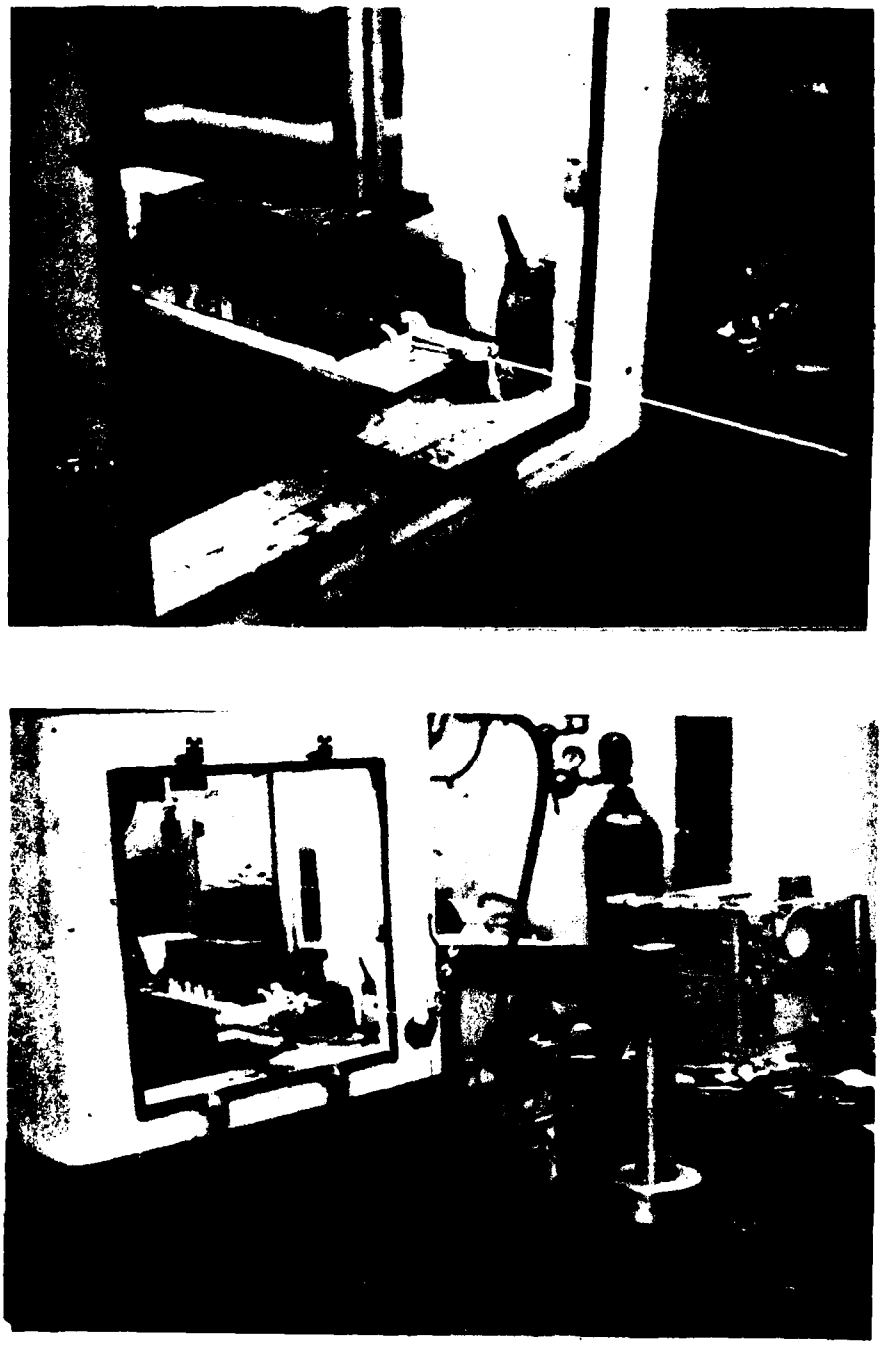

Figure 31. Test setup for simulated thermal loads

CHAPTER VI
DATA ANALYSIS

6.1 Fatigue Tests

The fatigue testing of the laboratory beams was conducted under controlled applied load conditions. Fatigue analysis, however, requires the determination of critical tensile strain in the asphaltic concrete and relating this strain to the allowable number of load applications, i.e., the fatigue response is given by

$$N_f = A\epsilon^{-B} \qquad (99)$$

where

N_f is the number of load applications to failure
ϵ is the critical tensile strain
A,B are material constants that depend also on temperature

The fundamental assumption of mechanistic stress/strain analysis is that Equation 99 can be used to describe the fatigue behavior of a particular material when the critical tensile strain is known, independent of how that strain is developed. All that is required is to determine the material constants (A, B in Equation 99) from some simple laboratory test, and, of course, the critical strain in the structure to be analized.

The analysis model described in Chapter IV is proposed as the analysis method to determine the critical strains resulting from loading.

The laboratory test data serves a two fold purpose in this study:

(a) to determine the material properties A, B in Equation 99

(b) to verify the stress/strain analysis model

The latter objective is the reason for the variety of conditions used in fatigue testing.

As was described in the previous chapter, control beams

(standard asphaltic concrete overlays) were tested under the following conditions:

(1) variable load
(2) variable thickness
(3) variable existing pavement

The significance of the latter is that stress/strain concentrations above the crack are a function of the existing layer properties, i.e., the concentration is more severe over a cracked concrete pavement than over a cracked asphaltic pavement.

The test data for the control beams at 72 degrees F (22 degrees C) is shown in Figure 32. The critical strains have been determined using the EFRON program described in Chapter IV. As can be seen from this figure, the regression equation fits the data points very well. There is some scatter in this data however, the correlation coefficient (R-square) for this data is 0.95 with a standard error of estimate (in terms of log Nf) of 0.125 - both values are better than generally reported for fatigue relationships where the only variable is applied load. The pertinent fatigue parameters are presented in Table 4.

The fatigue data for control beams at 40 degrees F (4 degrees C) is shown also in Figure 32. The variables for these sets were load and overlay thickness; the old pavement type was kept constant as concrete. It can again be seen that the analysis model explains the effect of the variables very satisfactorily.

The fatigue data for beams reinforced with the different fabrics are shown graphically in Figures 33 through 35 and summarized in Table 4. The test variables for these specimans were the same as for the control beams at 40 degrees F (4 degrees C), i.e., load and thickness were varied, but all overlays were over existing concrete pavements.

It should be noted that the slopes (the B value of Equation 99) of the fabric reinforced beams (indicated by dashed lines in Figures 33 through 35) are the same as the slopes (B values) obtained from regression analysis of the control beams. The fatigue data for the fabric-reinforced beams was analyzed assuming linear elastic response, i.e., that the stress and strain are proportional to applied load and that the material properties are independent of stress, as discussed in Chapter IV. Consequently, the fabric must behave in the same way in the system independent of the applied load/stress level.

Regression analysis of the fabric reinforced fatigue data indicates that the slopes at 72 degrees F (22 degrees C) are not drastically different from the control beam slope, but are substantially different at 40 degrees F (4 degrees C).

TABLE 4

FATIGUE PARAMETERS

	Temp	REGRESSION EQUATION A	B	R^2	SE	Assuming B = Constant A	B	SE
A	40	$2.59X10^{-12}$	4.425	.93	.143	$2.59X10^{-12}$	4.425	.143
B	40	$3.39X10^{-2}$	1.930	.85	.112	$2.30X10^{-10}$	4.425	.411
C	40	$1.02X10^{-2}$	2.109	.80	.143	$3.04X10^{-10}$	4.425	.423
D	40	$5.38X10^{-4}$	2.436	.74	.173	$2.22X10^{-10}$	4.425	.384
A	72	$1.26X10^{-11}$	4.558	.95	.125	$1.26X10^{-11}$	4.558	.125
B	72	$9.22X10^{-17}$	6.076	.89	.295	$4.19X10^{-11}$	4.558	.314
C	72	$4.83X10^{-5}$	2.579	.89	.136	$5.76X10^{-11}$	4.558	.366
D	72	$7.52X10^{-14}$	5.257	.94	.197	$7.33X10^{-11}$	4.558	.218

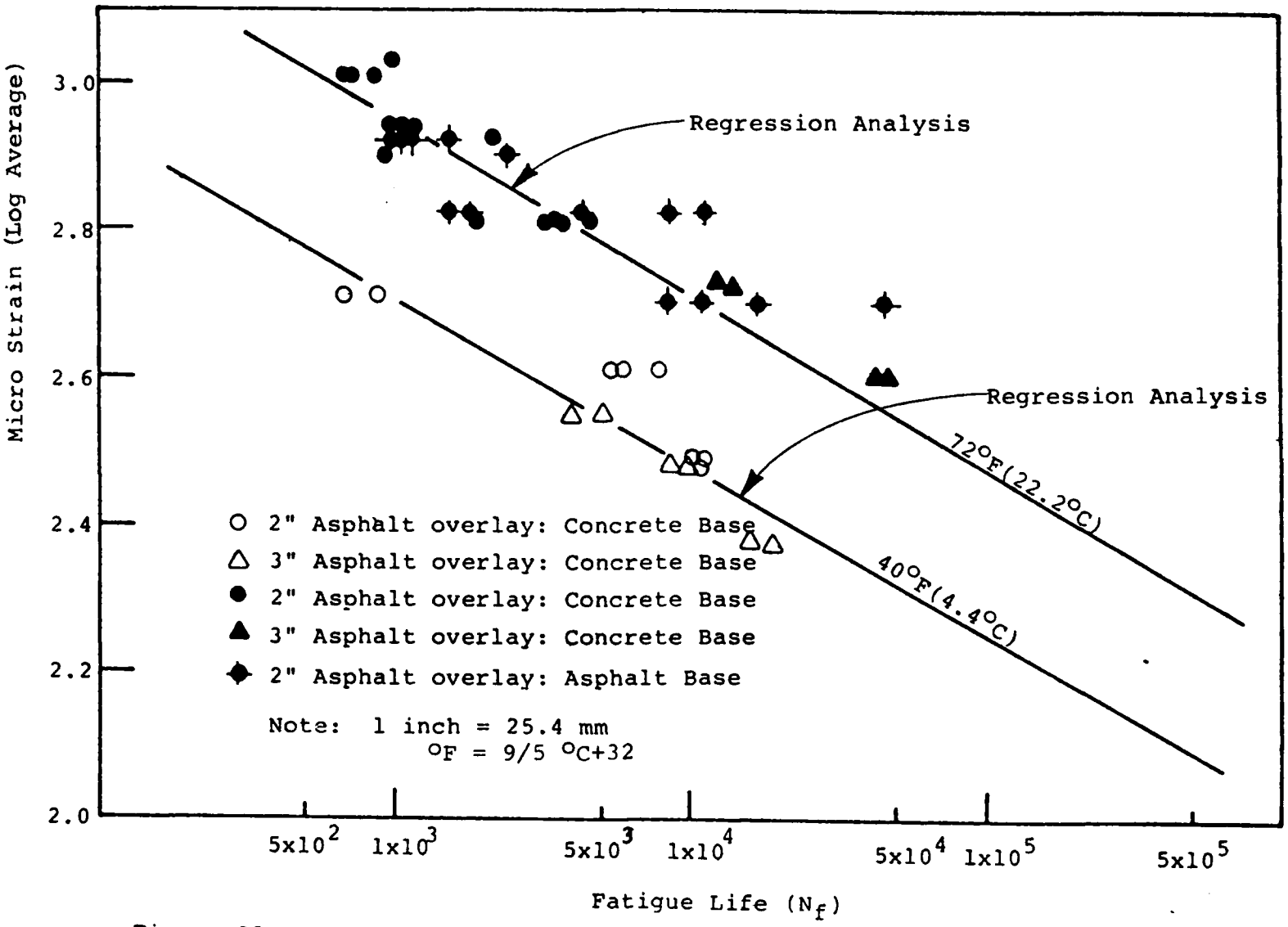

Figure 32. Laboratory Fatigue data for Treatment $\underline{\underline{A}}$ at 40°F and 72°F

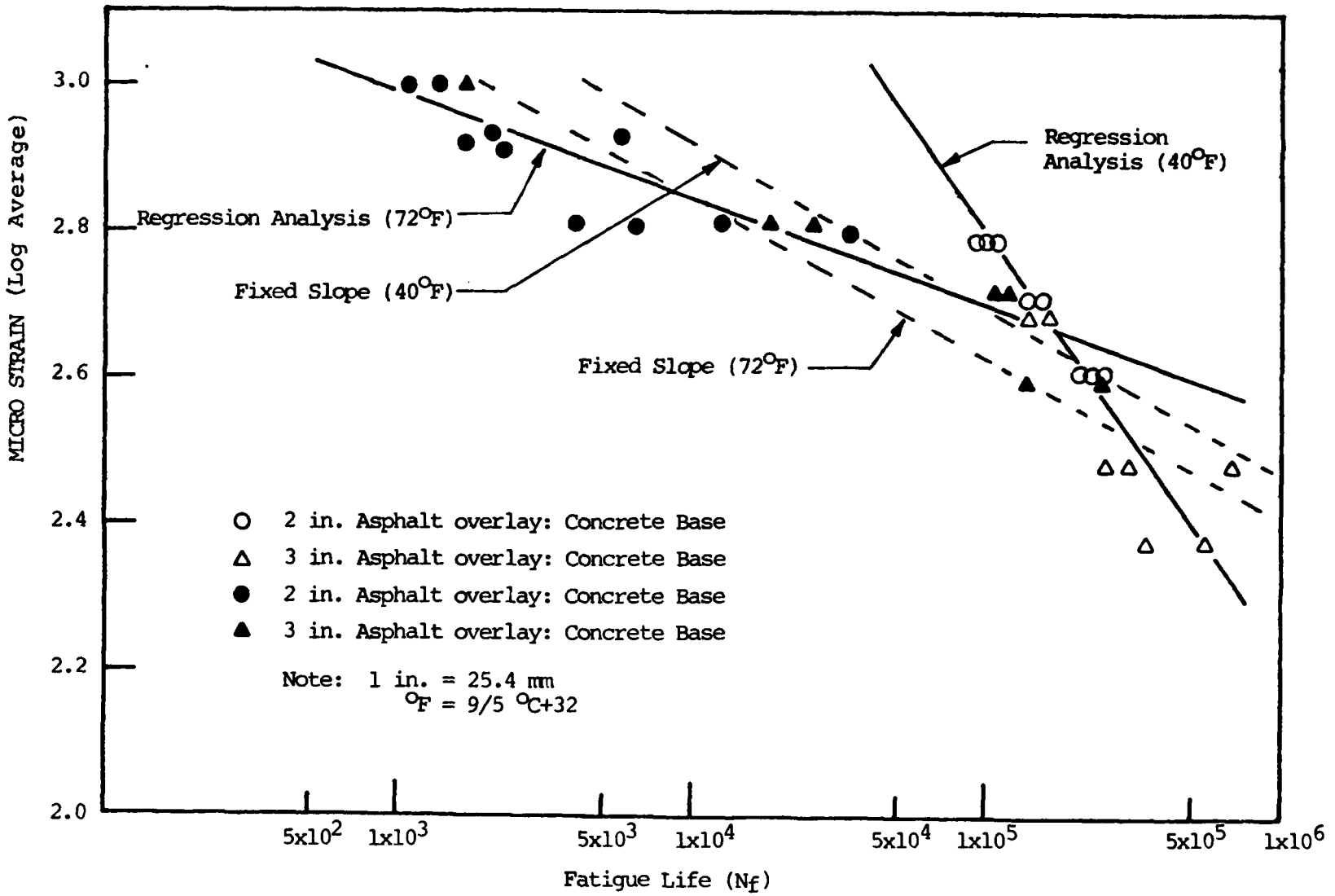

Figure 33. Laboratory fatigue data for treatment B at 40°F and 72°F

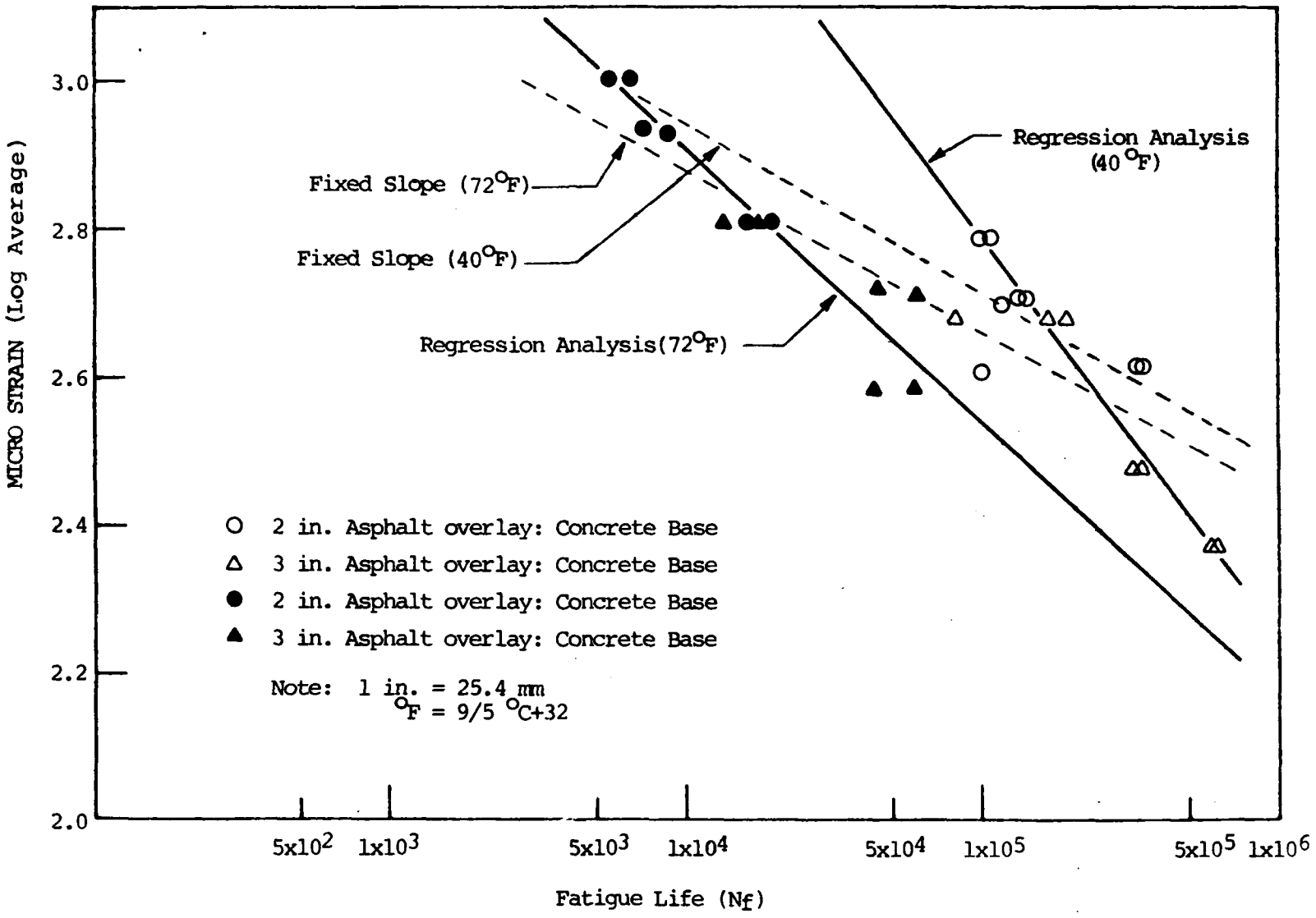

Figure 34. Laboratory fatigue data for treatment C at 40°F and 72°F

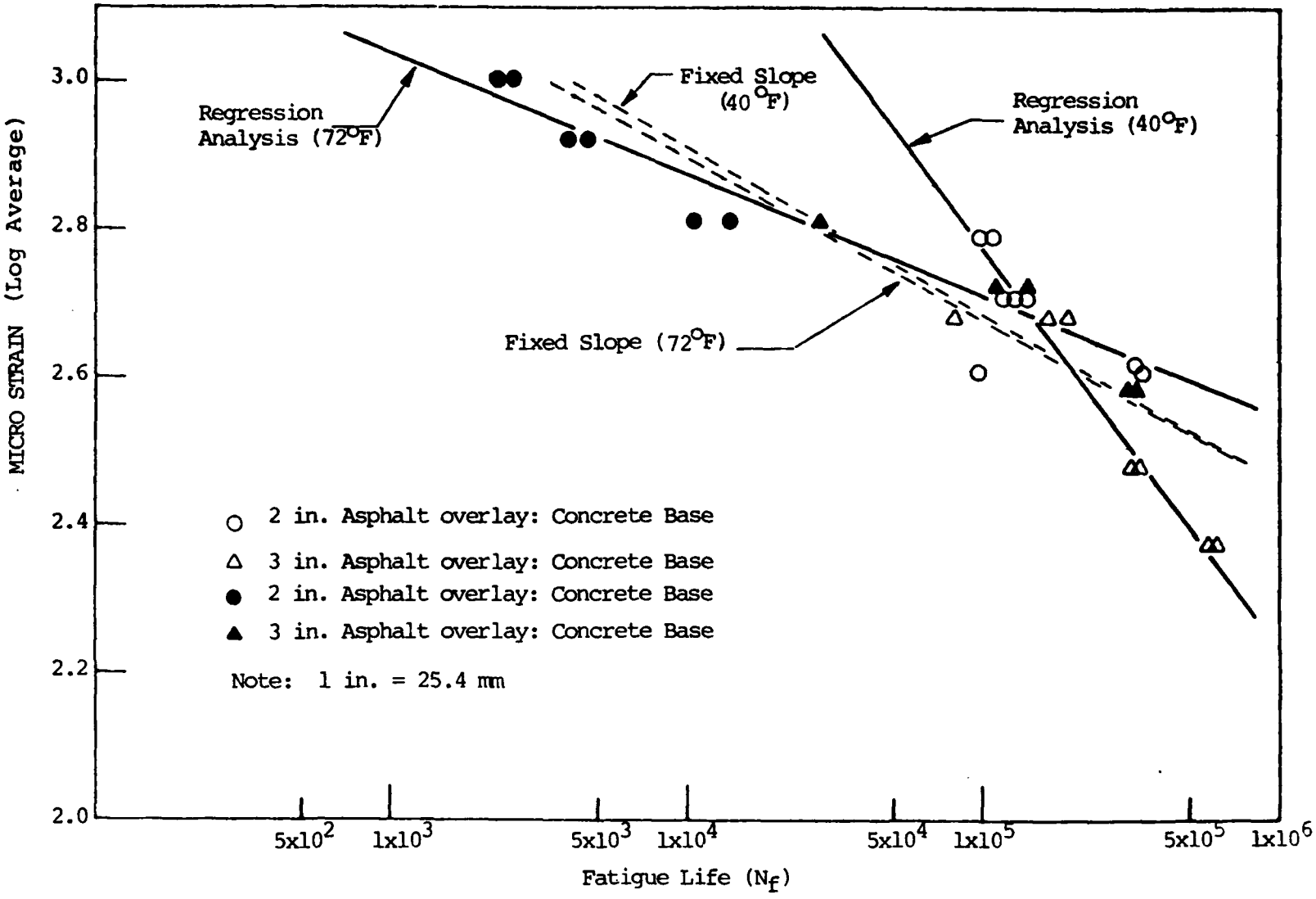

Figure 35. Laboratory fatigue data for treatment D at 40°F and 72°F

Thus, the assumption of linear elasticity are not entirely valid; however, non-linear elastic and/or elasto-plastic analysis is beyond the scope of this project. Furthermore, as is indicated by the standard error values in Table 4, the assumptions of linear elasticity do not increase the standard error values by much - the slight loss in precision is amply compensated by the great simplification in the analysis method.

Of course, the regression analysis results could be used in a phenomenological model to predict the fatigue response. The disadvantage of this approach is that fatigue response cannot be predicted from fabric properties alone but would require laboratory testing. However, the amount of testing is not extensive, and the improved confidence level in the predicted response may outweigh the disadvanatage.

The 40 and 72 degrees F (4 and 22 degrees C) test data are summarized in Figures 36 and 37, respectively. It is appparent from Figure 36 that fabric reinforcement has a significant beneficial effect at 40 degrees F (4 degrees C) but that the difference between fabrics is rather small. Figure 37 shows that the effect of fabrics on performance at 72 degrees F (22 degrees C) is not very great, nor is the difference between fabrics. The most probable explanation for this phenomenon is that although the off-the-shelf fabric properties are different among the various fabrics, the fabric-tack coat system properties are not that different. Furthermore, the in-situ fabric-tack coat system properties at 72 degrees F (22 degrees C) are not that different from asphaltic concrete properties, so that fabric effectiveness in relieving stresses is not great. At 40 degrees F (4 degrees C), however, the difference between fabric system and asphaltic concrete increases, leading to greater stress relief and fabric effectiveness.

6.2 Simulated Thermal Stress Tests

The test data using the procedure discussed in Section 5.2 is presented in Appendix B in graphical form. The fundamental objective of this test series was to establish the allowable joint opening at which failure (reflection cracking) begins, i.e., what is the critical allowable strain in the asphalt overlay, and how various factors, such as strain rate, mean temperaure, overlay thickness, reinforcement type, affect this value. The analysis of this data is on somewhat more uncertain grounds than the fatigue relationships since well-defined models for prediciting allowable critical strains are not available. The problems are complicated further by the fact that since asphaltic concrete is a viscoelastic material, loading rate is likely to influence the results. However, simulation of actual seasonal temperature effects is hardly practical since tests would have to be conducted over a several month period. Therefore, laboratory testing was conducted at loading rates that are representative of daily and weekly temperature cycles.

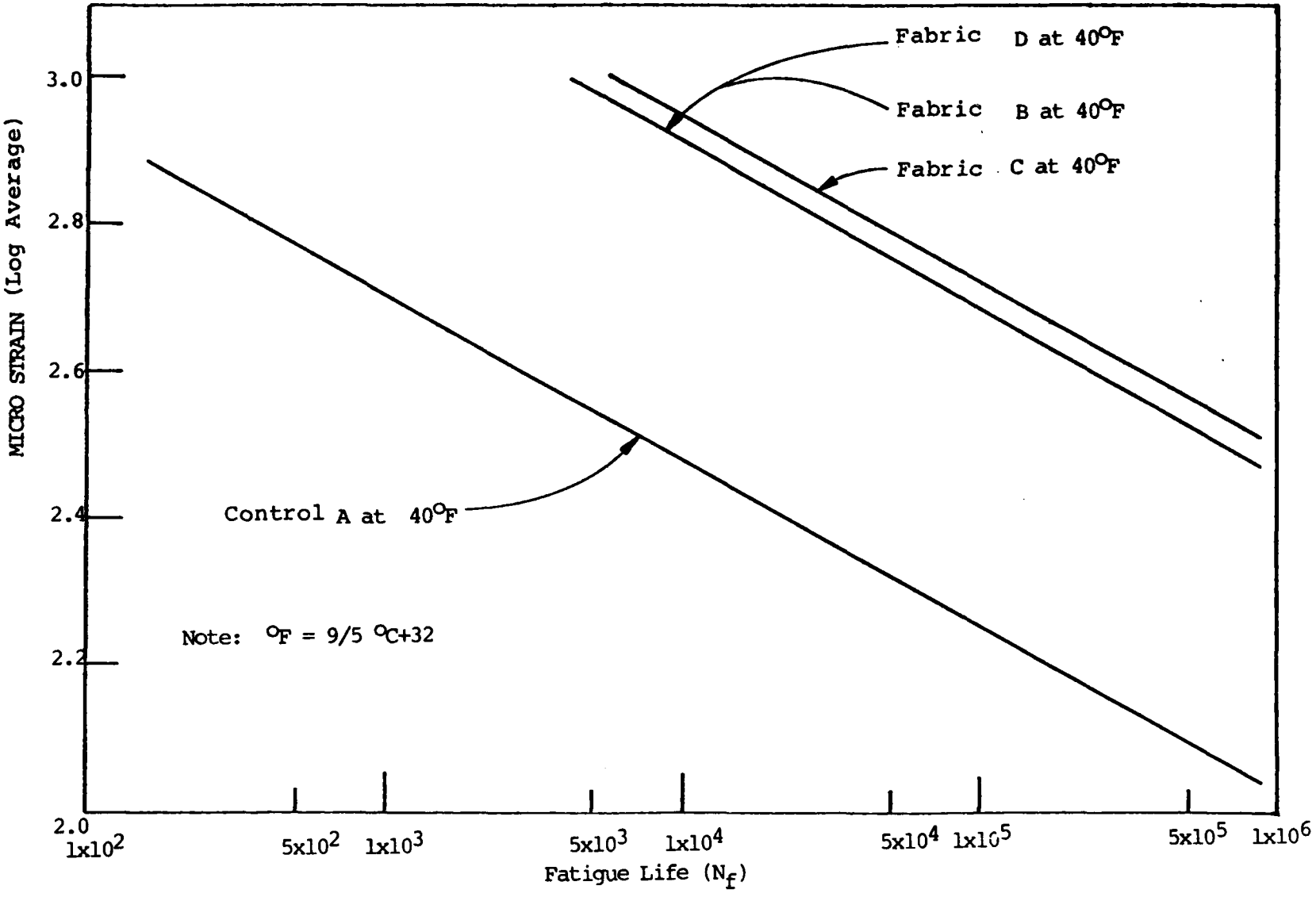

Figure 36. Laboratory fatigue data for fabrics A, B, C & D at fixed slope

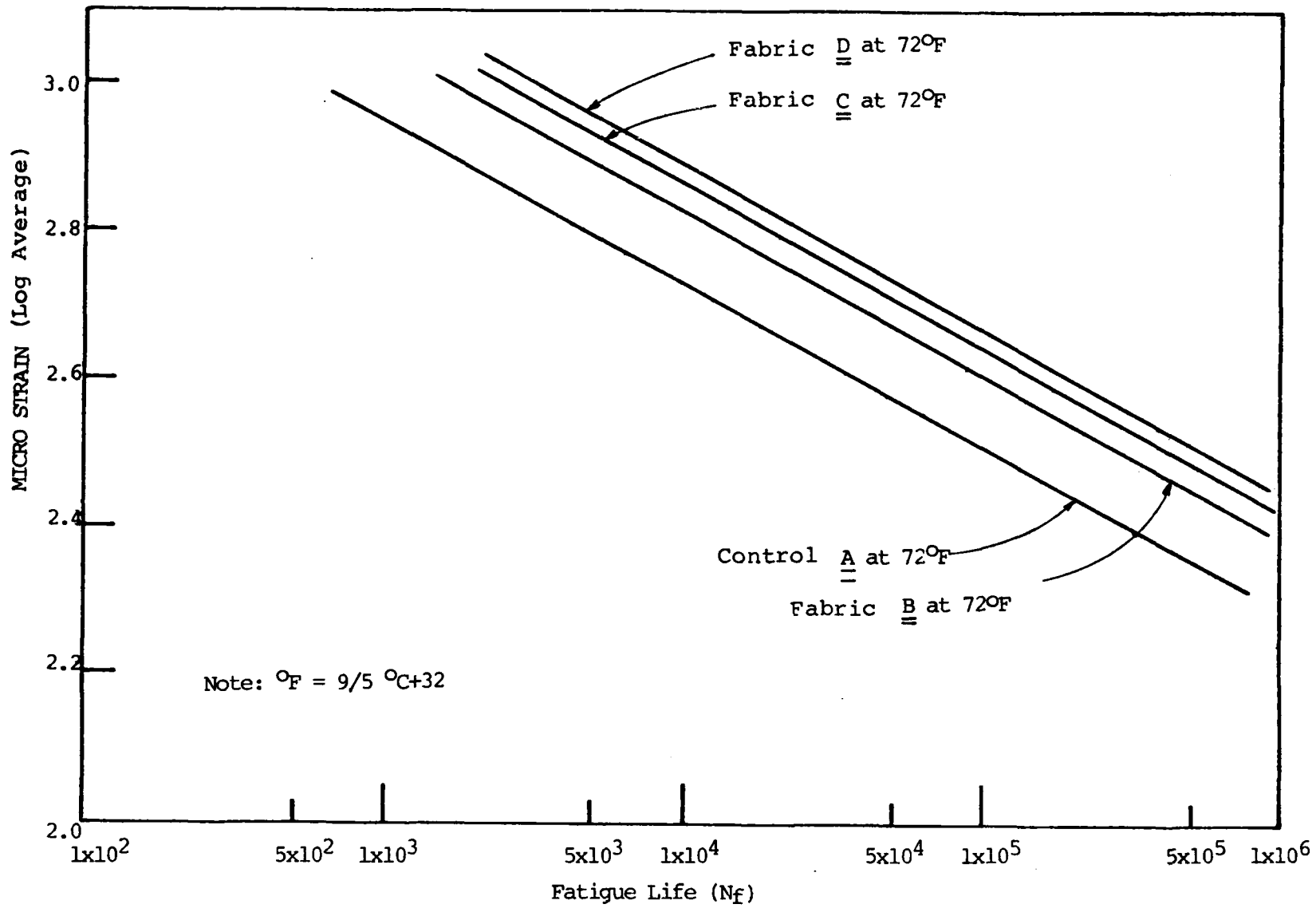

Figure 37. Laboratory fatigue data for control A, and Fabrics B, C & D at fixed slope

Figure 38 is more or less typical of the creep data obtained in this series of tests and shows the increase in joint opening as a function of time. This joint opening curve can be interpreted to consist of a linear (with time) and a non-linear portion, as shown in the above figure. The point at which the curve becomes non-linear can be interpreted as the maximum allowable joint opening for no cracking. Small cracks were observed on occasion at lower joint openings than the allowable value but for other tests cracks were not observed until the opening had exceeded the linear region, and in general the first observed crack occurred at openings near the critical value defined above.

Table 5 shows a summary of the test data for different treatments. The data presented in this table shows that for treatment A (control), there is very little difference in the allowable critical joint opening with thickness or with temperature. Figure 39 shows the results of a finite element analysis (using the EFRON program) of unreinforced overlays subjected to thermally induced joint openings. As can be seen from this figure, the overlay modulus has an insignificant effect on stresses below about 200,000 psi (1.4 MPa), and increasing the overlay thickness from 2 to 3 in (51 to 76mm) decreases stress by around 7 percent only. The reason that critical stress is insensitive to overlay thickness is that this stress is the result of stress concentration over the crack in the concrete rather than average stress in the overlay. Thus the measured data for the control beams agree quite well with the theoretical analysis.

The data in Table 5 shows also that reinforcement of the overlay with a fabric (Fabrics B, C, D) substantially increases the critical joint opening, and that the difference in performance between fabrics is not very significant. The same conclusion was reached also from the analysis of the fatigue data. The data for fabric C at 72 degrees F (22 degrees C) seems to indicate superior performance of this material. This data is suspect, however, since the bond between the concrete and the overlay failed on many specimens before any apparent damage to the overlay; the large joint opening most likely represents some slippage between the concrete and overlay.

AD-A147 199 MECHANISTIC METHODOLOGY FOR AIRPORT PAVEMENT DESIGN WITH ENGINEERING FABR..(U) RESOURCE INTERNATIONAL INC COLUMBUS OH K MAJIDZADEH ET AL. AUG 84 2/2

UNCLASSIFIED DOT/FAA/PM-84/9-1 DTFA01-81-C-10043 F/G 13/2 NL

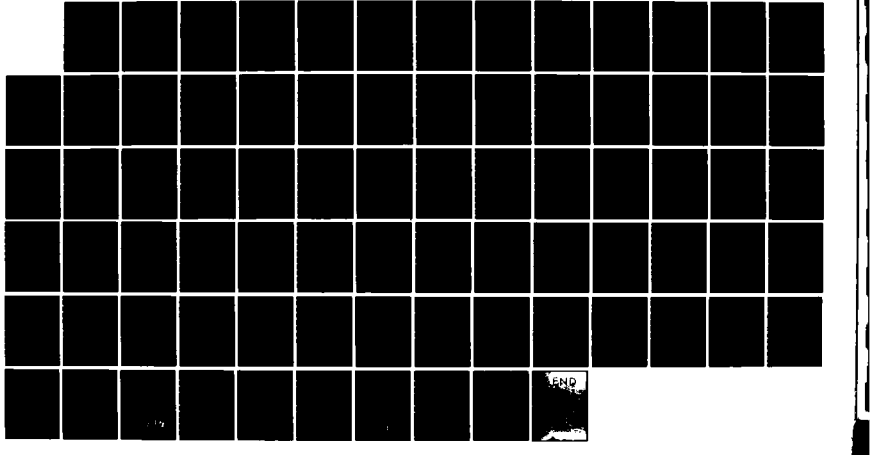

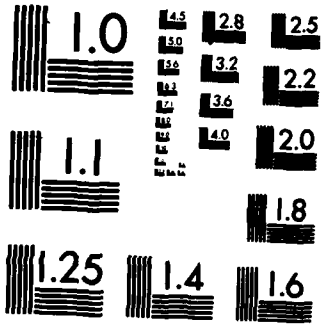
1.0
1.1
1.25
1.4
1.6
1.8
2.0
2.2
2.5
2.8
3.2
3.6
4.0
4.5
5.0
5.6

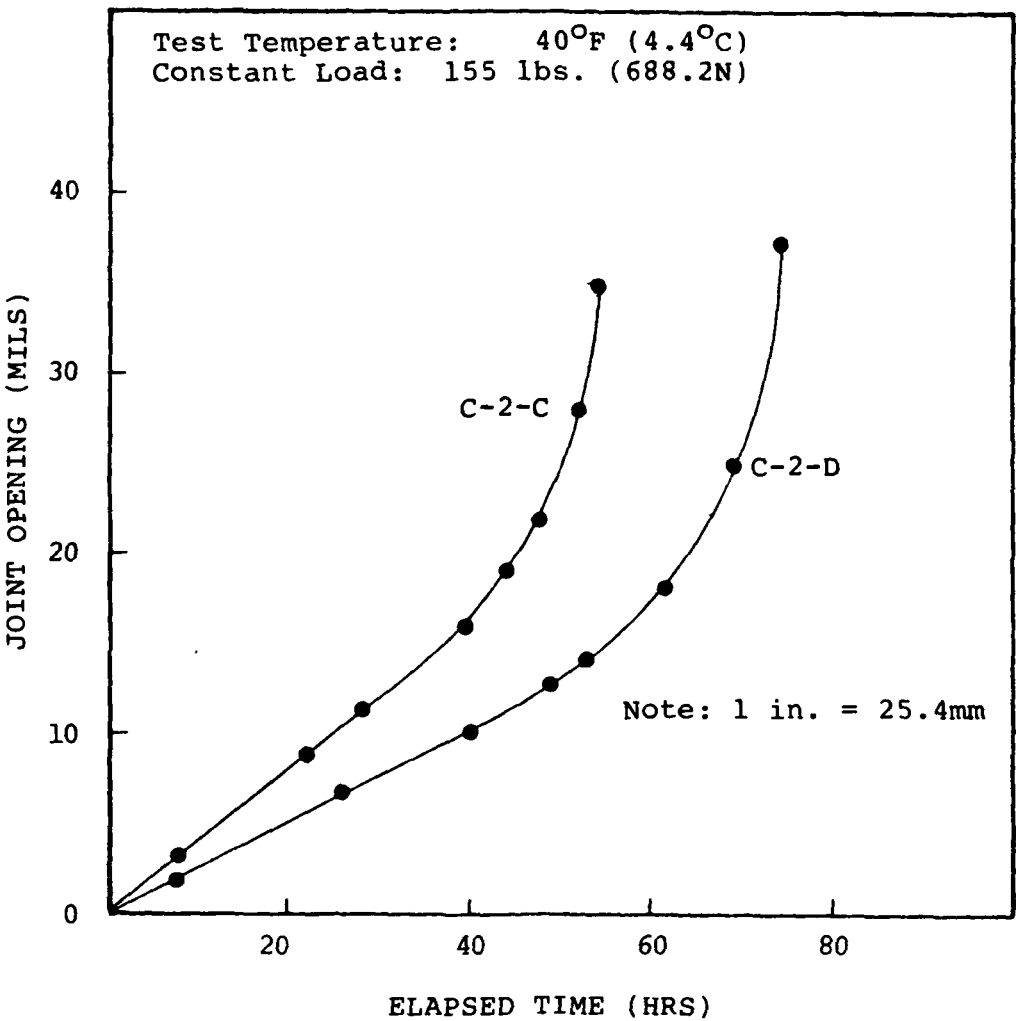

Figure 38. Typical joint opening creep curve

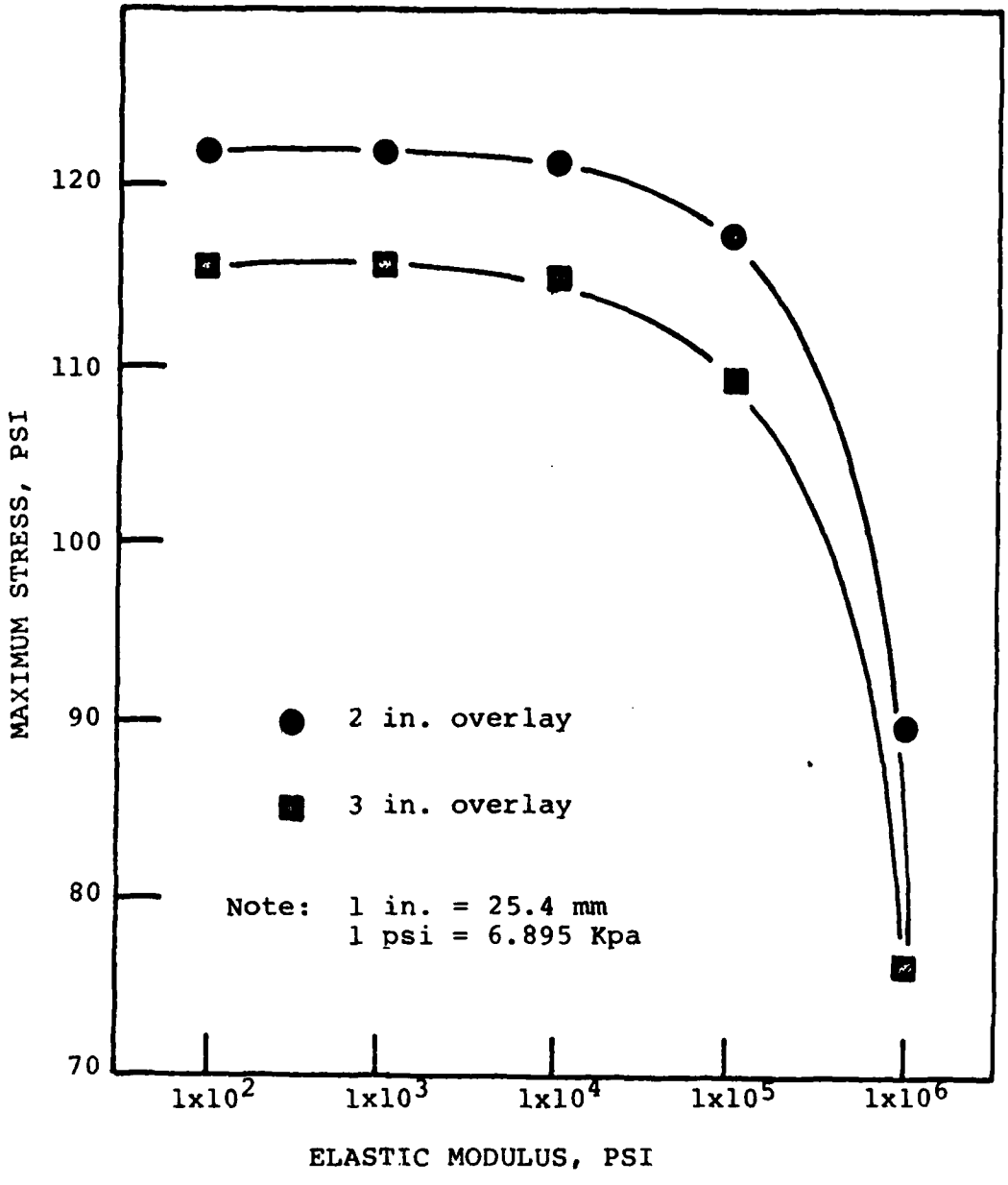

Figure 39. Maximum Stress in Overlay Due to Joint Opening

TABLE 5

CRITICAL JOINT OPENING FOR TREATMENT

Treatment	Temperature F (C)	Thickness in. (mm)	Joint Opening mils (mm)
A	40 (4)	2 (51)	10 (.25)
A	40 (4)	3 (76)	14 (.36)
B	40 (4)	2 (51)	23 (.58)
B	40 (4)	3 (76)	39 (.99)
C	40 (4)	2 (51)	19 (.48)
C	40 (4)	3 (76)	30 (.76)
D	40 (4)	2 (51)	20 (.51)
D	40 (4)	3 (76)	36 (.91)
A	72 (22)	2 (51)	12 (.30)
A	72 (22)	3 (76)	11 (.28)
B	72 (22)	2 (51)	26 (.66)
B	72 (22)	3 (76)	52 (1.32)
C	72 (22)	2 (51)	85 (2.16)[1]
C	72 (22)	3 (76)	-- ----- [2]
D	72 (22)	2 (51)	30 (.76)
D	72 (22)	3 (76)	45 (1.14)

[1] Value erroneous due to slippage between concrete and overlay

[2] Bond strength between concrete and overlay insufficient to conduct test

CHAPTER VII

CONCLUSIONS AND RECOMMENDATIONS

7.1 Conclusions

In this research investigation, a mechanistic methodology for design of fabric reinforced flexible overlays has been presented. It has been shown that the analytical model can satisfactorily predict the performance of flexible overlays of rigid airport pavements. To validate this model, laboratory fatigue tests have been carried out under controlled load and temperature environments. The three engineering fabrics used in this laboratory investigation correspond to low, medium and high tensile moduli fabrics. The following major conclusions are drawn from this study.

1. The results of the laboratory fatigue tests clearly demonstrates the effectiveness of fabrics in retarding the formation of reflective cracking of flexible overlays of rigid airport pavements.

2. The beneficial effects of fabrics are greatest at the lower temperatures where most help is needed. At these temperature levels, it has been shown that the allowable strain values are lower, requiring a greater contribution by fabric. The results of the temperature simulation tests also demonstrate the beneficial effect of using fabric reinforcement in retarding the formation of reflective cracks.

3. For the range of variables investigated, the test results show very little difference in the performance of the three engineering fabrics used in this study. However, the results of this research study is not applicable to the metallic reinforcement and other woven fabric types.

4. In this study, an SS-1H emulsion was used as a tack coat with application temperature of 77 F and application rate of 0.15 gallon per square yard (0.68 liter per square meter). The selection of optimum quantity of tack coat and tack coat type shall depend on the Concrete Surface Conditions as well as the asphalt retention of the fabrics.

5. An optimum fabric performance can only be achieved under limited horizontal and vertical displacement of underlying concrete pavement. The horizontal and vertical displacements under load and temperature are known to cause reflective cracking of flexible overlays. It is

shown that at the 40 F, the measured values of the joint opening above which a crack will develop ranges between 10 mils to 14 mils (0.25 to 036 mm) for a no fabric overlay, and ranges between 19 mils to 36 mils (0.48 to 0.91 mm) for the fabric reinforced overlays. Further, at 72 F (22C) a threshhold value of joint opening is about 11 mils (0.28 mm) for a no fabric overlay while it ranges from 26 mils to 52 mils (0.66 to 1.32 mm) for the fabric reinforced overlays.

6. As a general conclusion, the reinforcement of the overlay with a fabric substantially increases the critical joint opening, and that the difference in performance between fabrics tested in this study, is not very significant. On the other hand the large joint opening most likely represents some slippage between the concrete and overlay based on the laboratory observation that the bond between the concrete and the overlay failed on many of these specimens before any apparent damage occurred to the overlay.

7. For reinforced overlays subject to thermally induced joint openings, a threshhold modulus value of 200,000 psi (1.4 mpa) was found using EFRON program, below which the modulus has no effect on the maximum stress in the overlays.

In summary, it should be pointed out that the above conclusions could be slightly extrapolated beyond laboratory conditions used in this study. The comparison of the test results with the analysis using Mechanistic Model EFRON program shows that the analysis techniques utilized in that program realistically model the behavior of the overlay system in the laboratory tests, and there is every expectation that the model (EFRON) will satisfactorily predict the performance of overlays of actual runways also.

The verification of the applicability of the EFRON program to runway overlays is the major task of Volume II of this study. EFRON program is available at the FAA library.

7.2 Recommendations

Based on this research study, it is recommended that:

1. The type of fabric membrane to be used to improve the fatigue life of pavement shall be non-woven having a tensile strength of not less than 90 lbs. (41 kgs) determined according to ASTM D 1682 and a density in the range of 3 to 5.5 ozs. per square yard (40 to 70 gms per square yard).

2. Non-woven fabric membranes are to be used where the horizontal displacement is not in excess of 50 mils and vertical displacement is not in excess of 20 mils.

3. Tack coat to be used for most non-woven fabrics shall be emulsified asphalt with the rate of application ranging from 0.15 to 0.30 gallons per square yard. The optimum tack coat quantity shall depend on the type of fabric membrane used and the surface condition of the airport pavement to be overlaid.

4. The asphalt concrete overlay thickness when fabric membranes are used shall not be less than 3 inches (75 mm).

Construction specifications to be adopted for fabric reinforced overlays will be detailed in Volume II of this report and the above recommendations may be subject to change based on the final findings of this research study.

APPENDIX A

LABORATORY FATIGUE TEST DATA ON BEAMS

All beams 3 in (76 mm) wide x 24 in (610 mm) long

Treatment A - control, or conventional overlay

Treatment B - overlay reinforced with fabric B

Treatment C - overlay reinforced with fabric C

Treatment D - overlay reinforced with fabric D

Note: For properties of fabrics
refer to Table 1: page 67

TABLE 6

FATIGUE TEST DATA AT 72 DEGREES F

Beam Number	Base Thickness (inches)	Base Type	Overlay Thickness (inches)	Specific Gravity	Test Load (lbs)	Fatigue Life
A-2-1	1.5	conc.	2.0	2.37	150	1.90
A-2-2	1.51	conc.	2.0	2.37	150	3.30
A-2-3	1.5	conc.	2.0	2.36	150	4.80
A-2-4	1.5	conc.	2.0	2.34	150	3.70
A-2-5	1.48	conc.	2.0	2.34	200	1.10
A-2-6	1.48	conc.	2.0	2.38	200	1.00
A-2-7	1.48	conc.	2.0	2.37	200	1.20
A-2-8	1.48	conc.	2.05	2.36	200	2.20
A-2-9	1.5	conc.	2.10	2.37	250	0.90
A-2-10	1.5	conc.	2.00	2.36	250	1.00
A-2-11	1.5	conc.	2.10	2.36	250	0.70
A-2-12	1.5	conc.	2.10	2.36	250	0.75
B-2-1	1.5	conc.	2.0	2.37	150	4.20
B-2-2	1.5	conc.	2.0	2.37	150	12.71
B-2-3	1.5	conc.	2.0	2.37	150	6.50
B-2-4	1.5	conc.	2.05	2.36	150	34.84
B-2-5	1.6	conc.	2.05	2.37	200	1.70
B-2-6	1.6	conc.	2.0	2.35	200	2.10
B-2-7	1.6	conc.	2.1	2.35	200	2.30
B-2-8	1.5	conc.	2.0	2.35	200	5.80
B-2-9	1.5	conc.	2.05	2.36	250	1.10
B-2-10	1.5	conc.	2.05	2.36	250	1.40
B-2-11	1.6	conc.	2.05	2.37	250	1.38
B-2-12	1.5	conc.	2.05	2.36	250	1.68
C-2-1	2.0	conc.	2.00	2.35	150	20.4
C-2-2	2.0	conc.	2.00	2.36	150	16.7
C-2-3	2.0	conc.	2.00	2.36	200	9.0
C-2-4	2.0	conc.	2.00	2.36	200	7.5
C-2-5	2.0	conc.	2.00	2.35	250	6.8
C-2-6	2.0	conc.	2.00	2.35	250	5.8
D-2-1	1.5	conc.	2.00	2.36	150	14.50
D-2-2	1.5	conc.	2.0	2.36	150	11.30
D-2-3	2.0	conc.	2.05	2.35	200	4.90
D-2-4	2.0	conc.	2.05	2.35	200	4.30
D-2-5	2.0	conc.	1.98	2.38	250	2.70
D-2-6	2.0	conc.	1.97	2.38	250	2.50
CB-7	1.0	A.C.	1.98	2.37	150	11.30
CB-8	1.0	A.C.	1.98	2.36	150	11.70
CB-9	1.05	A.C.	2.00	2.36	150	10.95
CB-13	1.0	A.C.	2.00	2.35	150	17.50
CB-14	1.02	A.C.	2.00	2.35	150	8.70

TABLE 6 (continued)

FATIGUE TEST DATA AT 72 DEGREES F

Beam Number	Base Thickness (inches)	Base Type	Overlay Thickness (inches)	Specific Gravity	Test Load (lbs)	Fatigue Life
CB-15	1.01	A.C.	2.00	2.36	150	46.00
CB-1	1.0	A.C.	2.00	2.36	200	4.40
CB-2	1.05	A.C.	2.00	2.36	200	11.40
CB-3	1.0	A.C.	2.00	2.35	200	8.79
CB-4	1.0	A.C.	2.00	2.35	200	2.70
CB-5	1.0	A.C.	2.00	2.36	200	1.85
CB-6	1.0	A.C.	2.00	2.36	200	1.60
CB-10	1.0	A.C.	2.00	2.37	250	1.02
CB-11	1.1	A.C.	2.00	2.37	250	1.09
CB-12	1.1	A.C.	2.05	2.36	250	0.96
CB-16	1.1	A.C.	2.05	2.35	250	2.50
CB-17	1.0	A.C.	2.00	2.33	250	1.60
CB-18	1.05	A.C.	2.00	2.32	250	1.20
A-3-1	1.5	conc.	3.00	2.37	150	48.00
A-3-2	1.5	conc.	2.98	2.37	150	44.00
A-3-3	1.5	conc.	2.97	2.37	200	12.80
A-3-4	1.5	conc.	2.99	2.37	200	14.30
A-3-5	1.5	conc.	3.00	2.38	250	3.70
A-3-6	1.5	conc.	3.01	2.35	250	3.60
B-3-1	1.5	conc.	3.00	2.36	150	137.8
B-3-2	1.5	conc.	3.00	2.36	150	251.4
B-3-3	1.5	conc.	3.00	----	200	122.0
B-3-4	1.5	conc.	3.00	----	200	112.0
B-3-5	1.5	conc.	3.00	2.37	250	26.5
B-3-6	1.5	conc.	3.00	2.35	250	18.8
C-3-1	1.5	conc.	3.00	2.36	150	42.5
C-3-2	1.5	conc.	3.00	2.38	150	58.0
C-3-3	1.5	conc.	2.99	2.38	200	44.0
C-3-4	1.5	conc.	3.01	2.37	200	60.4
C-3-5	1.5	conc.	3.03	2.36	250	18.2
C-3-6	1.5	conc.	3.01	2.35	250	14.0
D-3-1	1.5	conc.	3.00	2.36	150	301.5
D-3-2	1.5	conc.	3.00	2.37	150	326.0
D-3-3	1.5	conc.	3.00	2.37	200	110.3
D-3-4	1.5	conc.	3.00	2.32	200	140.5
D-3-5	1.5	conc.	3.00	2.36	250	27.9
D-3-6	1.5	conc.	3.00	2.37	250	28.2

TABLE 7

FATIGUE TEST DATA AT 40 DEGREES F

Beam Number	Base Thickness (inches)	Base Type	Overlay Thickness (inches)	Specific Gravity	Test Load (lbs)	Fatigue Life
A-2-13	2.0	conc.	2.0	2.36	150	10.2
A-2-14	2.0	conc.	2.0	2.32	150	11.1
A-2-15	2.0	conc.	2.05	2.32	150	10.9
A-2-16	2.0	conc.	2.0	2.37	200	6.0
A-2-17	2.0	conc.	2.0	2.35	200	8.0
A-2-18	2.0	conc.	2.0	2.35	200	5.5
A-2-19	2.0	conc.	2.0	2.36	250	0.7
A-2-20	2.0	conc.	2.0	2.36	250	0.9
A-2-21	2.0	conc.	2.0	2.36	250	0.9
B-2-13	2.0	conc.	2.0	2.35	200	236.85
B-2-14	2.0	conc.	2.0	2.35	200	252.74
B-2-15	2.0	conc.	2.0	2.36	200	210.63
B-2-16	2.0	conc.	2.0	2.36	250	142.70
B-2-17	2.0	conc.	2.0	2.37	250	140.80
B-2-18	2.0	conc.	2.0	2.33	250	156.30
B-2-19	2.0	conc.	2.0	2.33	300	110.72
B-2-20	2.0	conc.	2.0	2.38	300	98.63
B-2-21	2.0	conc.	2.0	2.38	300	95.36
C-2-7	2.0	conc.	1.98	----	200	356.75
C-2-8	2.0	conc.	2.00	----	200	332.86
C-2-10	2.0	conc.	2.05	----	250	186.75
C-2-11	2.0	conc.	2.05	----	250	193.82
C-2-13	2.0	conc.	2.00	----	300	140.65
C-2-14	2.0	conc.	2.00	----	300	130.76
C-2-15	2.0	conc.	2.0	----	300	76.35
D-2-10	2.0	conc.	1.98	2.37	200	316.7
D-2-11	2.0	conc.	2.00	2.35	200	98.3
D-2-12	2.0	conc.	2.00	----	200	328.5
D-2-7	2.0	conc.	1.99	----	250	141.8
D-2-8	2.0	conc.	1.99	----	250	134.3
D-2-9	2.0	conc.	2.01	2.36	250	115.1
D-2-13	2.0	conc.	2.0	2.35	300	97.67
D-2-14	2.0	conc.	2.0	2.35	300	108.34
A-3-7	1.5	conc.	3.0	----	200	16.2
A-3-8	1.5	conc.	3.05	----	200	19.3
A-3-10	1.5	conc.	3.0	----	250	8.6
A-3-11	1.5	conc.	3.0	----	250	10.3
A-3-13	1.5	conc.	3.05	2.36	300	5.2
A-3-14	1.5	conc.	3.02	2.37	300	4.1
B-3-7	1.5	conc.	3.0	2.36	200	365.90

TABLE 7 (continued)

FATIGUE TEST DATA AT 40 DEGREES F

Beam Number	Base Thickness (inches)	Base Type	Overlay Thickness (inches)	Specific Gravity	Test Load (lbs)	Fatigue Life
B-3-8	1.5	conc.	3.0	2.34	200	535.0
B-3-10	1.5	conc.	3.0	2.33	250	696.43
B-3-11	1.5	conc.	3.0	2.37	250	256.38
B-3-12	1.5	conc.	3.0	----	250	301.60
B-3-13	1.5	conc.	2.98	2.31	400	148.8
B-3-14	1.5	conc.	3.0	2.38	400	166.5
C-3-7	1.5	conc.	3.0	2.36	200	610.07
C-3-8	1.5	conc.	3.0	2.37	200	680.39
C-3-10	1.5	conc.	3.0	2.35	250	386.95
C-3-11	1.5	conc.	3.0	2.38	250	350.31
C-3-13	1.5	conc.	3.0	2.37	400	407.30
C-3-14	1.5	conc.	3.0	2.36	400	196.0
C-3-15	1.5	conc.	3.0	2.34	400	180.[illegible]
D-3-7	1.5	conc.	3.0	2.36	200	565
D-3-8	1.5	conc.	3.0	2.35	200	593
D-3-10	1.6	conc.	3.0	2.37	250	312.
D-3-11	1.6	conc.	3.0	2.37	250	323.47
D-3-13	1.6	conc.	3.0	2.32	400	80.63
D-3-14	1.5	conc.	3.0	2.36	400	165.39
D-3-15	1.5	conc.	3.0	2.35	400	190.29

APPENDIX B

SIMULATED THERMAL LOADING OF LABORATORY SPECIMENS

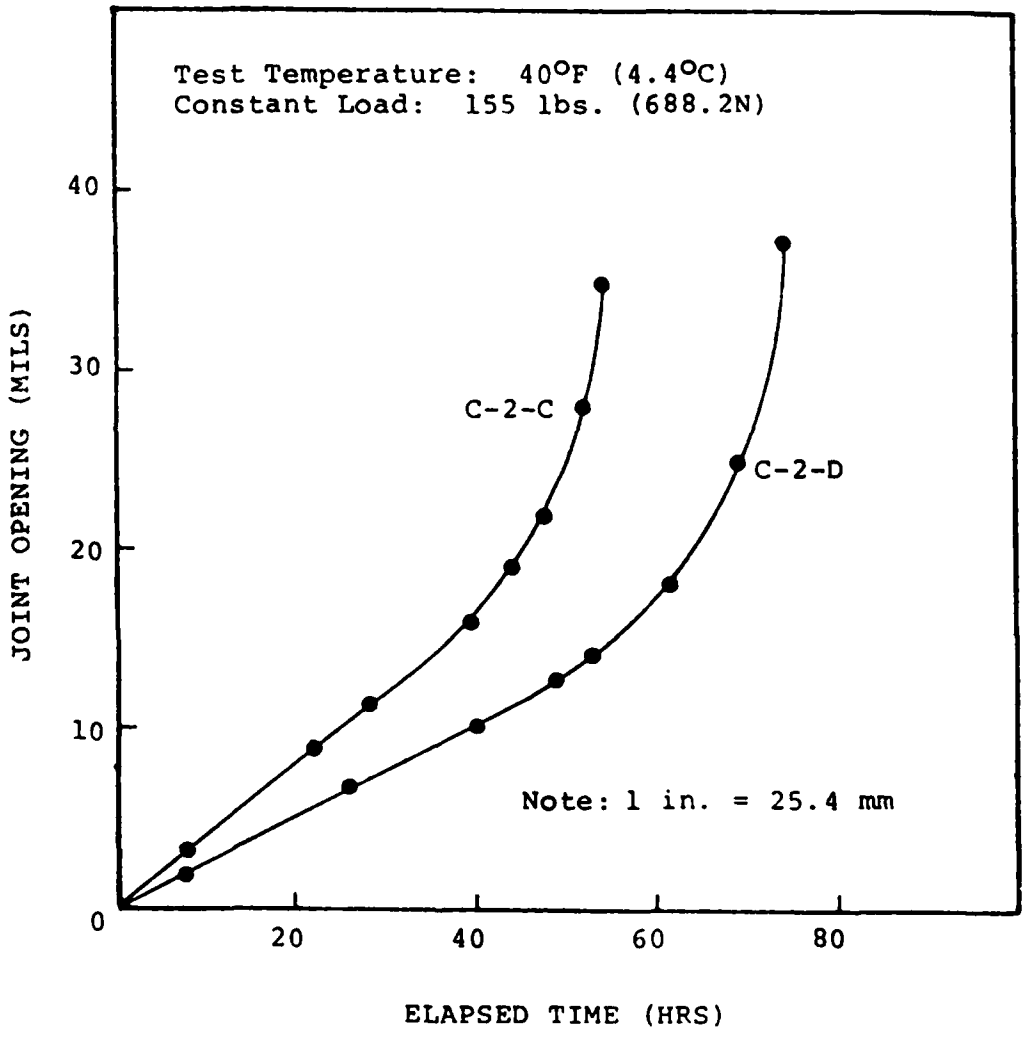
Test Temperature: 40°F (4.4°C)
Constant Load: 155 lbs. (688.2N)
C-2-C
C-2-D
Note: 1 in. = 25.4 mm
JOINT OPENING (MILS)
ELAPSED TIME (HRS)
0
10
20
30
40
20
40
60
80

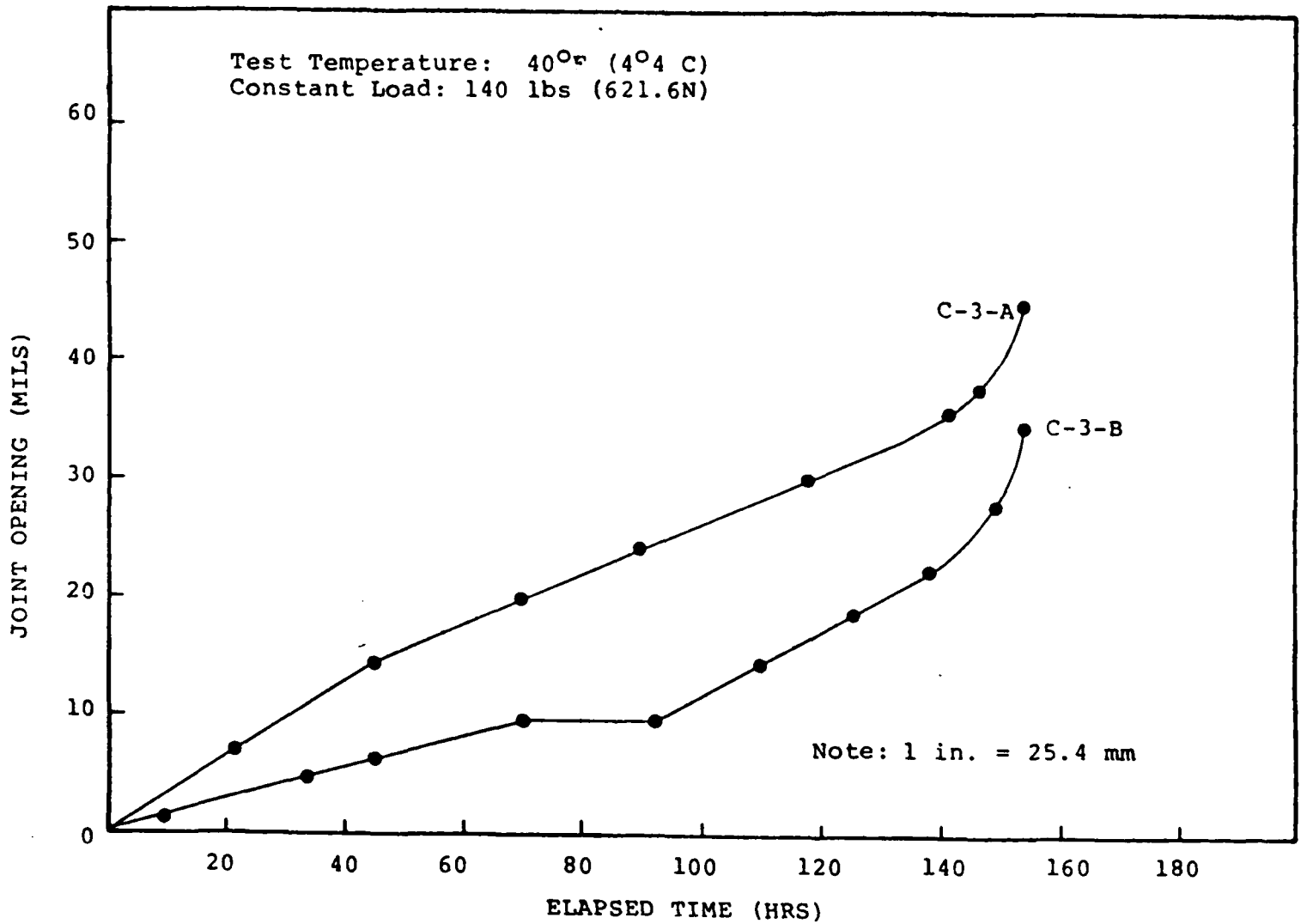
Test Temperature: 40°F (4°4 C)
Constant Load: 140 lbs (621.6N)
C-3-A
C-3-B
Note: 1 in. = 25.4 mm
JOINT OPENING (MILS)
ELAPSED TIME (HRS)
0
10
20
30
40
50
60
20
40
60
80
100
120
140
160
180

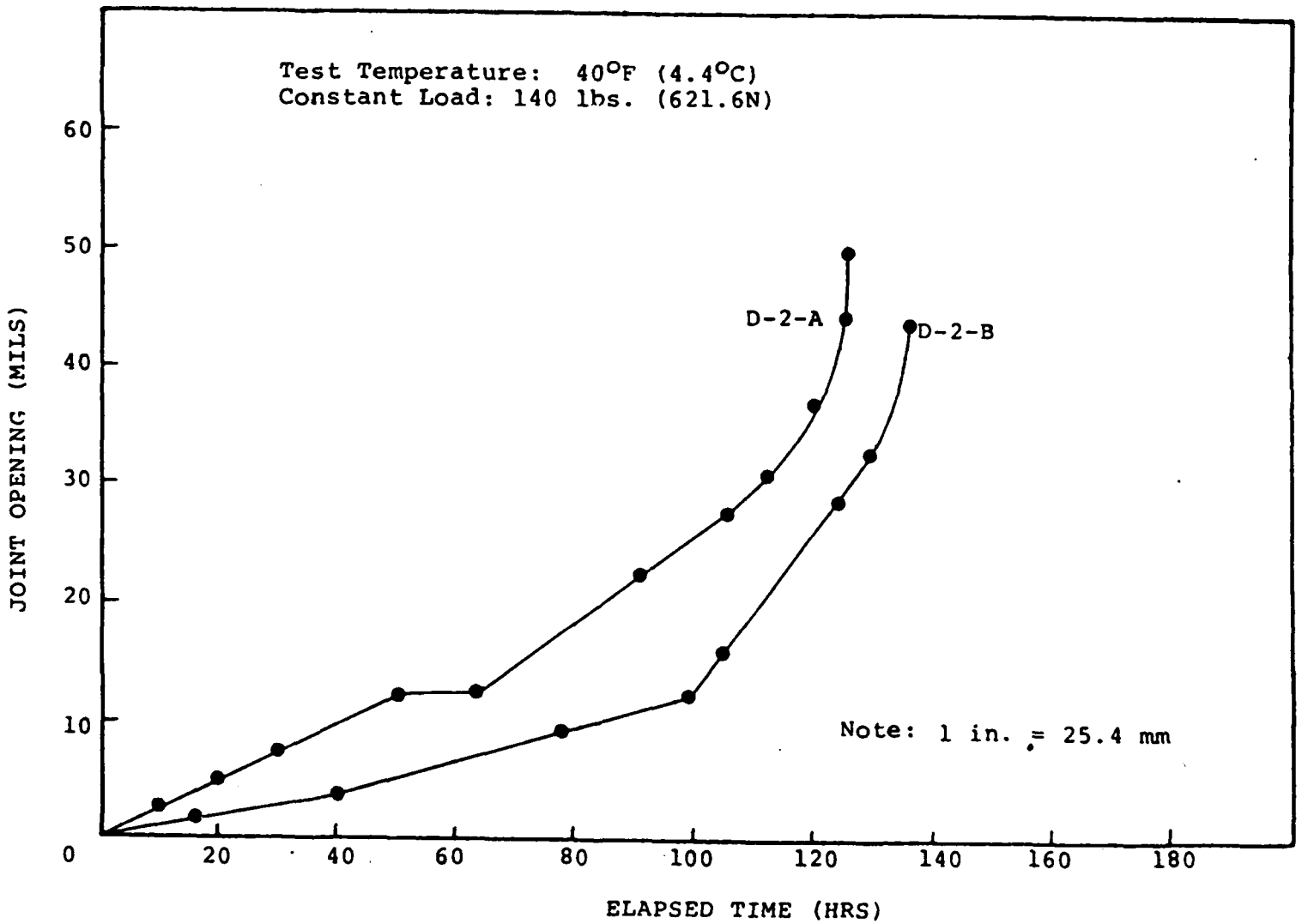
Test Temperature: 40°F (4.4°C)
Constant Load: 140 lbs. (621.6N)
D-2-A
D-2-B
Note: 1 in. = 25.4 mm
JOINT OPENING (MILS)
ELAPSED TIME (HRS)
0
10
20
30
40
50
60
20
40
60
80
100
120
140
160
180

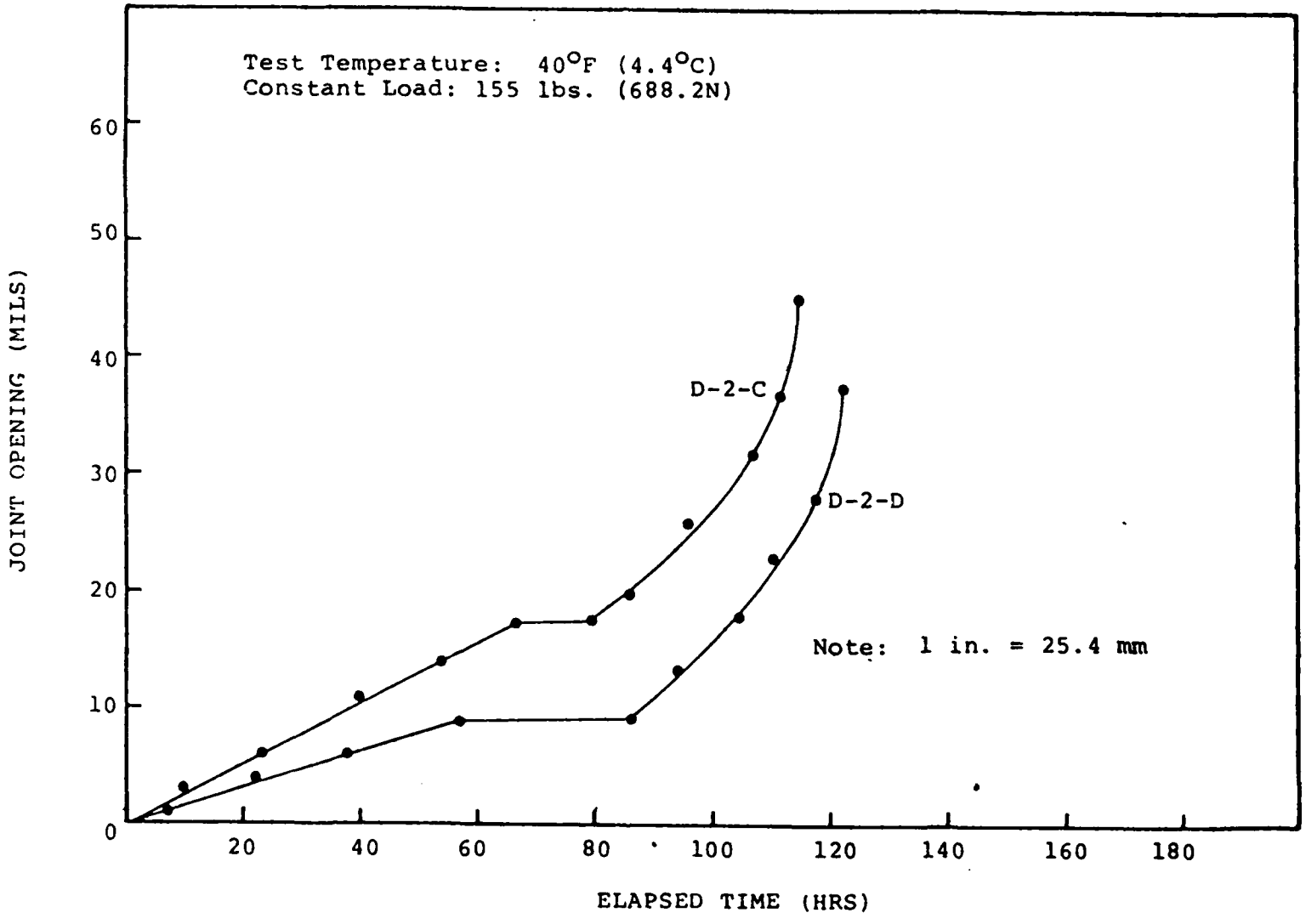
Test Temperature: 40°F (4.4°C)
Constant Load: 155 lbs. (688.2N)
JOINT OPENING (MILS)
ELAPSED TIME (HRS)
D-2-C
D-2-D
Note: 1 in. = 25.4 mm
0
10
20
30
40
50
60
20
40
60
80
100
120
140
160
180

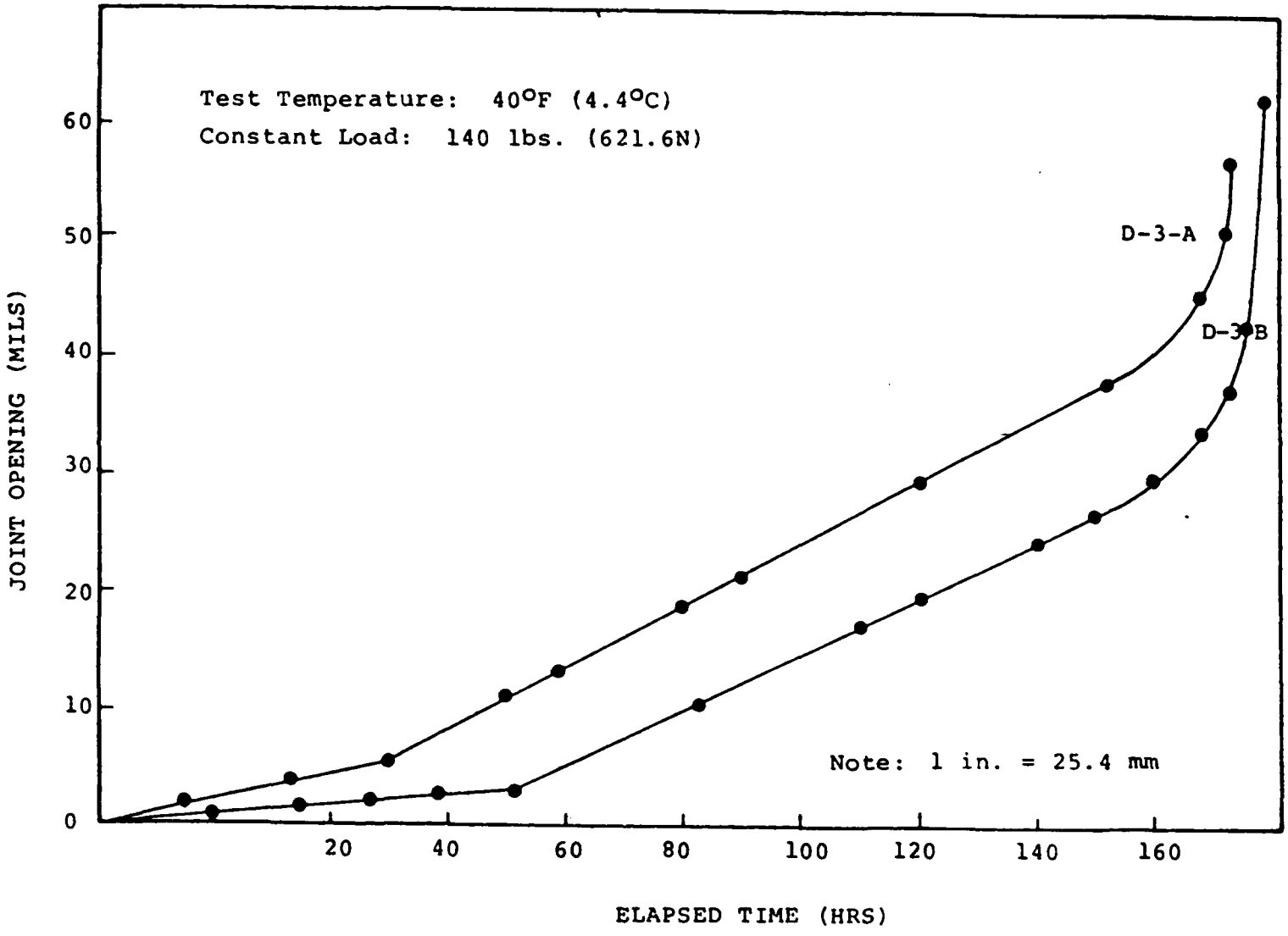
Test Temperature: 40°F (4.4°C)
Constant Load: 140 lbs. (621.6N)
D-3-A
D-3-B
Note: 1 in. = 25.4 mm
JOINT OPENING (MILS)
ELAPSED TIME (HRS)
0
10
20
30
40
50
60
20
40
60
80
100
120
140
160

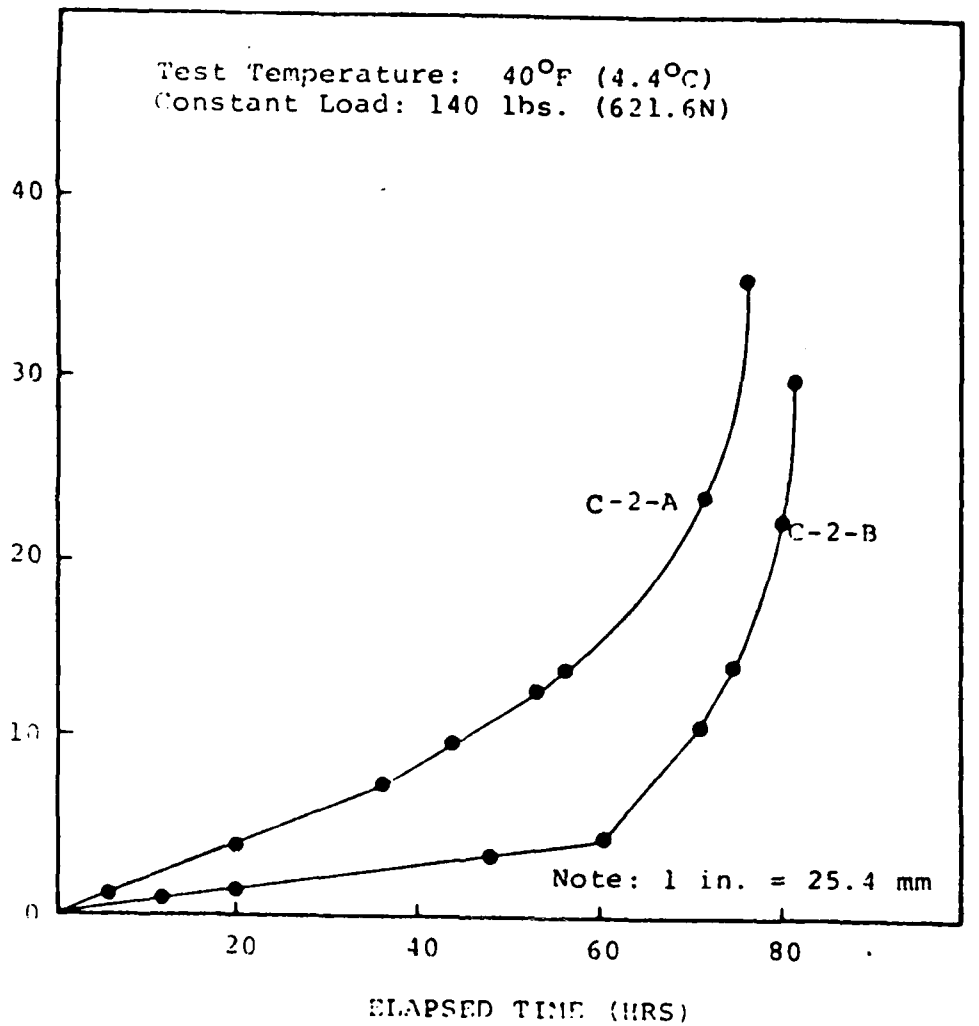
Test Temperature: 40°F (4.4°C)
Constant Load: 140 lbs. (621.6N)
40
30
20
10
0
C-2-A
C-2-B
Note: 1 in. = 25.4 mm
20
40
60
80
ELAPSED TIME (HRS)

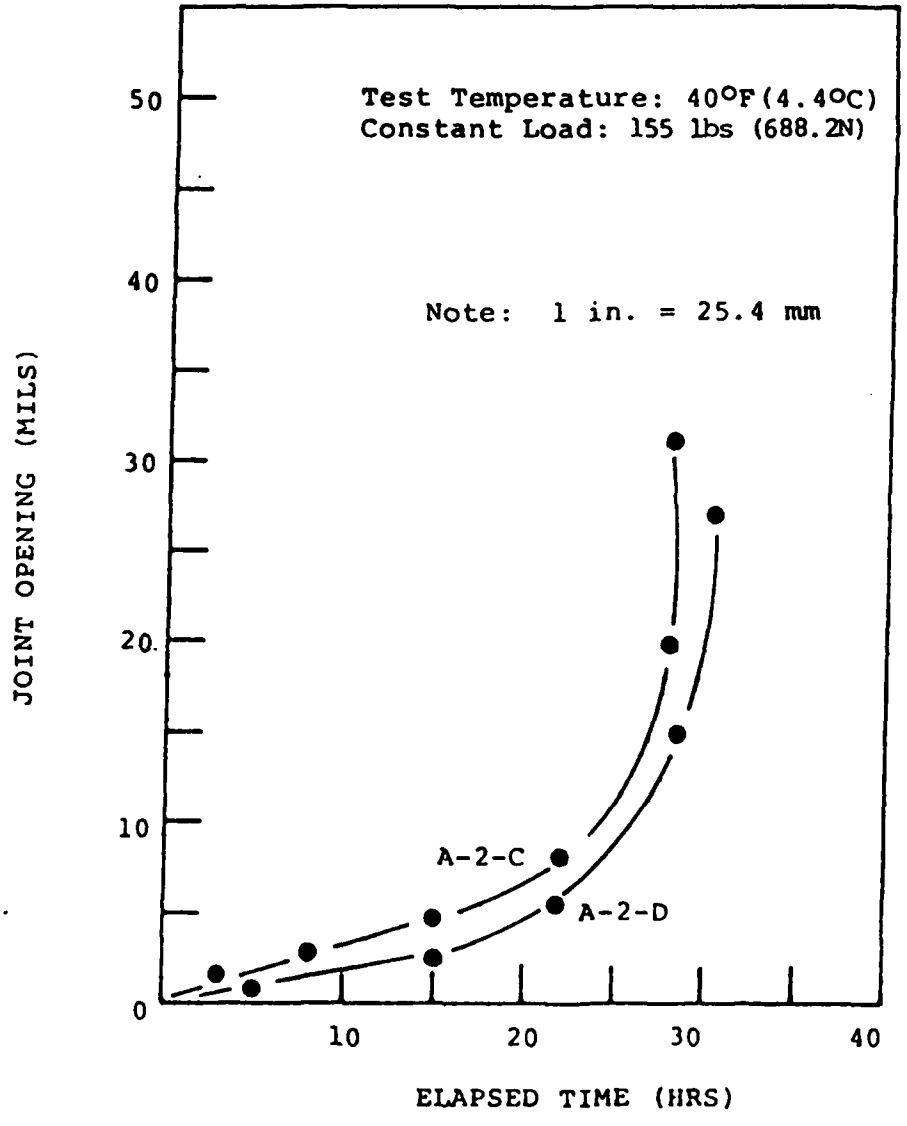
Test Temperature: 40°F (4.4°C)
Constant Load: 155 lbs (688.2N)
Note: 1 in. = 25.4 mm
JOINT OPENING (MILS)
ELAPSED TIME (HRS)
A-2-C
A-2-D
0
10
20
30
40
50
10
20
30
40

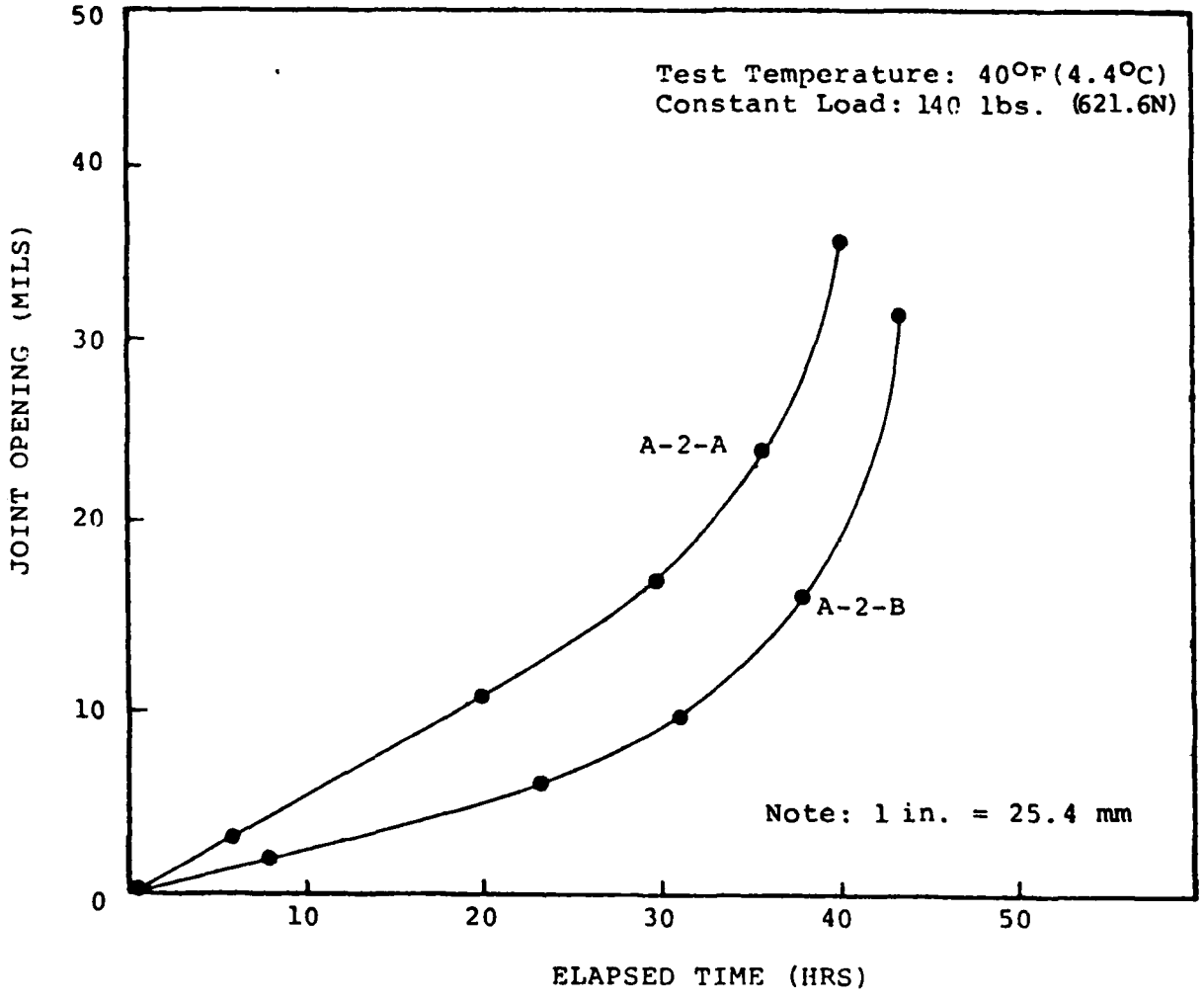
Test Temperature: 40°F (4.4°C)
Constant Load: 140 lbs. (621.6N)
A-2-A
A-2-B
Note: 1 in. = 25.4 mm
JOINT OPENING (MILS)
ELAPSED TIME (HRS)
0
10
20
30
40
50

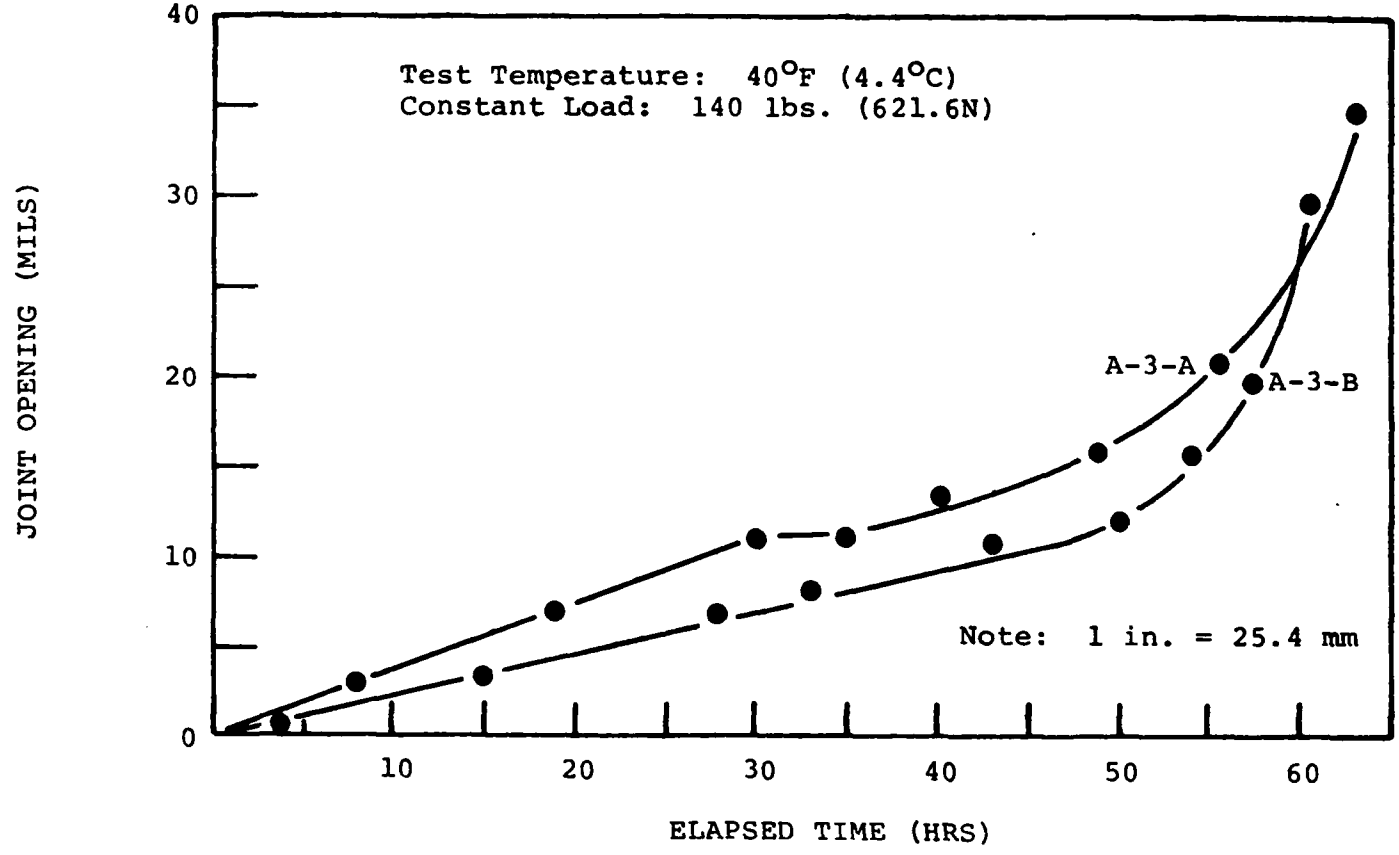
Test Temperature: 40°F (4.4°C)
Constant Load: 140 lbs. (621.6N)
A-3-A
A-3-B
Note: 1 in. = 25.4 mm
JOINT OPENING (MILS)
ELAPSED TIME (HRS)
0
10
20
30
40
10
20
30
40
50
60

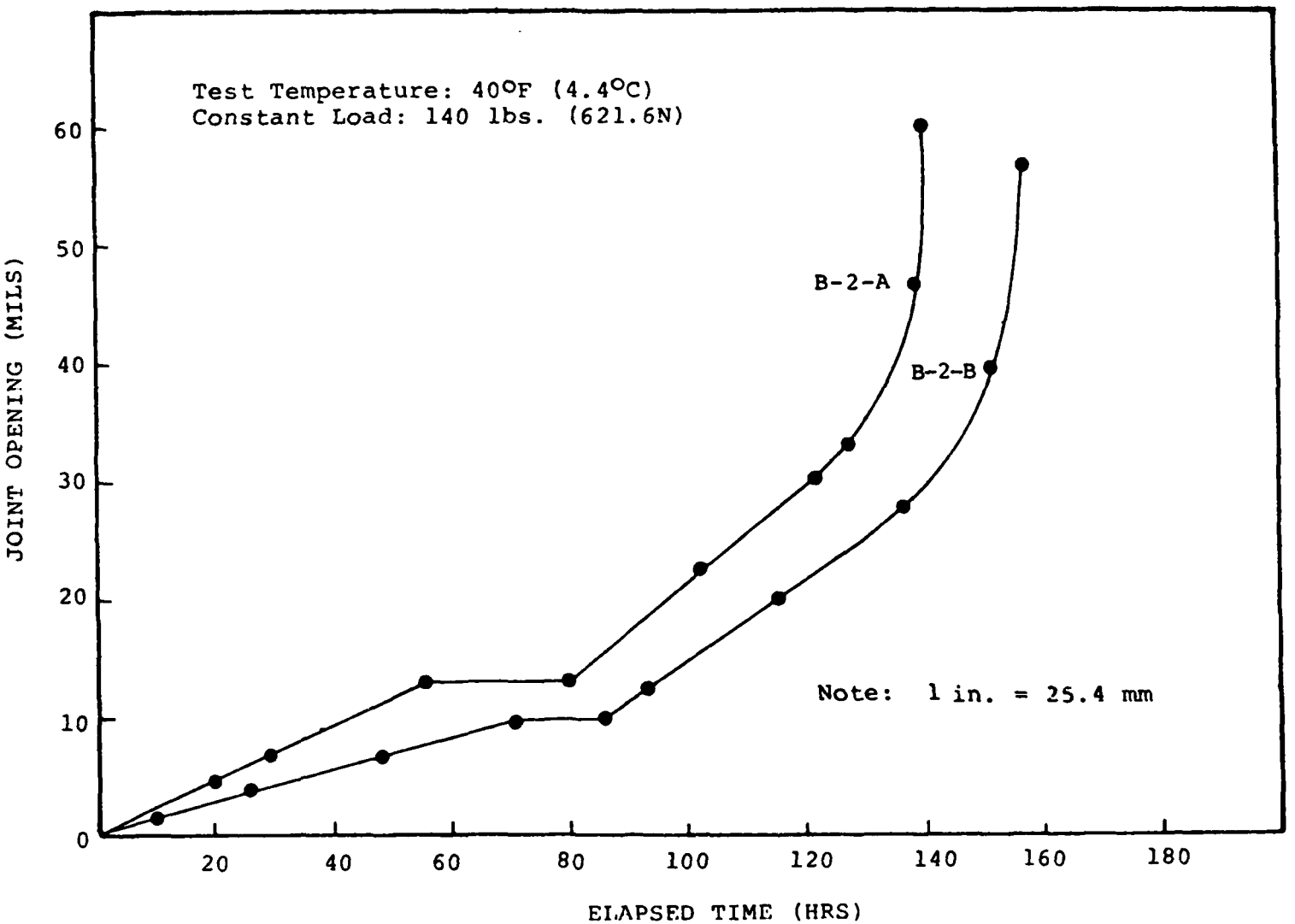
Test Temperature: 40°F (4.4°C)
Constant Load: 140 lbs. (621.6N)
B-2-A
B-2-B
Note: 1 in. = 25.4 mm
JOINT OPENING (MILS)
0
10
20
30
40
50
60
20
40
60
80
100
120
140
160
180
ELAPSED TIME (HRS)

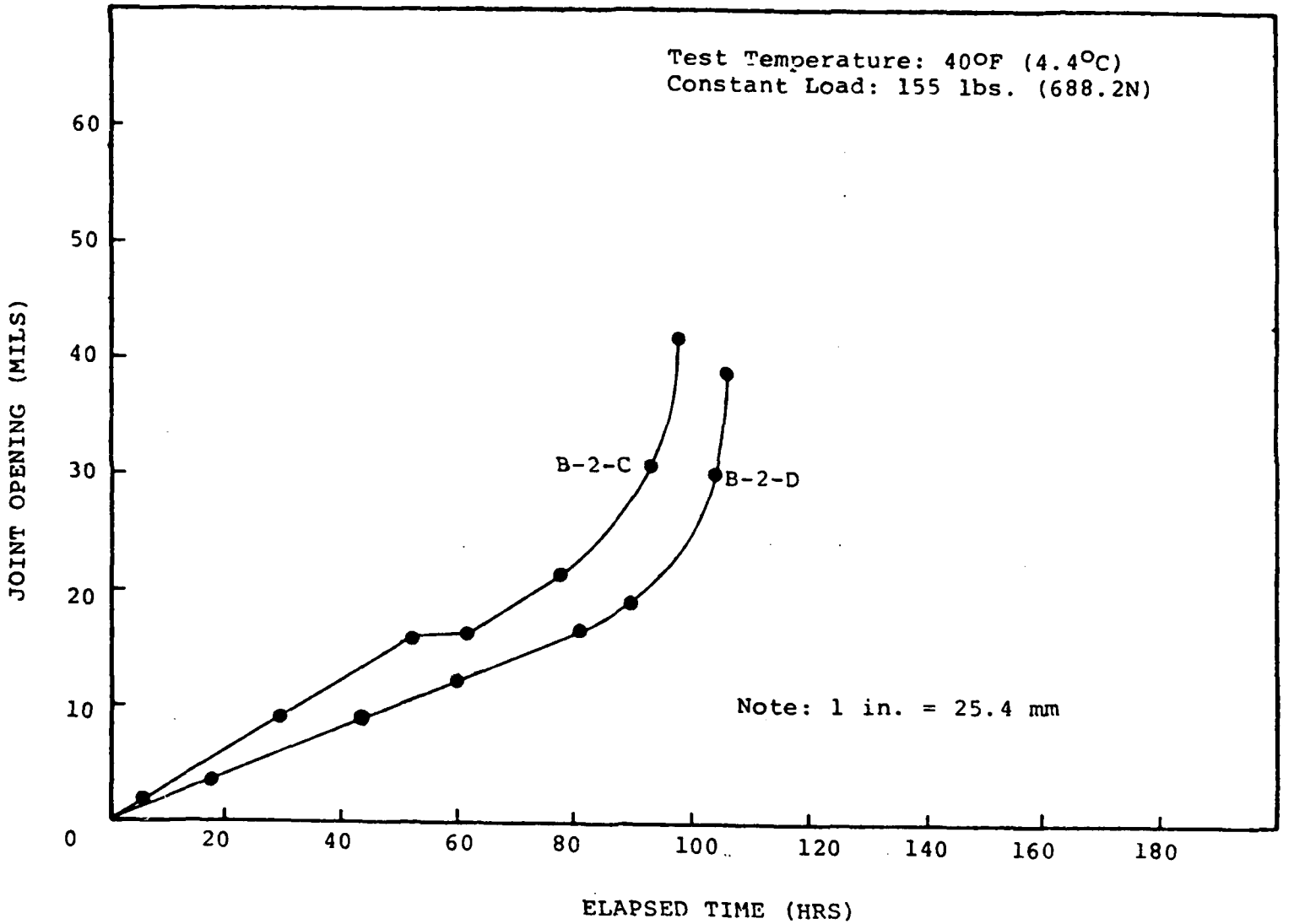
Test Temperature: 40°F (4.4°C)
Constant Load: 155 lbs. (688.2N)
B-2-C
B-2-D
Note: 1 in. = 25.4 mm
JOINT OPENING (MILS)
ELAPSED TIME (HRS)
0
10
20
30
40
50
60
20
40
60
80
100
120
140
160
180

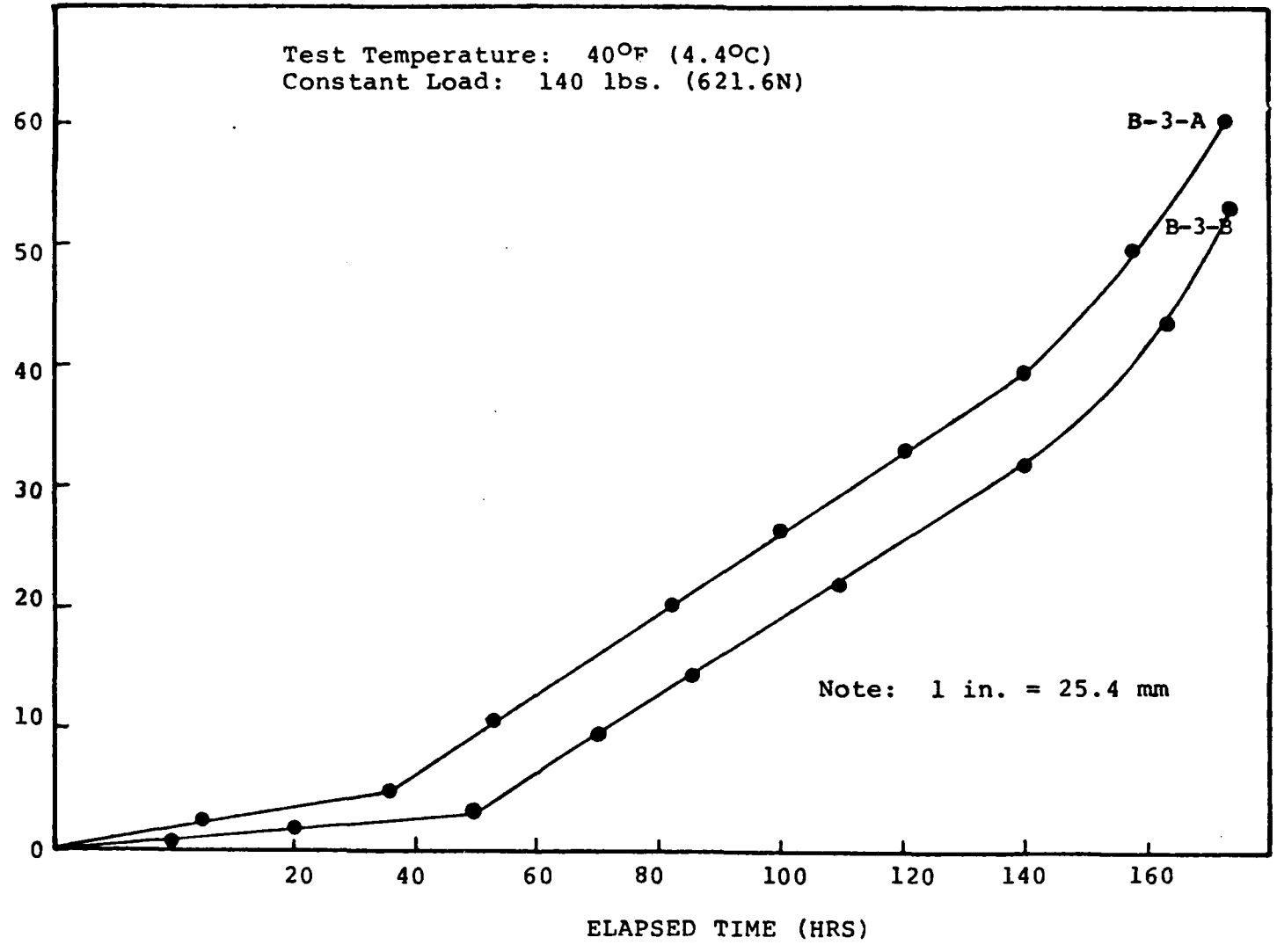
Test Temperature: 40°F (4.4°C)
Constant Load: 140 lbs. (621.6N)
B-3-A
B-3-B
Note: 1 in. = 25.4 mm
60
50
40
30
20
10
0
20
40
60
80
100
120
140
160
ELAPSED TIME (HRS)

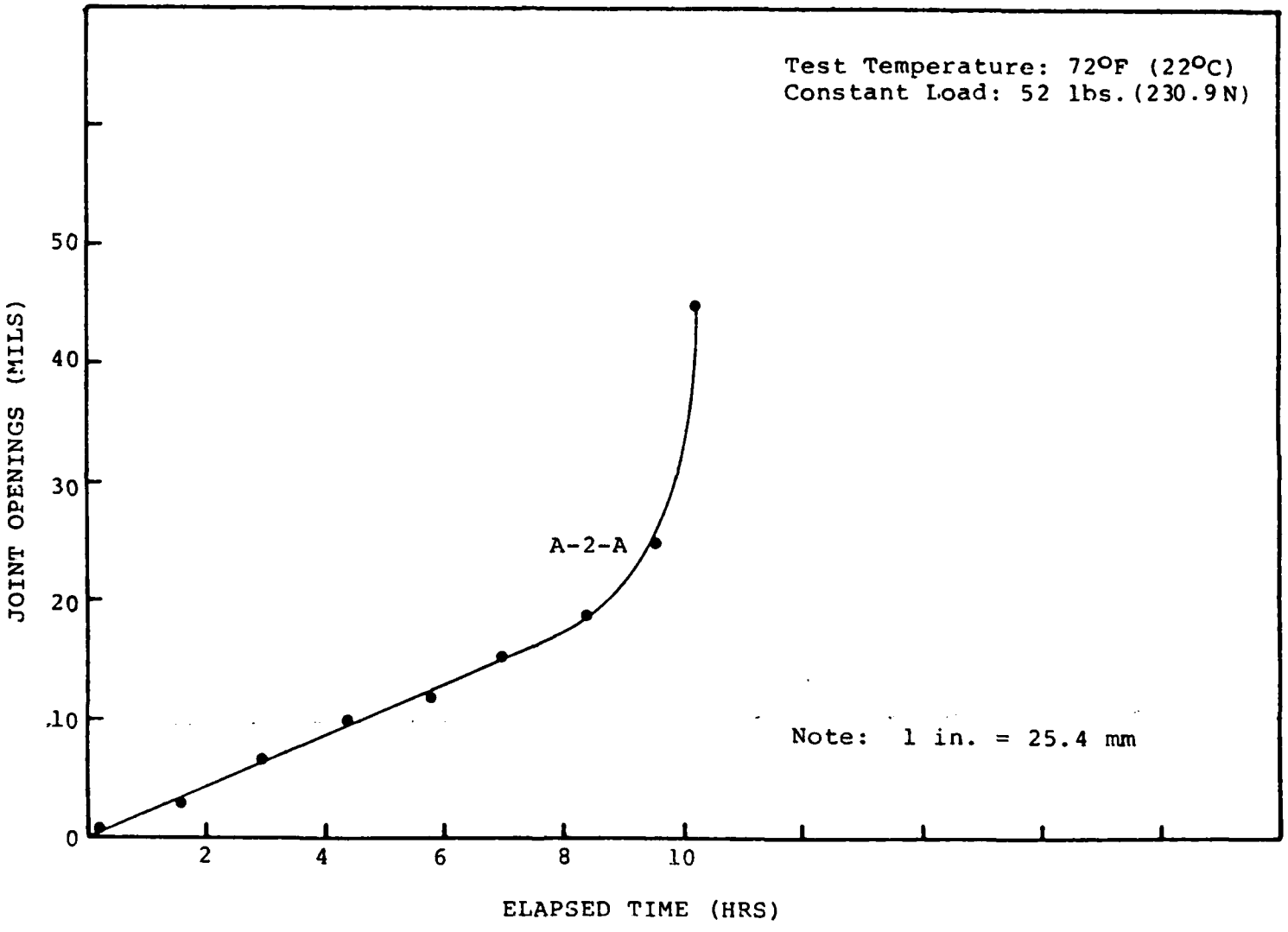
Test Temperature: 72°F (22°C)
Constant Load: 52 lbs. (230.9 N)
JOINT OPENINGS (MILS)
0
10
20
30
40
50
A-2-A
2
4
6
8
10
ELAPSED TIME (HRS)
Note: 1 in. = 25.4 mm

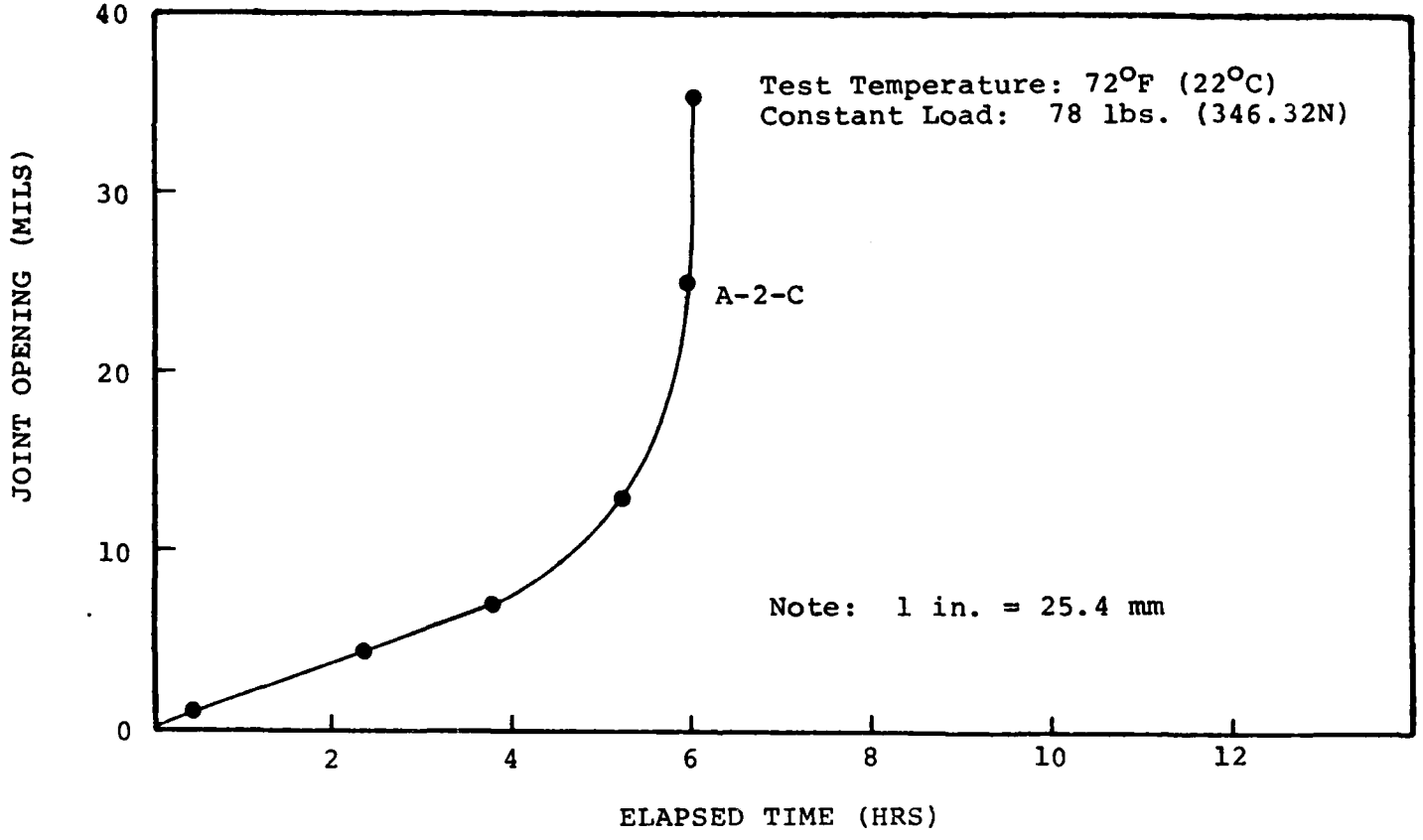
40
30
20
10
0
JOINT OPENING (MILS)
Test Temperature: 72°F (22°C)
Constant Load: 78 lbs. (346.32N)
A-2-C
Note: 1 in. = 25.4 mm
2
4
6
8
10
12
ELAPSED TIME (HRS)

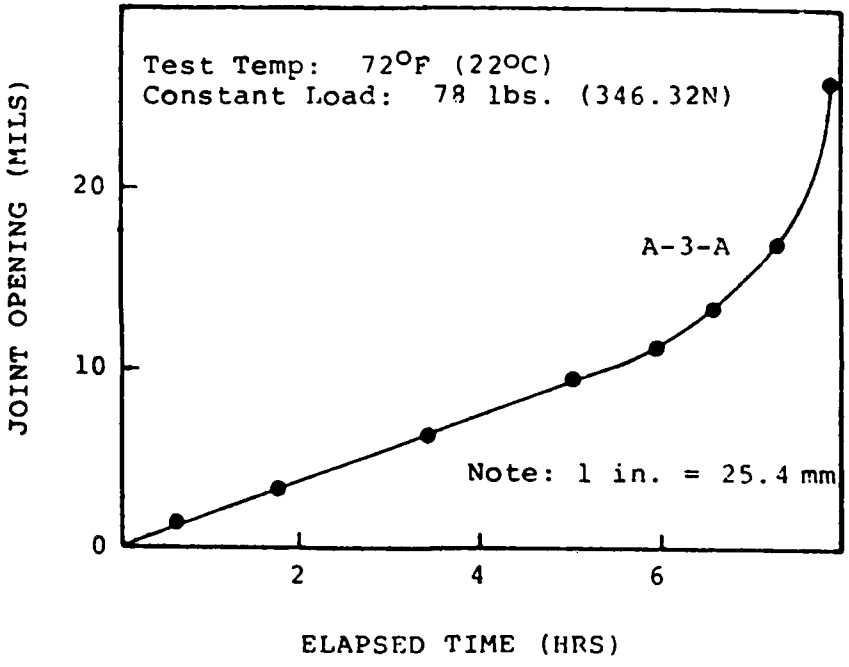
Test Temp: 72°F (22°C)
Constant Load: 78 lbs. (346.32N)
A-3-A
Note: 1 in. = 25.4 mm
JOINT OPENING (MILS)
0
10
20
2
4
6
ELAPSED TIME (HRS)

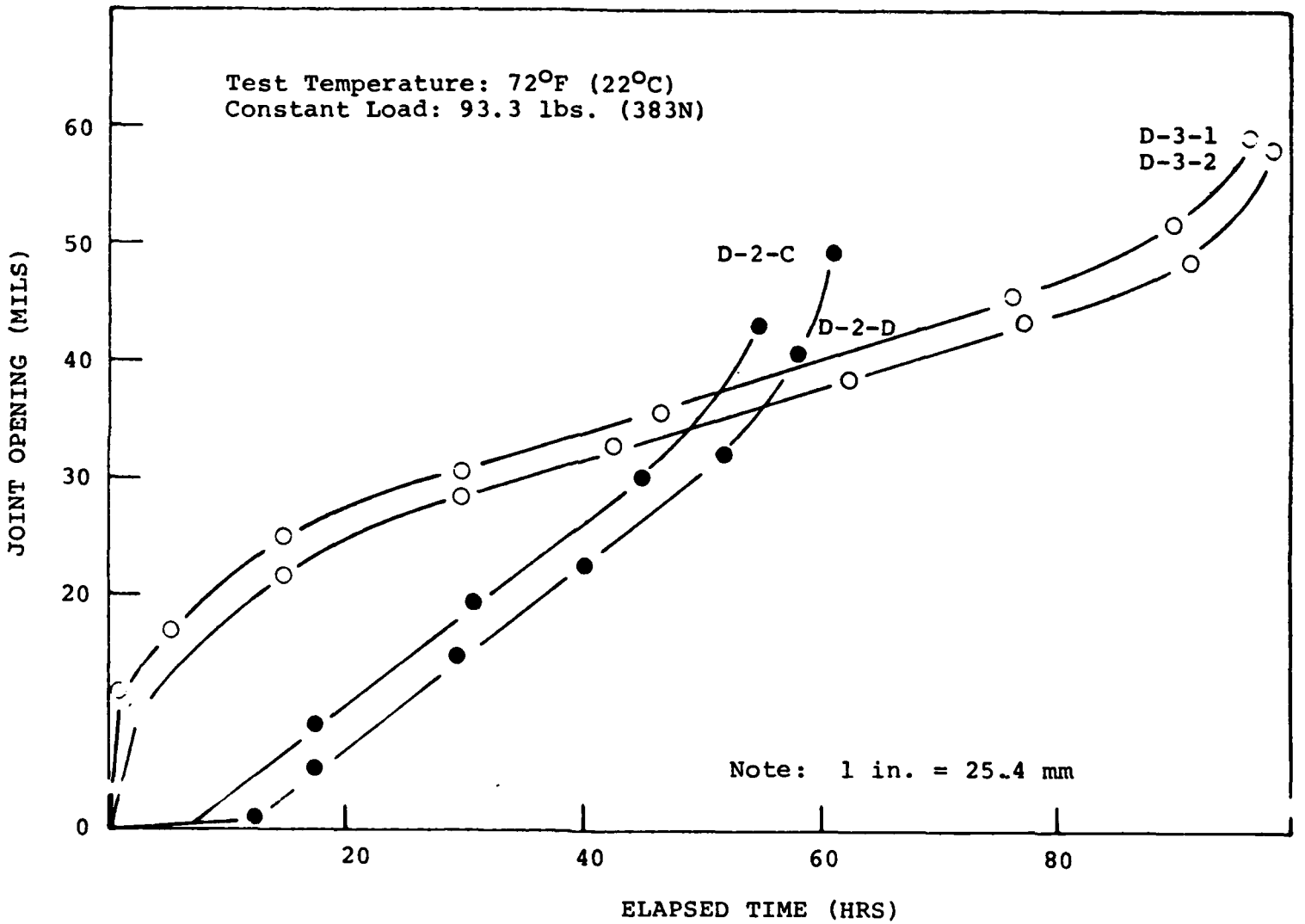
Test Temperature: 72°F (22°C)
Constant Load: 93.3 lbs. (383N)
D-3-1
D-3-2
D-2-C
D-2-D
Note: 1 in. = 25.4 mm
JOINT OPENING (MILS)
0
20
30
40
50
60
20
40
60
80
ELAPSED TIME (HRS)

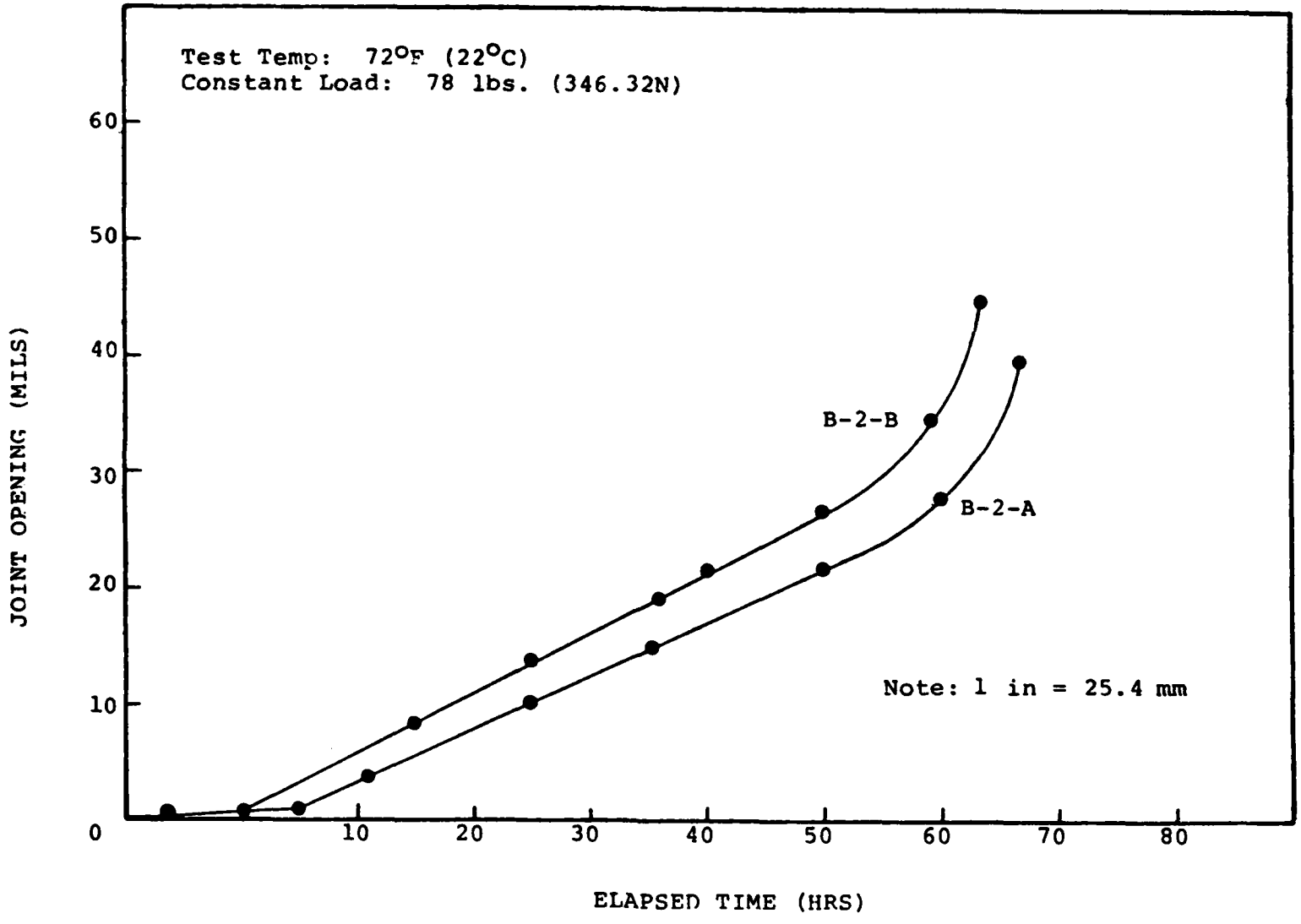
Test Temp: 72°F (22°C)
Constant Load: 78 lbs. (346.32N)
JOINT OPENING (MILS)
ELAPSED TIME (HRS)
B-2-B
B-2-A
Note: 1 in = 25.4 mm
0
10
20
30
40
50
60
70
80

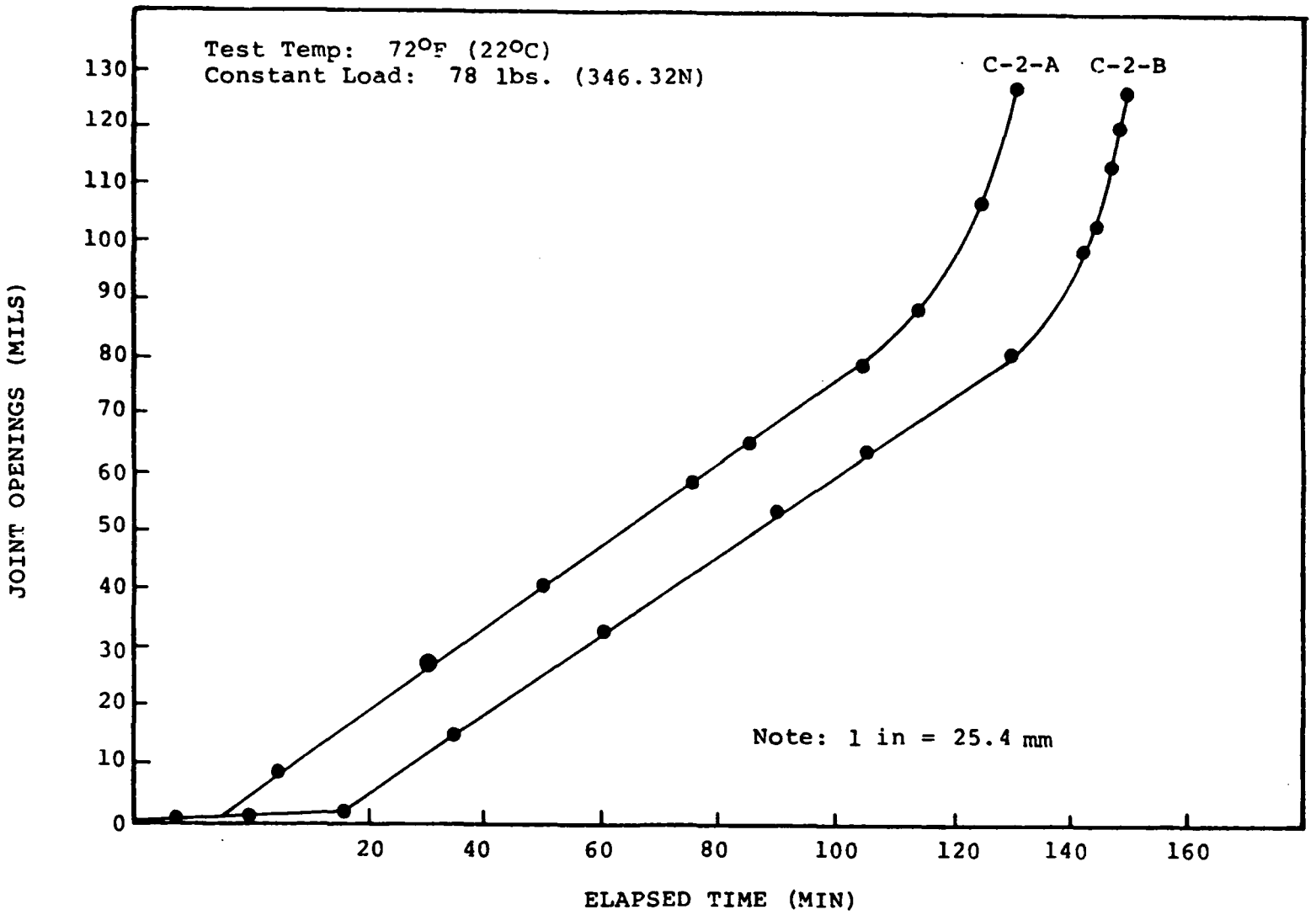
Test Temp: 72°F (22°C)
Constant Load: 78 lbs. (346.32N)
C-2-A
C-2-B
Note: 1 in = 25.4 mm
JOINT OPENINGS (MILS)
ELAPSED TIME (MIN)
0
10
20
30
40
50
60
70
80
90
100
110
120
130
20
40
60
80
100
120
140
160

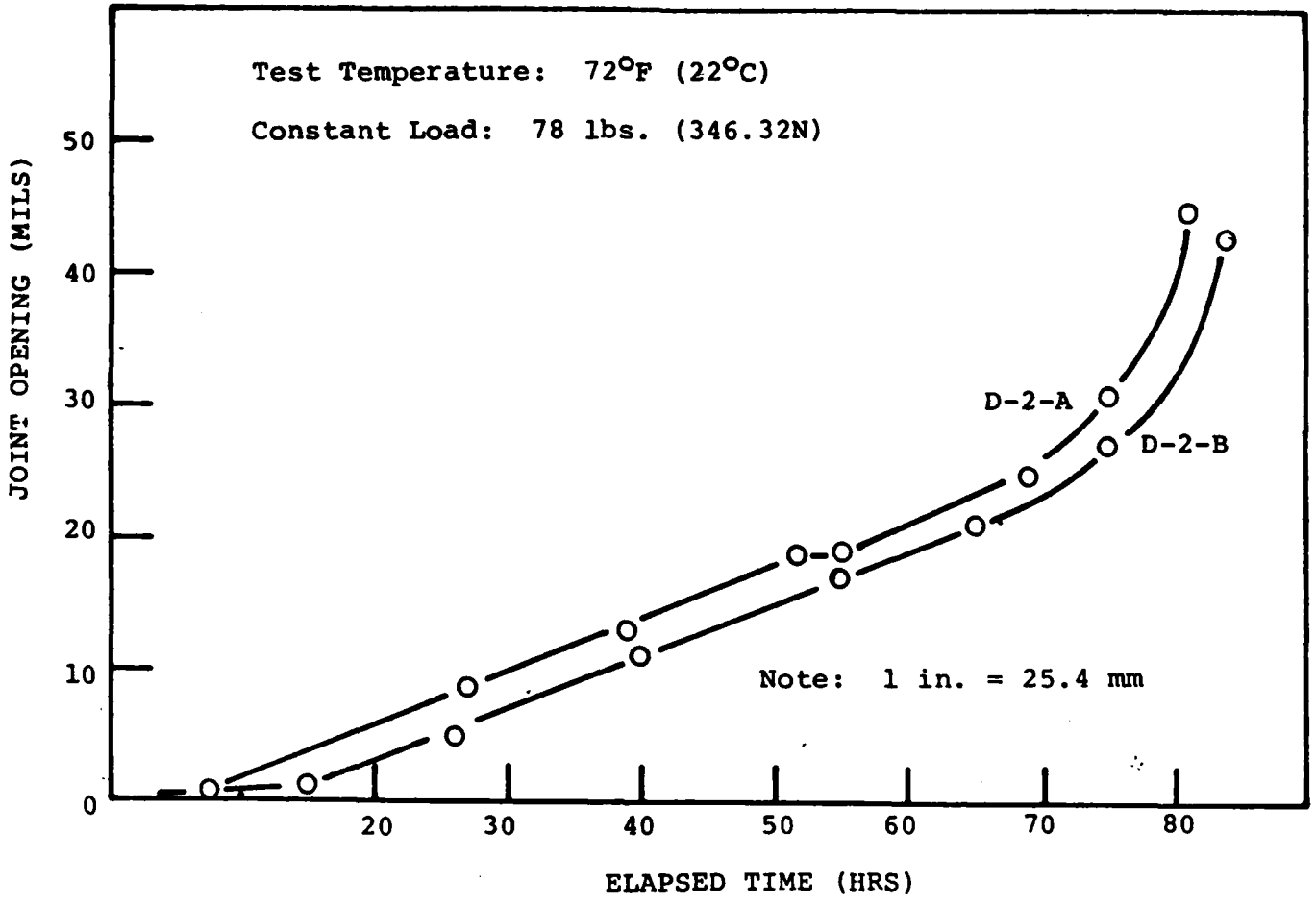
Test Temperature: 72°F (22°C)
Constant Load: 78 lbs. (346.32N)
JOINT OPENING (MILS)
0
10
20
30
40
50
D-2-A
D-2-B
Note: 1 in. = 25.4 mm
20
30
40
50
60
70
80
ELAPSED TIME (HRS)

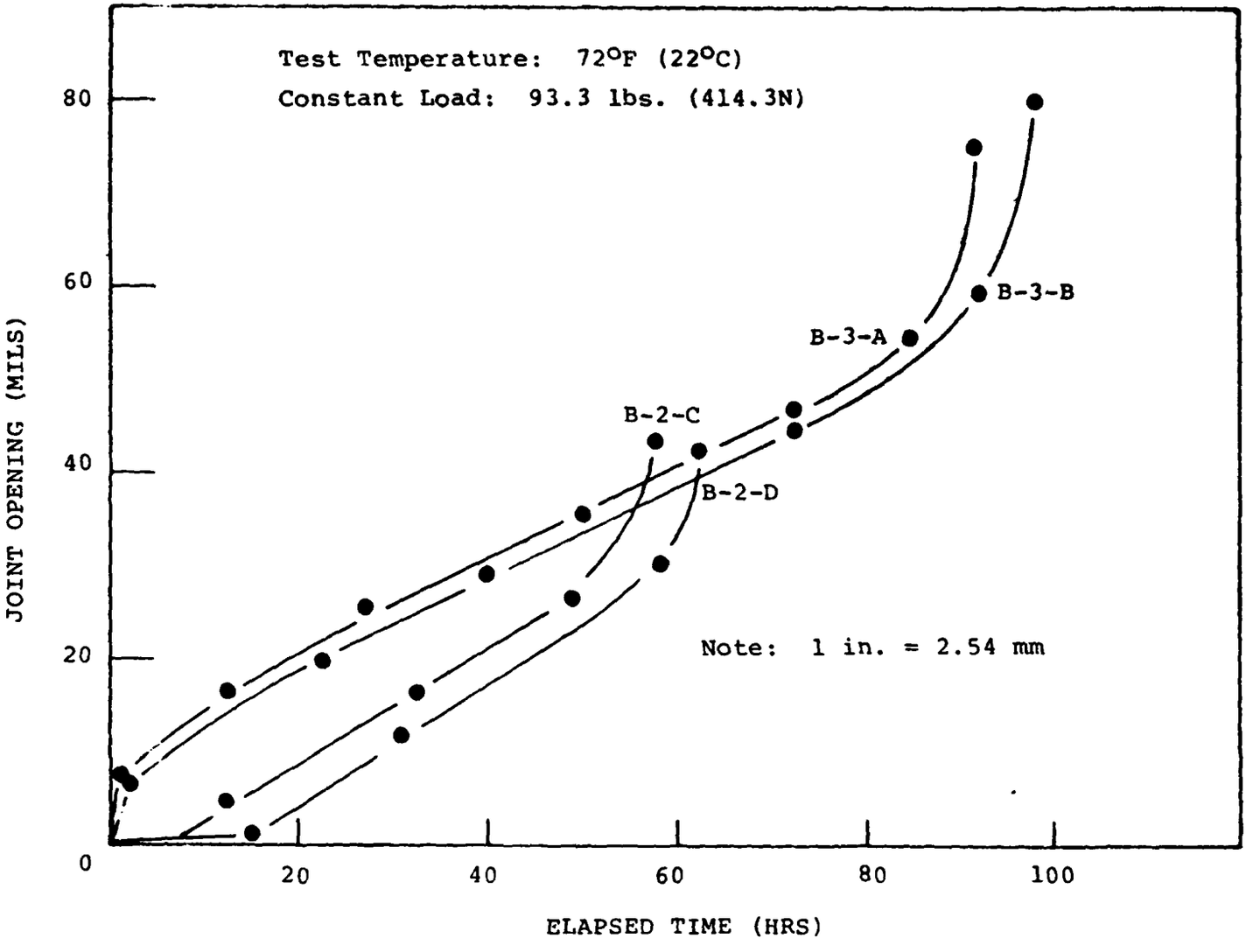
Test Temperature: 72°F (22°C)
Constant Load: 93.3 lbs. (414.3N)
B-3-B
B-3-A
B-2-C
B-2-D
Note: 1 in. = 2.54 mm
JOINT OPENING (MILS)
ELAPSED TIME (HRS)
0
20
40
60
80
100

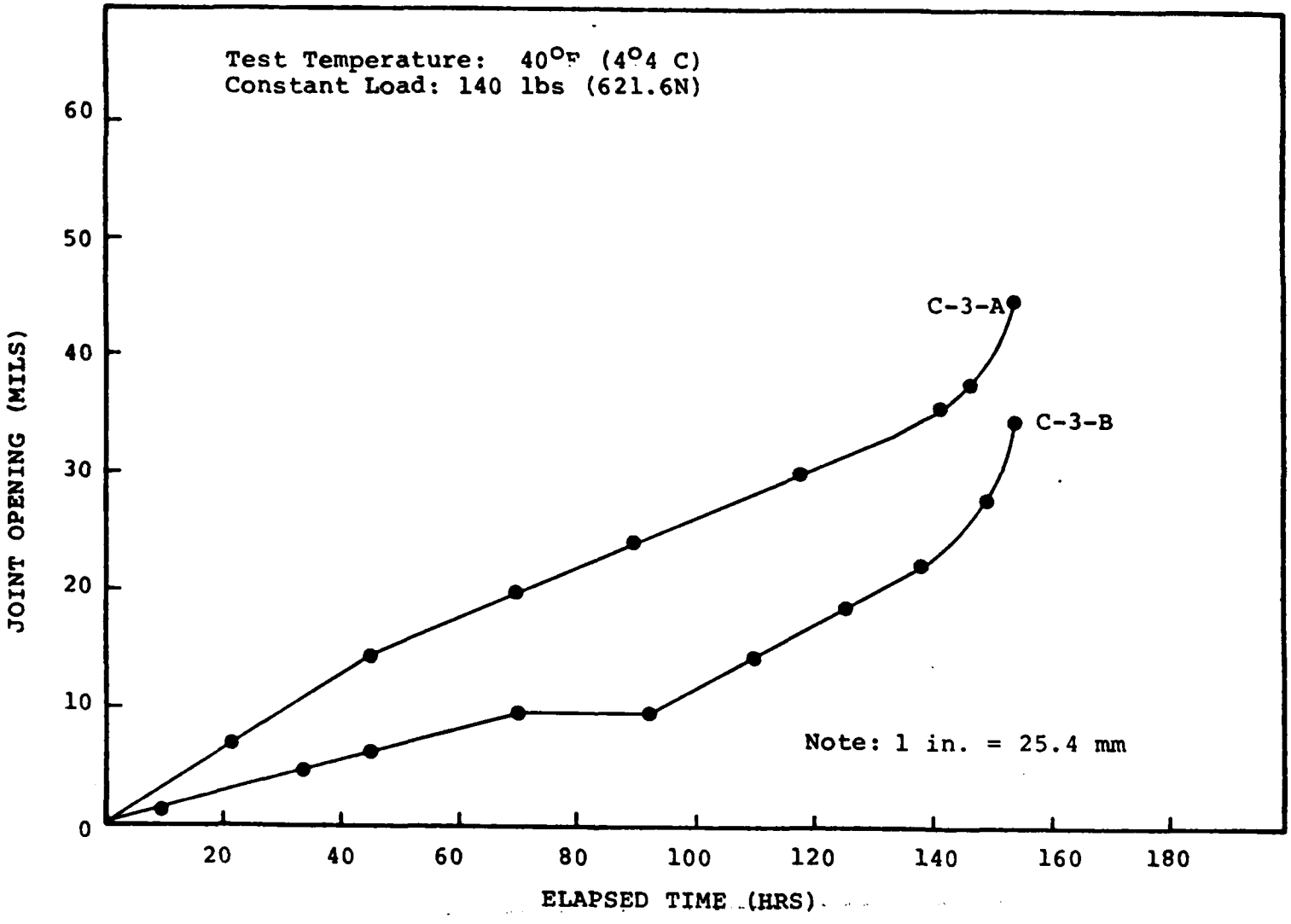
Test Temperature: 40°F (4°4 C)
Constant Load: 140 lbs (621.6N)
JOINT OPENING (MILS)
ELAPSED TIME (HRS)
C-3-A
C-3-B
Note: 1 in. = 25.4 mm
0
10
20
30
40
50
60
20
40
60
80
100
120
140
160
180

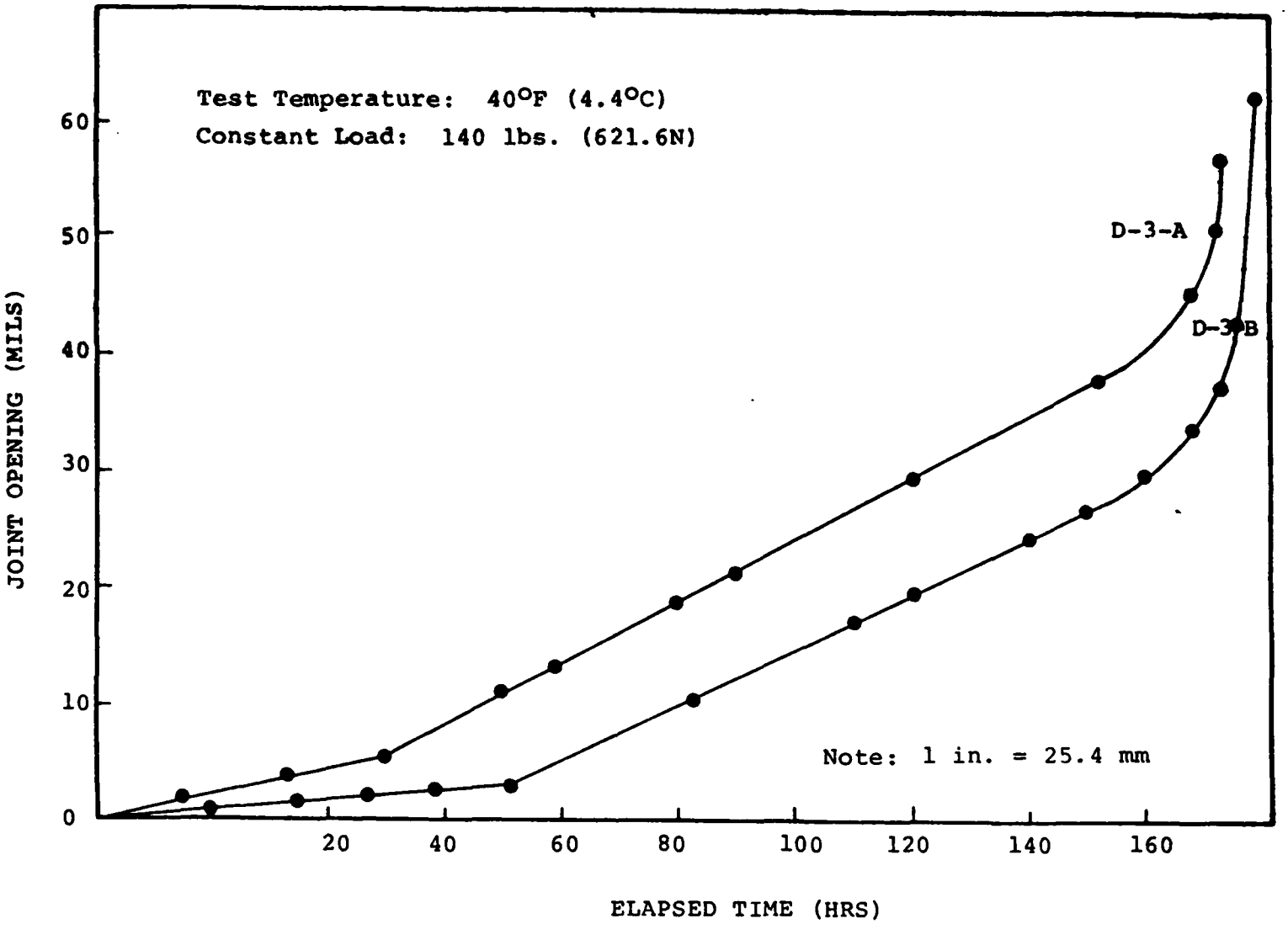
Test Temperature: 40°F (4.4°C)
Constant Load: 140 lbs. (621.6N)
D-3-A
D-3-B
Note: 1 in. = 25.4 mm
JOINT OPENING (MILS)
0
10
20
30
40
50
60
20
40
60
80
100
120
140
160
ELAPSED TIME (HRS)

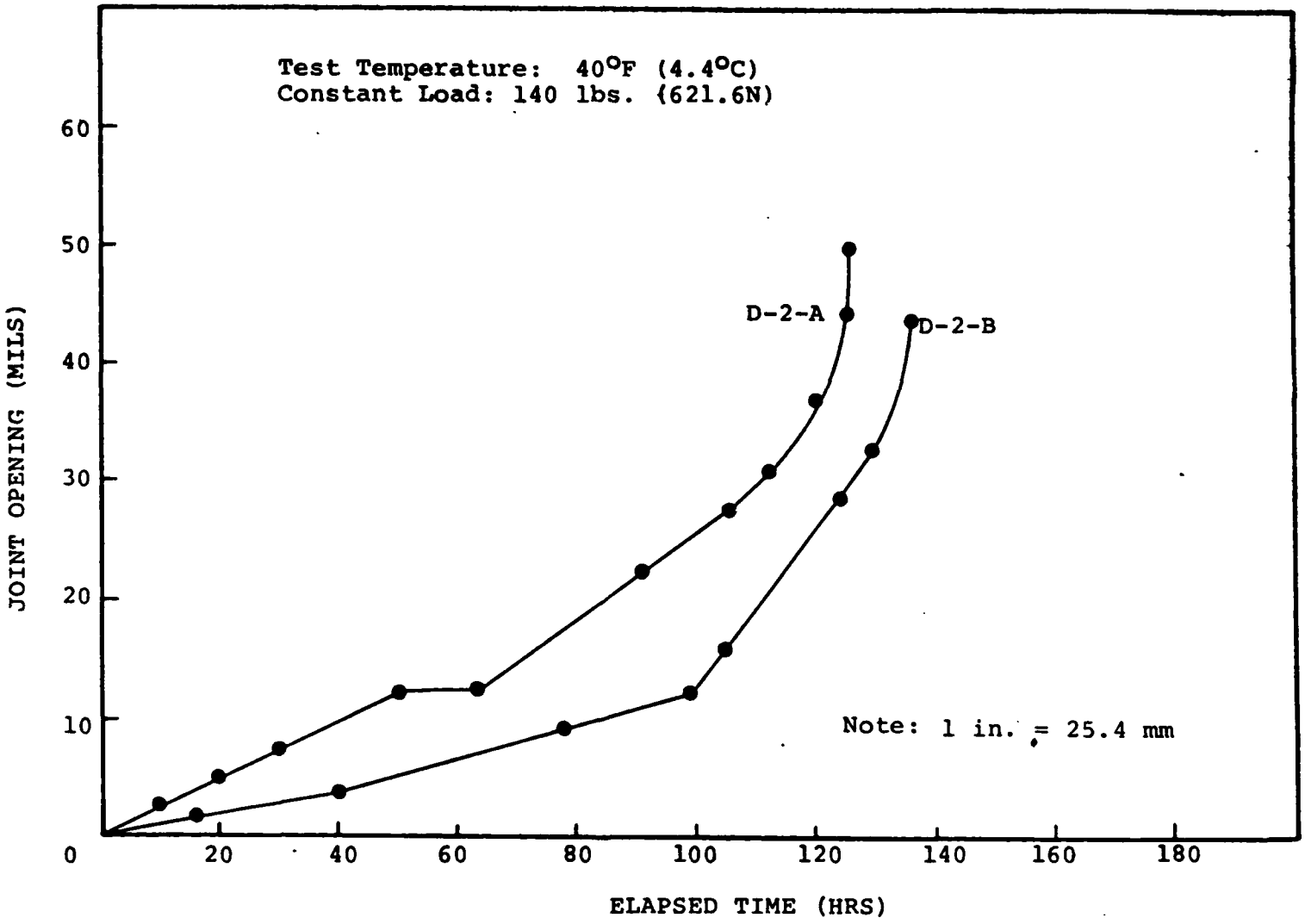
Test Temperature: 40°F (4.4°C)
Constant Load: 140 lbs. (621.6N)
D-2-A
D-2-B
Note: 1 in. = 25.4 mm
JOINT OPENING (MILS)
ELAPSED TIME (HRS)
0
10
20
30
40
50
60
20
40
60
80
100
120
140
160
180

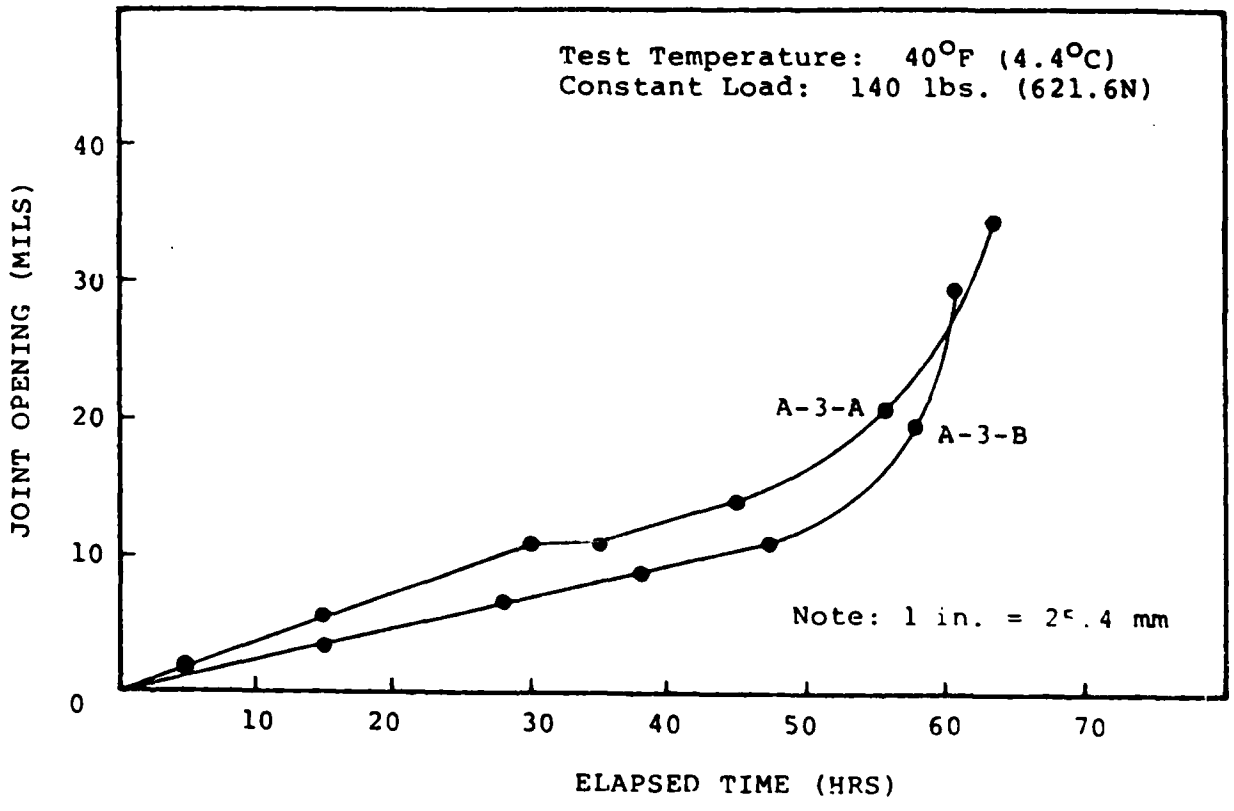
Test Temperature: 40°F (4.4°C)
Constant Load: 140 lbs. (621.6N)
JOINT OPENING (MILS)
0
10
20
30
40
A-3-A
A-3-B
Note: 1 in. = 25.4 mm
10
20
30
40
50
60
70
ELAPSED TIME (HRS)

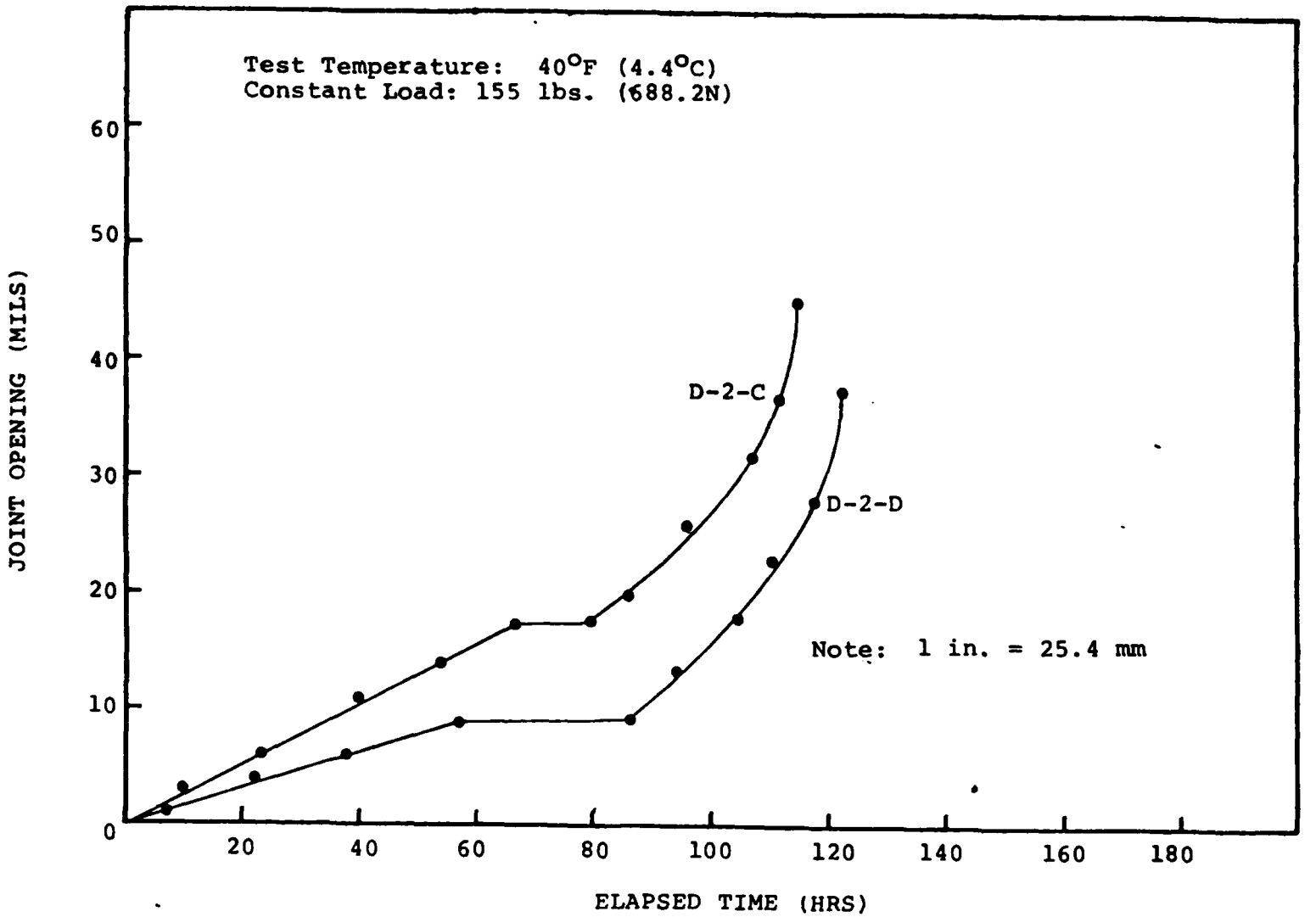
Test Temperature: 40°F (4.4°C)
Constant Load: 155 lbs. (688.2N)
JOINT OPENING (MILS)
0
10
20
30
40
50
60
D-2-C
D-2-D
Note: 1 in. = 25.4 mm
20
40
60
80
100
120
140
160
180
ELAPSED TIME (HRS)

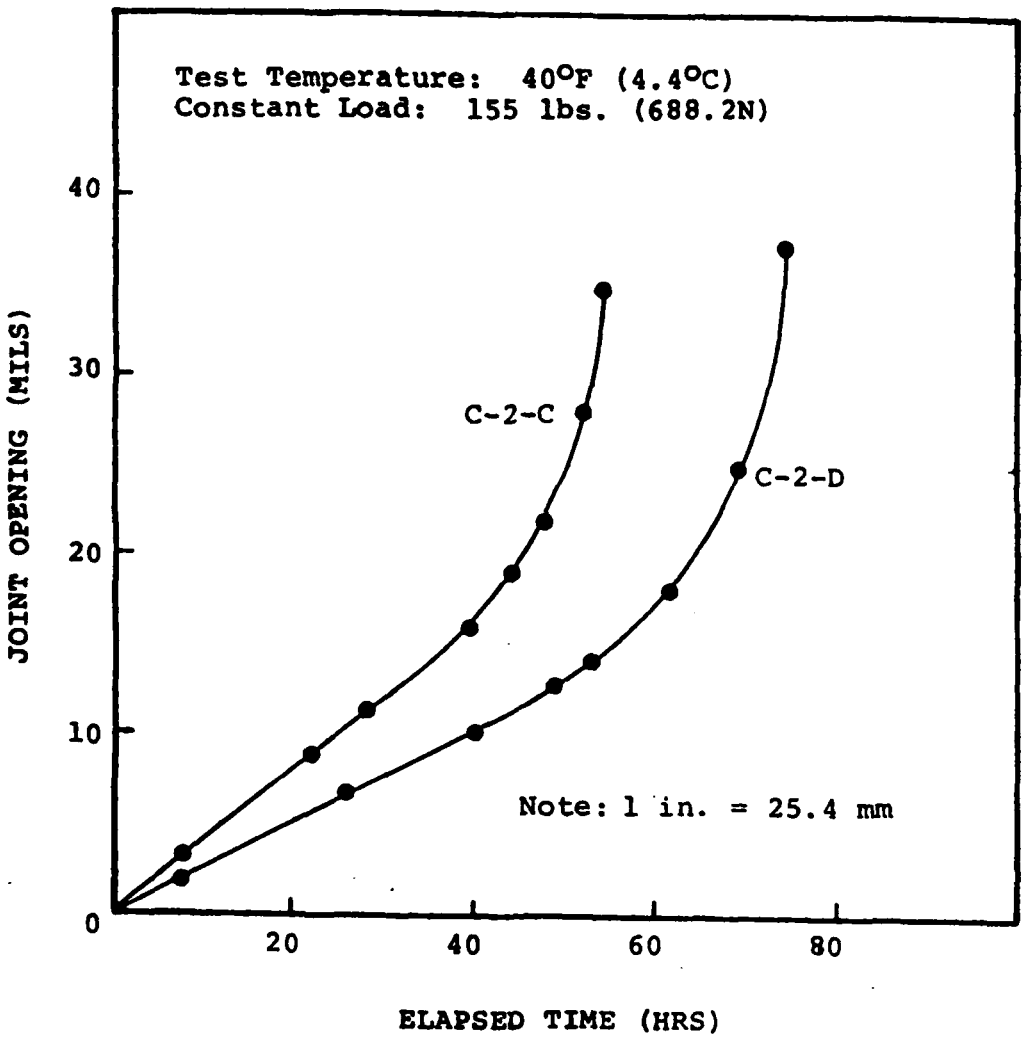
Test Temperature: 40°F (4.4°C)
Constant Load: 155 lbs. (688.2N)
C-2-C
C-2-D
Note: 1 in. = 25.4 mm
JOINT OPENING (MILS)
ELAPSED TIME (HRS)
0
10
20
30
40
20
40
60
80

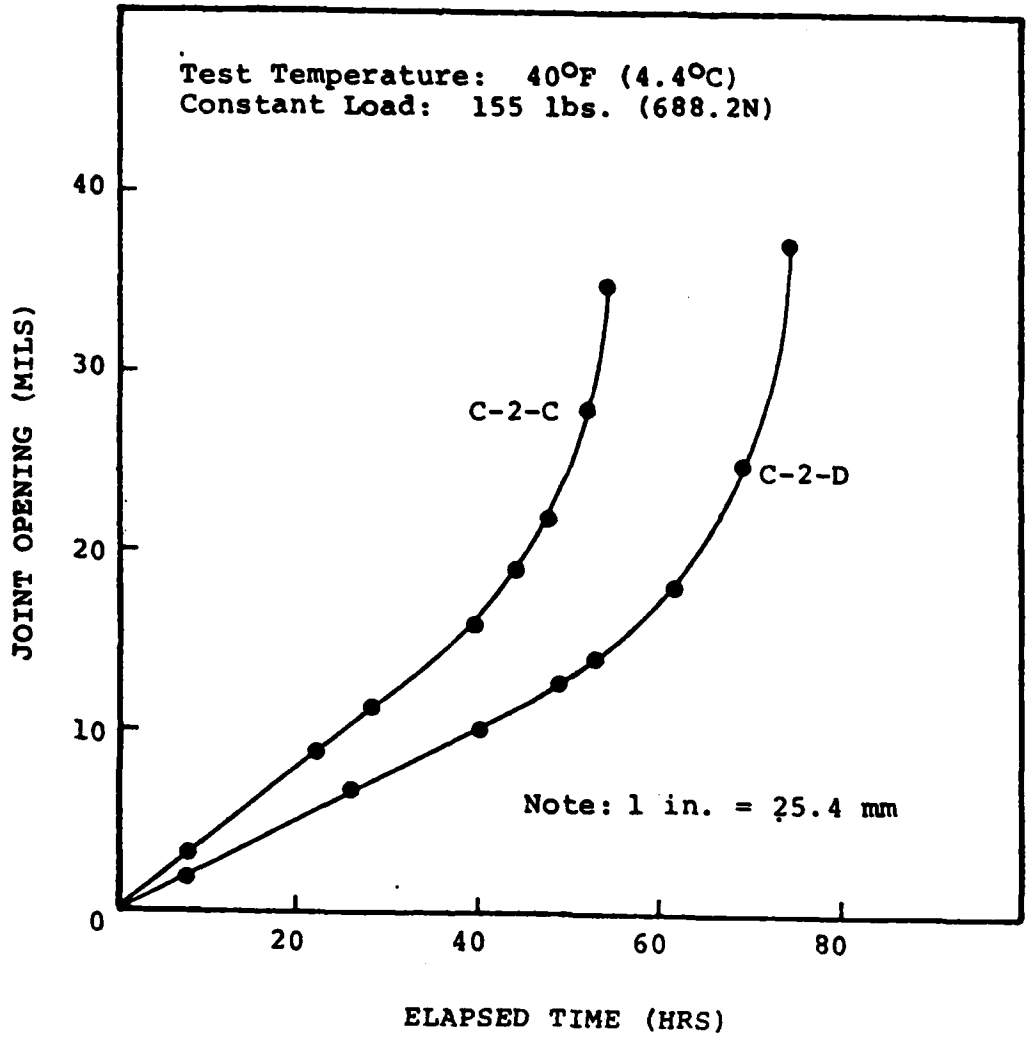
Test Temperature: 40°F (4.4°C)
Constant Load: 155 lbs. (688.2N)
JOINT OPENING (MILS)
0
10
20
30
40
C-2-C
C-2-D
Note: 1 in. = 25.4 mm
20
40
60
80
ELAPSED TIME (HRS)

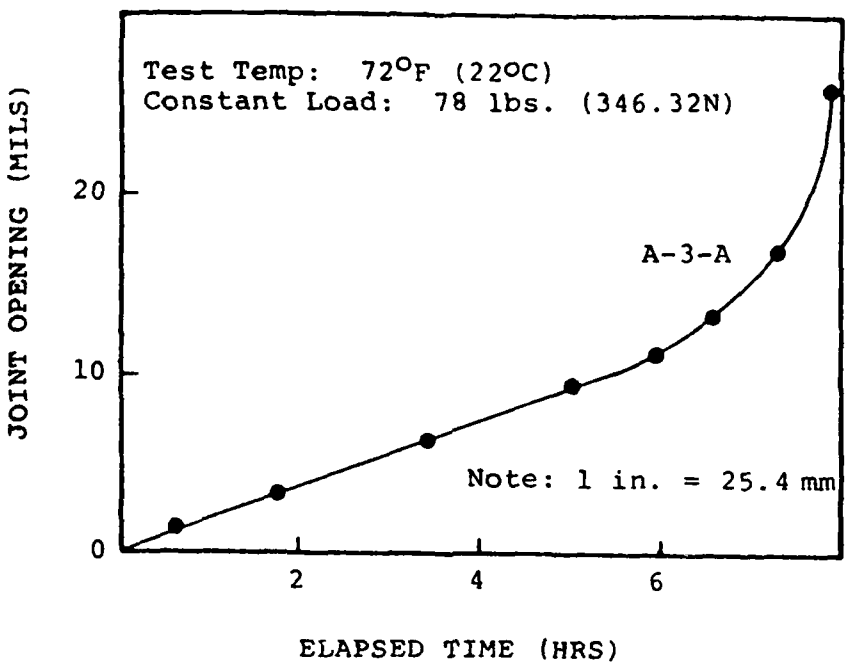
Test Temp: 72°F (22°C)
Constant Load: 78 lbs. (346.32N)
A-3-A
Note: 1 in. = 25.4 mm
JOINT OPENING (MILS)
0
10
20
2
4
6
ELAPSED TIME (HRS)

APPENDIX C

MECHANISTIC METHODOLOGY FOR AIRPORT PAVEMENT DESIGN WITH ENGINEERING FABRICS

PHASE II: USER GUIDE

EFRON USERS MANUAL

1. PROGRAM CAPACITY

EFRON is a computer program designed to analyze stress-strain distribution for existing pavements covered with rigid or flexible overlays. It is based on the theory described in Volume 1 of this report.

An existing pavement structure can be supported by an N-layered elastic foundation (N<3) which is represented in this program by a stiffness matrix computed based upon Burmeister's solution of 3 dimentional semi-infinite space. Overlay structure can contain an engineering fabric which can act as a bond breaker and/or as a reinforcement. EFRON utilizes a two-dimentional finite element approach and has the following capabilities:

1. Slabs can have a variable length and can be divided for regular or irregular infinite element mesh, which is automatically created by the program.

2. Boundary conditions are assumed by the program depending on assumed load type, support structure and boundary condition option.

3. Three types of the foundations can be specified as an option:
   a) solid elastic
   b) Winkler
   c) Rigid

4. Three load types, or any combination of these, are available:

   a) Vertical Load (mechanical)
   b) Vertical temperature gradient (daily temperature change)
   c) Uniform temperature load (seasonal temperature change)

5. Number of support layers can be varied from 1 to 3.

6. Iteration procedure can be specified as an option due to partial contact and/or elasto-plastic shear resistance between slab and foundation. A special bond type element has been applied for this feature.
7. Engineering fabric is simulated by N-layered stripe which can be placed at any position in the overlay. The number of fabric layers (N) can vary from 0 (no fabric) to 4. Each layer of this stripe can have separate material and geometric properties.

8. All material properties of the structure may be orthotropic and/or temperature dependent. This feature is extremely important for fabric whose modulus in vertical directon is different from horizontal.

9. Transverse joint may be plain or doweled.

10. Dowel bar looseness can be specified between 0 and 8 mil (0 and .2 mm) by a stiffness reduction function developed by Resource International Inc.

11. Variable size void under the slabs can be specified.

12. Plane stress or plane strain analysis can be specified.

13. New pavement or overlay design can be performed.

14. Up to 10 different cracks can be specified in different locations of the slabs.

A Simplified flow chart of the EFRON computer program is shown in Figure 1.

2. FINITE ELEMENTS MESH AND BOUNDARY CONDITIONS

A finite element mesh, as well as boundary conditions, will be generated automatically by the program depending on imput parameters (see below for input instructions and mesh examples). However, the following recommendations for the use of boundary

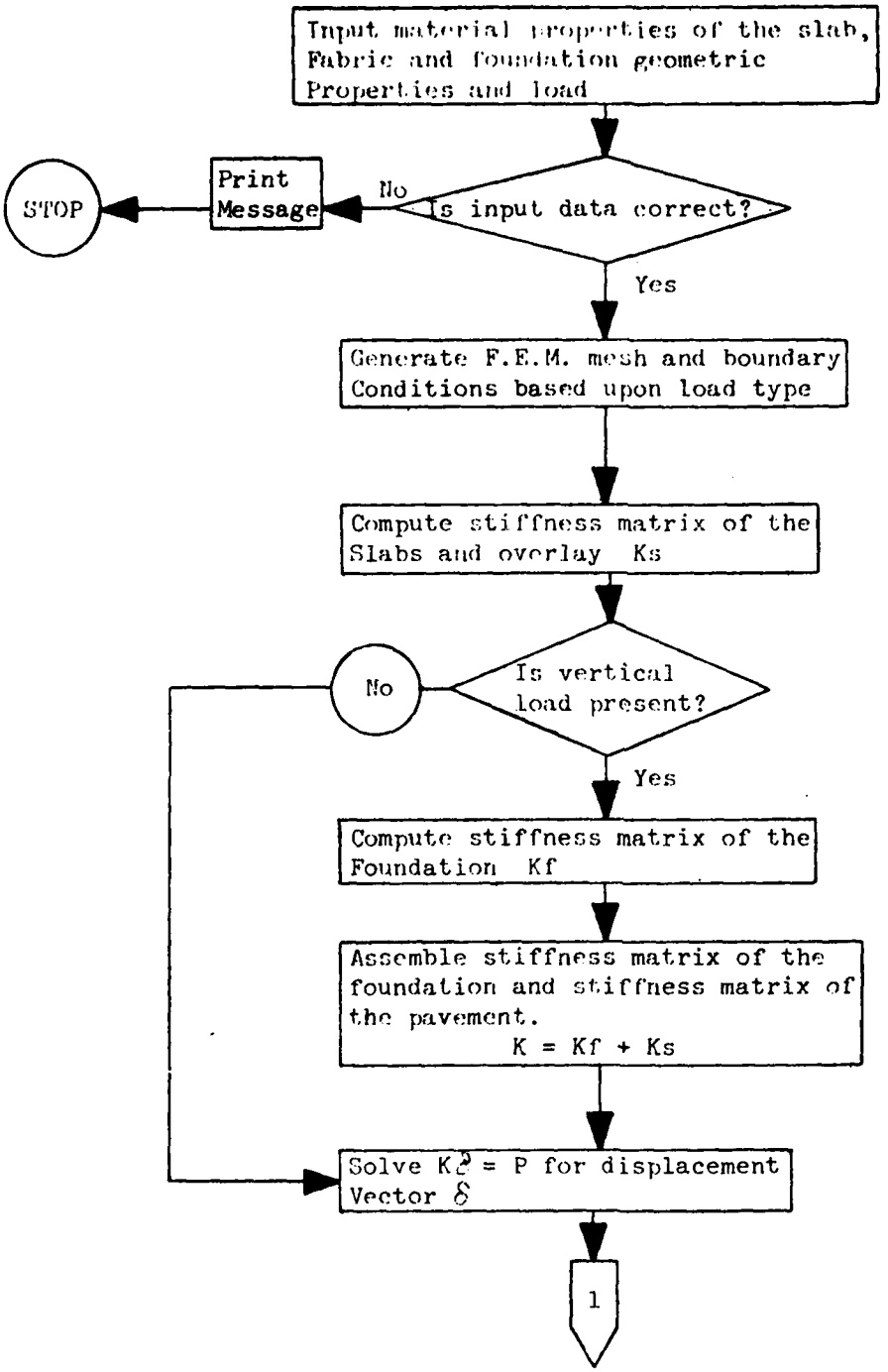

Figure 1. Flow Chart of EFRON

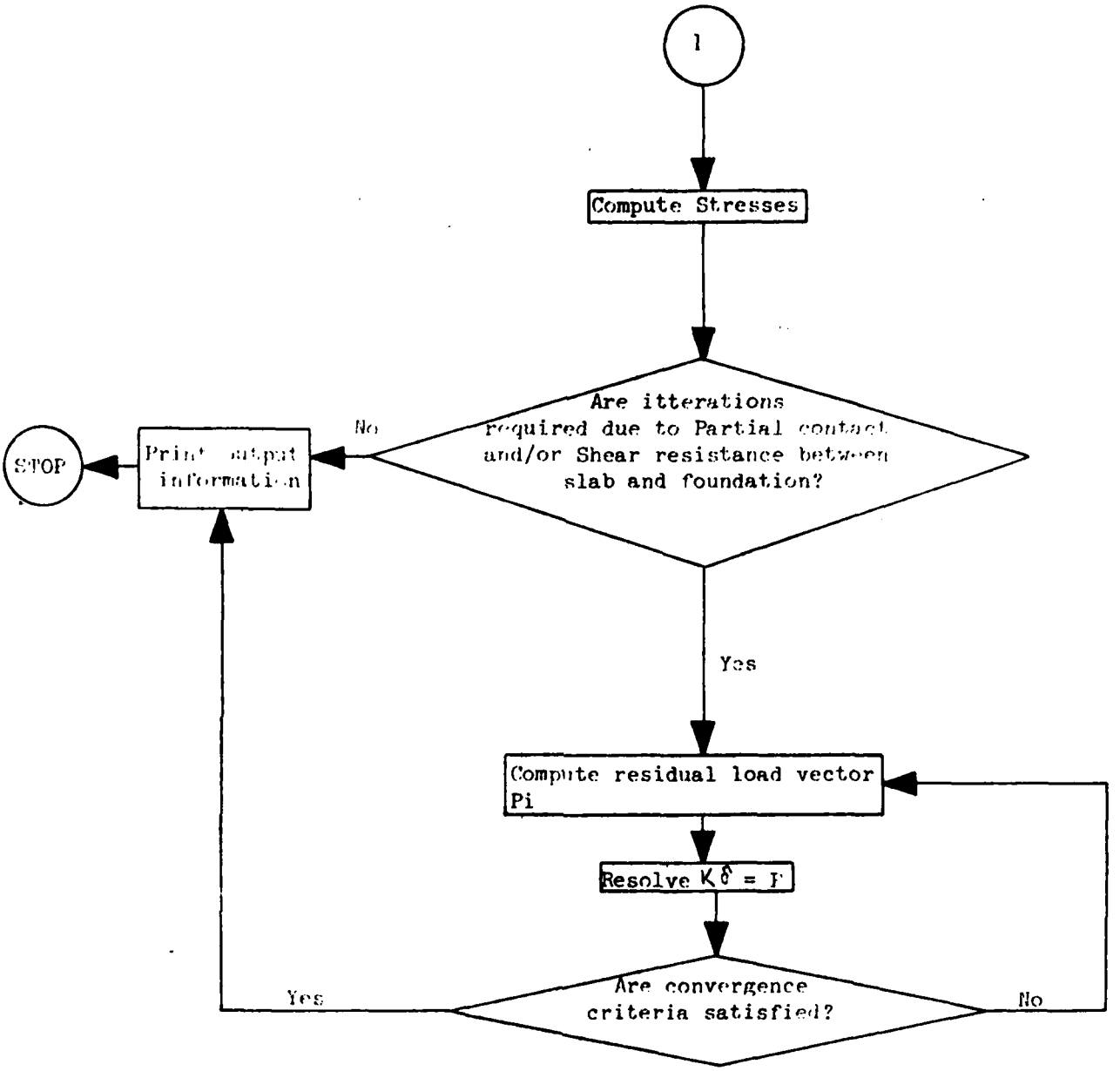

Figure 1 (cont'd). Flow Chart of EFRON

conditions option and mesh type options should be considered:

1. Use regular mesh in case of no mechanical load applied on the structure (IR=0).

2. Restrict horizontal movement on each edge in the above case (IBC=0). This boundary condition means that this is a double symmetry case.

3. Using a partial restriction in x,y directions is recommended in case of a simulation of the support of the infinite or very long slab. This is a Winkler type of spring and its axial stiffness calculation is not very precise.

4. Do not use a very small or very large element size in case of regular mesh. A very small size significantly increases computation time. A very large size decreases result credibility. Recommended size is 1/12 - 1/15 of a single slab length.

5. Assume a minimum vertical element size (DLSIZE) equal

   DLSIZE =.2*TH(1)

where

   TH(1) overlay thickness

   This assumption will result in a more correct stress above the joint.

Figure 2 shows a two-dimentional representation of the overlayed pavement structure used in the finite element (EFRON) program. This figure shows also the definition of several of the input variables. Figure 3 shows a possible FEM mesh for this pavement which is an irregular mesh in this case. As was stated above, the irregular mesh is recommended in the case of wheel load (mechanical load), but a regular mesh should be used with thermal loads.

The information required as input is described in Table 1 in conjunction with Figures 2 through 4. The makeup of the data deck is shown in Figure 5. It may seem from these figures as of a great deal of data is required; however, the imput data is in

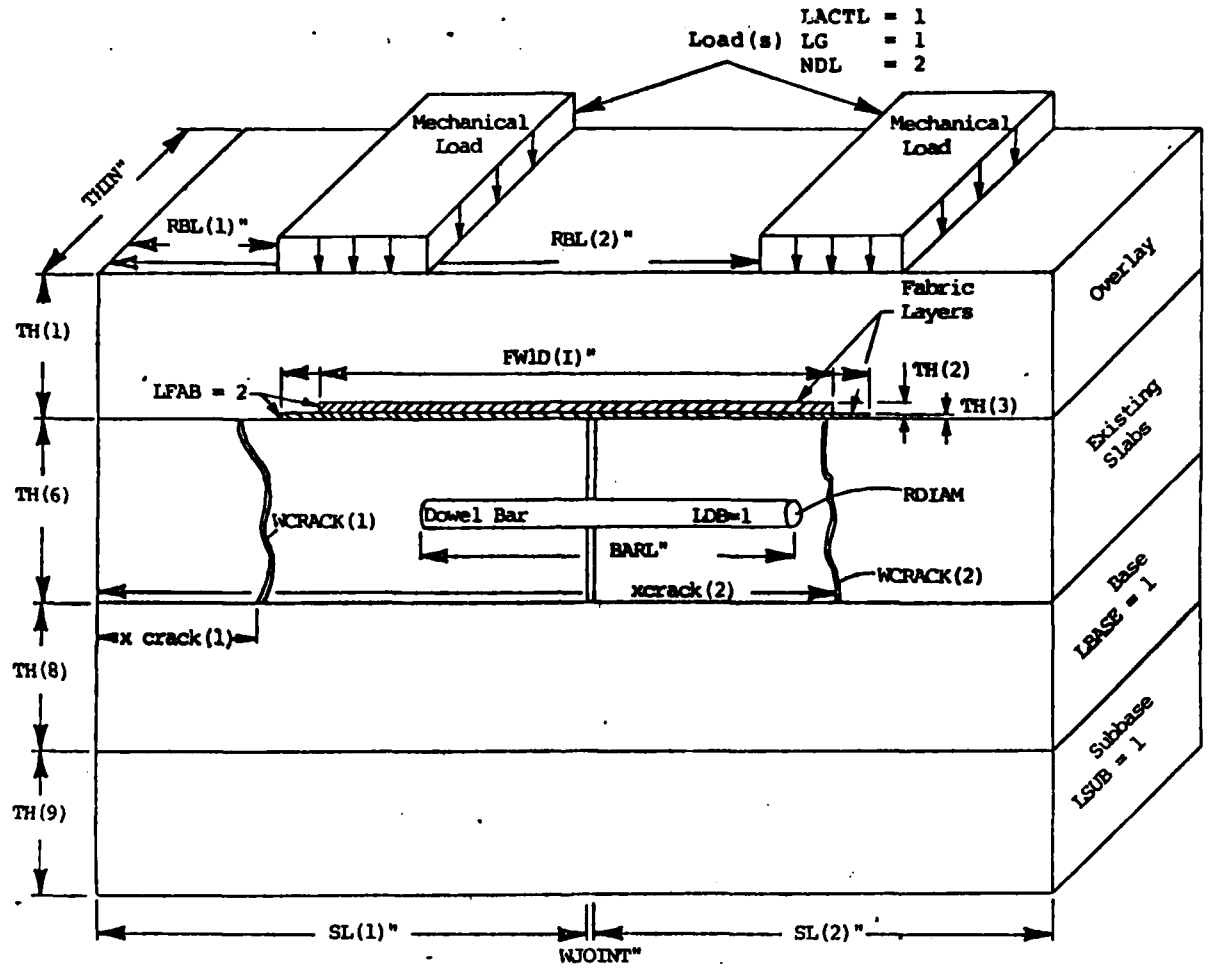

Figure 2. 2-Dimensional Representation of Pavement System

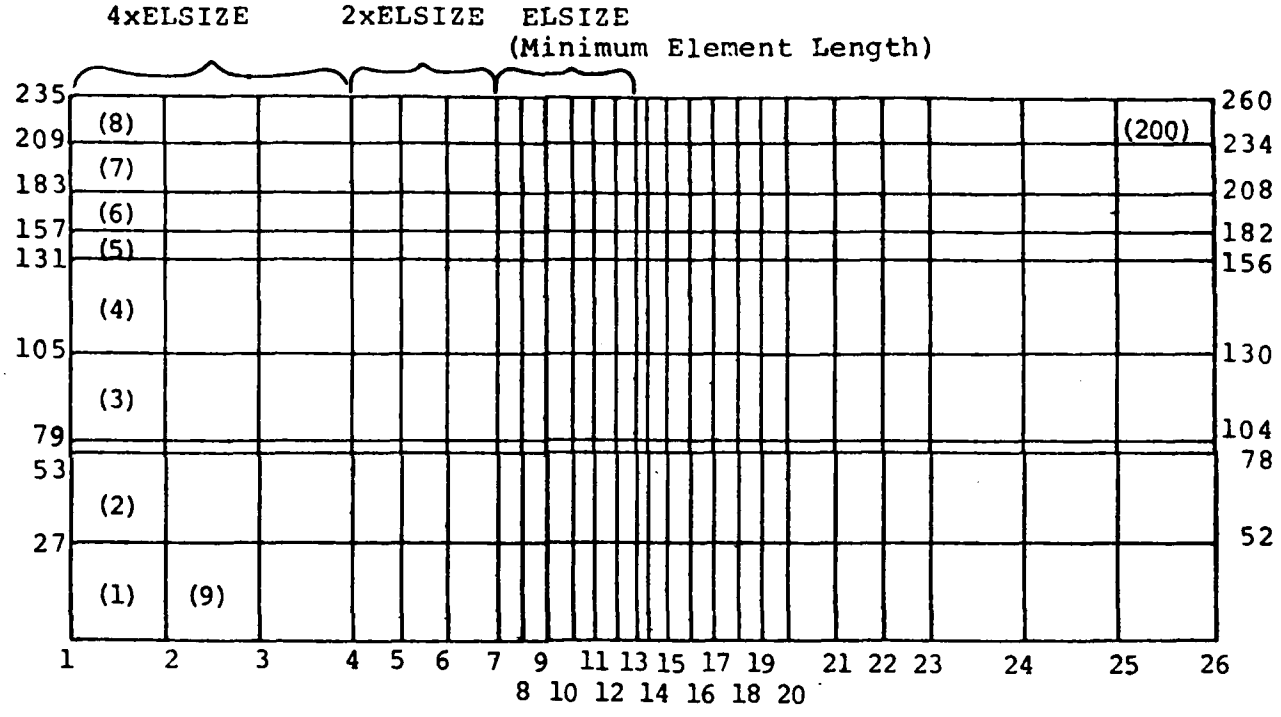

NOTE: The minimum element size (ELSIZE) is not uniform within an irregular mesh.

Figure 3. Example of an irregular mesh, IR = 1

If output is desired for one or N groups of elements only:

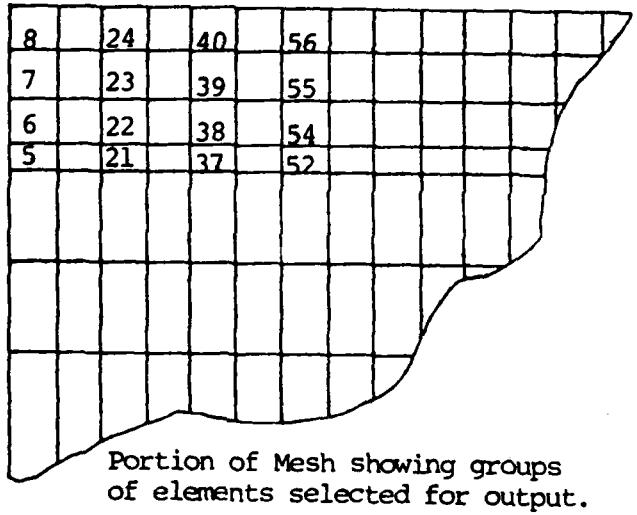

Portion of Mesh showing groups of elements selected for output.

Input cards, starting from card XXIII to N cards would be:

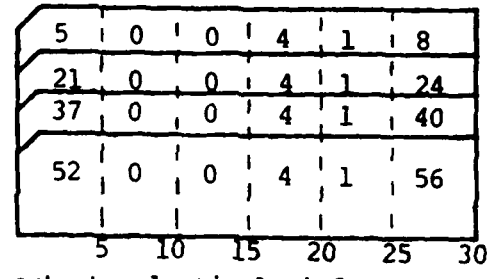

To output selectively information on N groups of elements, N cards must be used. LASTEL on all but the very last card must be blank; this indicates to the program that there are more cards to follow, on the last card LASTEL must be 777 to indicate there are no more cards or groups of elements to output.

Figure 4. Example of Selective Output, IO = ∅

Table #1

DESCRIPTION OF INPUT DATA

CARD	FORMAT	VARIABLE	COL.	DESCRIPTION & VALUE RANGE	COMMENTS
I	20A4	1 Title	1-80	Any alphanumeric data.	
II	A1	1 LDTYPE	1	Design Type Option. '1' - New Pavement Design. LDTYPE = '0' - Overlay Design.	
III	14I5	1 LACTL	1-5	Mechanical Load Indicator. '0' - No mechanical load. LACTL = 1 - 'Mechanical & Gravity'.	
		2 LTEMP	6-10	Horizontal Temperature Load Indicator. 0 - No uniform Temp. change LTEMP = 1 - 'Uniform Temp. change'.	
		3 LTG	11-15	Temperature Gradient Indicator. 0 - No vertical temp. gradient. LTG = 1 - 'Vertical Temp. Gradient'.	
		4 ITER	16-20	Number of Iterations. 0 - No iterations. ITER = N	$N \leq 25$

Table #1
cont'd
DESCRIPTION OF INPUT DATA

CARD	FORMAT	VARIABLE	COL.	DESCRIPTION & VALUE RANGE	COMMENTS
III cont'd		5 LDB	21-25	Dowel Bar Option. 0 - No dowel bars. LDB = 1 - Dowel joint	
		6 LFAB	26-30	Number of Fabric layers. 0 - No fabric LFAB = 1 2 3 4	Only 3 in case of "NEW" pavement design.
		7 LBASE	31-35	Base Option. 0 - No base. LBASE = 1 - Base.	Further explanation of LBASE in Fig. 2.
		8 LSUB	36-40	Subbase Option 0 - No subbase. LSUB = 1 - Subbase.	Further explanation of LSUB in Fig. 2.
		9 LVOID	41-45	Void Option. 0 - No void LVOID = 1 - Void.	
		10 LSHOUL	46-50	Shoulder Boundary Condition Option. 0 - No shoulder. LSHOUL = 1 - Shoulder.	Further explanation of LSHOUL in Fig. 2. If L should = 1 IBC must be 1

Table #1
cont'd
DESCRIPTION OF INPUT DATA

CARD	FORMAT	VARIABLE	COL.	DESCRIPTION & VALUE RANGE	COMMENTS
III cont'd		11 IBC	51-55	Side Boundary Condition Option. -1 - Free. IBC = 0 - Restricted in X Direction 1 - Partially restricted in X & Y direction	Further explanation of IBC in Fig. 2.
		12 IRIG	56-60	Support Condition Option. 0 - Elastic Subgrade. IRIG = 1 - Rigid Subgrade. -1 - Winkler type subgrade	For IRIG = 1 IBC must be ≤ 0
		13 NANAL	61-65	Design Type. 2 - Plane Stress Analysis. NANAL = 1 - Plane Stress Analysis	
		14 NCRACK	66-70	Number of Intermediate Crack 0 - No cracks. NCRACK = N $\leq$ 10	Further explanation of NCRACK in Fig. 2. Only for rigid or winkler support.
IV	6I5	1 NMG	1-5	Mesh Generator Option. 0 - Mesh will be created manually. NMG = 1 - Mesh will be created be program.	Extra information is necessary for NMG=0
		2 NGRAF	6-10	Graphical Output Option. 0 - No graphical output.	Required hardware-Tektronix 4025.

Table #1
cont'd
DESCRIPTION OF INPUT DATA

CARD	FORMAT	VARIABLE	COL.	DESCRIPTION & VALUE RANGE	COMMENTS
IV cont'd		2 NGRAF (Cont'd)		NGRAF = 1 - Graphical Output.	
		3 LG	11-15	Load Generator Option. 0 - Every Nudal Point Load Must be entered. LG = 1 - Load Vector will be calculated by given distributed load.	
		4 IR	16-20	Mesh Type Option. 0 - Regular Mesh. IR = 1 - Irregular Mesh.	Further explanation of IR in Fig. 3 & 4.
		5 INFROST	21-25	Stiffness Information Option. -1 - Complete Matrix Information NFOST = 0 - No matrix information 1 - Stiffness matrix information	Matrix information on Logical Unit 7.
		6 IO	26-30	Input/Output Option. -1 - Complete F.E.M. Information. IO = 0 - Selective Output. (Refer to Card XXIV.) 1 - Full output.	All information on Logical Unit 6.
V	8F10.0	1 XCRACK(1)	1-10	X Coordinate for Crack Location	Omit this card if NCRACK = 0 Use another card if necessary.
		2 WCRACK(1)	11-20	Crack Width	

Table #1
cont'd
DESCRIPTION OF INPUT DATA

CARD	FORMAT	VARIABLE	COL.	DESCRIPTION & VALUE RANGE	COMMENTS
V cont'd	8F10.0	2 WCRACK(1) (CONT'D) . . . . XCRACK(10) WCRACK(10)	11-20		
VI	4F10.0	1 SL(1)	1-10	Length of Slab #1.	(For Entire Card)
		2 SL(2)	11-20	Length of Slab #2.	Use Card #VIA
		3 WJOINT	21-30	Joint Width. (in.)	LDTYPE = '1'.
		4 ELSIZE	31-40	Minimum Element Length (in.)	Further explanation in Fig. 2.
		5 DLSIZE	41-50	Minimum Element Vertical Size(in)	Used only for bottom of Overlay.
VIA	2F10.0	1 SL(1)	1-10	Length of Slab.	Use this Card Only if LDTYPE = '1'.
		2 ELSIZE	11-20	Minimum Element Size. (in.)	

Table #1
cont'd
DESCRIPTION OF INPUT DATA

CARD	FORMAT	VARIABLE	COL.	DESCRIPTION & VALUE RANGE	COMMENTS
VIA cont'd		3 DLSIZE	21-30	Minimum Element Vertical Size (in)	
VII	6F10.0	1 TH(1)	1-10	Thickness of the Top Layer	
		2 E(1,1)	11-20	Elastic Modulus of the Top Layer.	
		3 V(1,1)	21-30	Poisson's Ratio of Top Layer.	
		4 ALFA(1)	31-40	Coefficient of Thermal Expansion.	
		5 E(1,4)	41-50	Shear Modulus of the Top Layer.	
		6 THIN	51-60	Width of the Slab.	Omit this Variable if NANAL = 1.
VIII	F10.0	FWID	1-10	Fabric Width for Fabric Layer #I. Minus joint width	1)Omit Cards VIII & IX if LFAB = 0.
IX	5F10.0	1 TH(I)	1-10	Thickness of Fabric Layer (I).	
		2 E(I,1)	11-20	Elastic Modulus of Fabric Layer(I)	2)Repeat Cards VIII & IX for LFAB times.
		3 V(i,1)	21-30	Poisson's Ratio of Fabric Layer(I)	
		4 ALFA(I)	31-40	Coefficient of Thermal Expansion.	I = 1, 2, 3, 4
		5 E(I,4)	41-50	Shear Modulus of Fabric Layer (I)	

Table #1
cont'd
DESCRIPTION OF INPUT DATA

CARD	FORMAT	VARIABLE	COL.	DESCRIPTION & VALUE RANGE	COMMENTS
X	F10.0	FPOS	1-10	Position of the Fabric From the Bottom of the Top Layer	Omit this Card if LDTYPE = 0
XI	5F10.0	1 TH(6)	1-10	Same as Card VII (for Layer #2)	
		2 E(6.1)	11-20	Same as Card VII (for Layer #2)	
		3 V(6,1)	21-30	"	
		4 ALFA(6)	31-40	"	
		5 E(6,4)	41-50	"	
XII	2F10.0	1 ESUB	1-10	Subgrade Modulus.	Omit this Card if IRIG = 1
		2 VSUB	11-20	Subgrade Poisson's Ratio.	
XIII	3F10.0	1 TH(8)	1-10	Base Thickness.	Omit this Card if LBASE =
		2 E(8,1)	11-20	Base Modulus.	Omit Cards XII, XIII, XIV if LACTL = 0
		3 V(8,1)	21-30	Base Poisson's Ratio	
XIV	3F10.0	1 TH(9)	1-10	Subbase Thickness	Omit this Card if LSUB =
		2 E(9,1)	11-20	Subbase Modulus.	
		3 V(9,1)	21-30	Subbase Poisson's Ratio.	

Table #1
cont'd
DESCRIPTION OF INPUT DATA

CARD	FORMAT	VARIABLE	COL.	DESCRIPTION & VALUE RANGE	COMMENTS
XV	2F10.0	1 VWID(1)	1-10	Void Size for Slab #1, measured from the joint.	Omit Card if LVOID = 0.
		2 VWID(2)	11-20	Void Size for Slab #2, measured from the joint.	
XVI	5F10.0	1 RDIAM	1-10	Diameter of the Dowel Bar (in.)	Omit Card if LDB = 0
		2 ALOOS	11-20	Looseness of the Dowel Bar (in.)	
	2F10.0	3 E(10,1)	21-30	Modulus of the Dowel Bar.	
		4 V(10,1)	31-40	Poisson's Ratio of the Dowel Bar.	
		5 BARL	41-50	Dowel Bar Length (inches).	
XVII	2F10.0	1 ARATIO	1-10	Convergence Criteria. Must be between 0 & 1.	If ARATIO = 0, Default Value of ARATIO = .1.
		2 TFORCE	11-20	(Presently Not Used in Program)	
XVIII	F10.0	UTEMP	1-10	Uniform Temperature Change (^{o}F).	Omit Card if LTEMP = 0.
XIX	F10.0	TG	1-10	Vertical Temperature Gradient	Omit Card if LTG = 0.
XX	5F10.0	1 SNORM	1-10	Normal Stiffness for Joint Element (psi)	
		2 SSHR	11-20	Shear Stiffness for Joint Element (psi)	

Table #1
cont'd
DESCRIPTION OF INPUT DATA

CARD	FORMAT	VARIABLE	COL.	DESCRIPTION & VALUE RANGE	COMMENTS
XX cont'd		3 THE	21-30	Coefficient of Thermal Expansion	
		4 FRIC	31-40	Coefficient of Friction.	
		5 COH	41-50	Cohesion.	
XXI	15,F10.0	1 NLO	1-5	**Nodal Point Number**	Omit Card if LG = 1.
		2 AFORCE	6-15	Load Magnitude.	Repeat Card XXI as many times as necessary.
		3 NDIR	16-20	Load Direction NDIR = 0 y direction NDIR = 1 x direction	Last Card of this set must be blank.
XXII	15	NDL	1-5	Number of Distributed Loads.	Omit Card if LG = 0.
XXIII	3F10.0	1 RBL	1-10	X Coordinate of Beginning of Dist. Load.	Omit this Card if LG = 0.
		2 RLOAD	11-20	Magnitude of Load.	Repeat this Card NDL times.
		3 PRES	21-30	Load Pressure.	
XXIV	6I5	1 NELM	1-5	Beginning element number (see mesh).	Use this Card only if IO = 1

Table #1
cont'd
DESCRIPTION OF INPUT DATA

CARD	FORMAT	VARIABLE	COL.	DESCRIPTION & VALUE RANGE	COMMENTS
XXIV cont'd		2 IOOP	6-10	Output options must always remain 1, 0, 8, 16, 20 or blank.	
		3 IOSTEP	11-15	Output options must always remain 1, 0, 8, 16, 20 or blank.	
		4 NMN	16-20	Number of repetitions (elements in the group).	
		5 NELST	21-25	Element step number.	Explained in Fig. 3.
		6 LASTEL	26-30	For more groups use or blank. For no more groups use 777.	Repeat this Card until LASTEL = 777 for as many groups of elements you would like to output.

CARD # \ COLUMN #	5	10	15	20	25	30	35	40	45	50	55	60	65	70	75	80	COMMENTS
I																	
II	1																
III	1	2	3	4	5	6	7	8	9	10	11	12	13	14			
IV	1	2	3	4	5	6											
V	1		2		3		4		5								
VI	1		2		3		4		5								
VIA	1		2		3												
VII	1		2		3		4		5		6						
VIII	1		2		3												
IX	1		2		3		4		5								
X	1																
XI	1		2		3		4		5								
XII	1		2														

Note: Numbers refer to variables, refer to Table #1.

Figure 5. Makeup of data deck

COLUMN # / CARD #	5	10	15	20	25	30	35	40	45	50	55	60	65	70	75	80	COMMENTS
XIII	1		2		3												
XIV	1		2		3												
XV	1		2														
XVI	1		2		3		4		5								
XVII	1		2														
XVIII	1																
XIX	1																
XX	1		2		3		4		5								
XXI	1	2															
XXII	1																
XXIII	1		2		3												
XXIV	1	2	3	4	5	6											

Note: Numbers refer to variables, refer to Table #1.

Figure 5 (cont'd). Makeup of data deck

general not difficult to generate once the user has decided on the appropriate options.

3. RECOMMENDATIONS OF INPUT MATERIAL PROPERTIES

As was stated previously, the slab support layers are characterized by using elastic layer theory; therefore, elastic material properties are required (Young's modulus, Poisson's ratio, and layer thickness) for each foundation layer as well as for the concrete slab. Additionally, flexural strength (28 day, 3 point loading) is required for concrete.

(a) The flexural strength (modulus of rupture) of most airport concretes is around 600 - 800 psi (4.1 to 5.5 MPa). This value is generally available from test data but may be estimated from unconfined compressive strength tests using the following ACI relationship:

$$fc = a\ f'c \qquad (1)$$

where

fc is the flexural strength
f'c is the compressive strength of standard 6 X 12 in. (152 X 305 mm) cylinders
a is a constant ranging from 7 to 10 for British units and 0.58 to 0.83 for International units.
The lower value should be used with high-strength concrete and the higher value for low strength concrete.

(b) The dynamic (tangent) modulus of highway concretes is around 5 million psi (34.5 GPa) within a range of 3.5 to 6 million psi (24.1 to 41.4 GPa). In the absence of specific test data, it may be estimated from the following ACI relationship:

$$Ec = 43 * {}^{1.5} * f'c \text{ (in psi)}$$

$$Ec = 0.056 {}^{1.5} f'c \text{ (in kPa)} \quad (2)$$

where

Ec is the tangent modulus
is the concrete unit weight
f'c is the compressive strength

Equation 2 is generally given for the secant modulus. Since the tangent modulus is usually 20 to 30 percent higher than the secant modulus, the coefficients in equation 2 have been increased by 30 percent over the values recommended by ACI for secant modulus (for a more conservative design) because critical stresses in concrete increase with increasing concrete modulus.

(c) The Poisson's ratio values in Table 2 are recommended. The analysis is rather insensitive to Poisson's ratio so that precise values are not required.

(d) Subgrade modulus may be obtained from laboratory tests in triaxial compression, or may be estimated from AASHTO soil classification, soil support values, or modulus of subgrade reaction, using Figure 6 to estimate the CBR value, and Equation 3 to compute the modulus.

$$Es = 1500 \text{ CBR (in psi)}$$

$$Es = 10.3 \text{ CBR (in MPa)} \quad (3)$$

(e) Granular base/subbase moduli may be obtained from laboratory tests in triaxial compression, or may be estimated from Equation 4:

$$En\text{-}l = 11.06 \, EN^{0.837} \text{ (in psi)} \quad (4)$$

TABLE 2

RECOMMENDED POISSON'S RATIOS

Material	Poisson's Ratio
Concrete	0.15
Asphaltic concrete	0.40
Granular base	0.37
Cement-treated base	0.20
Lime-stabilized soil	0.35
Subgrade	0.45

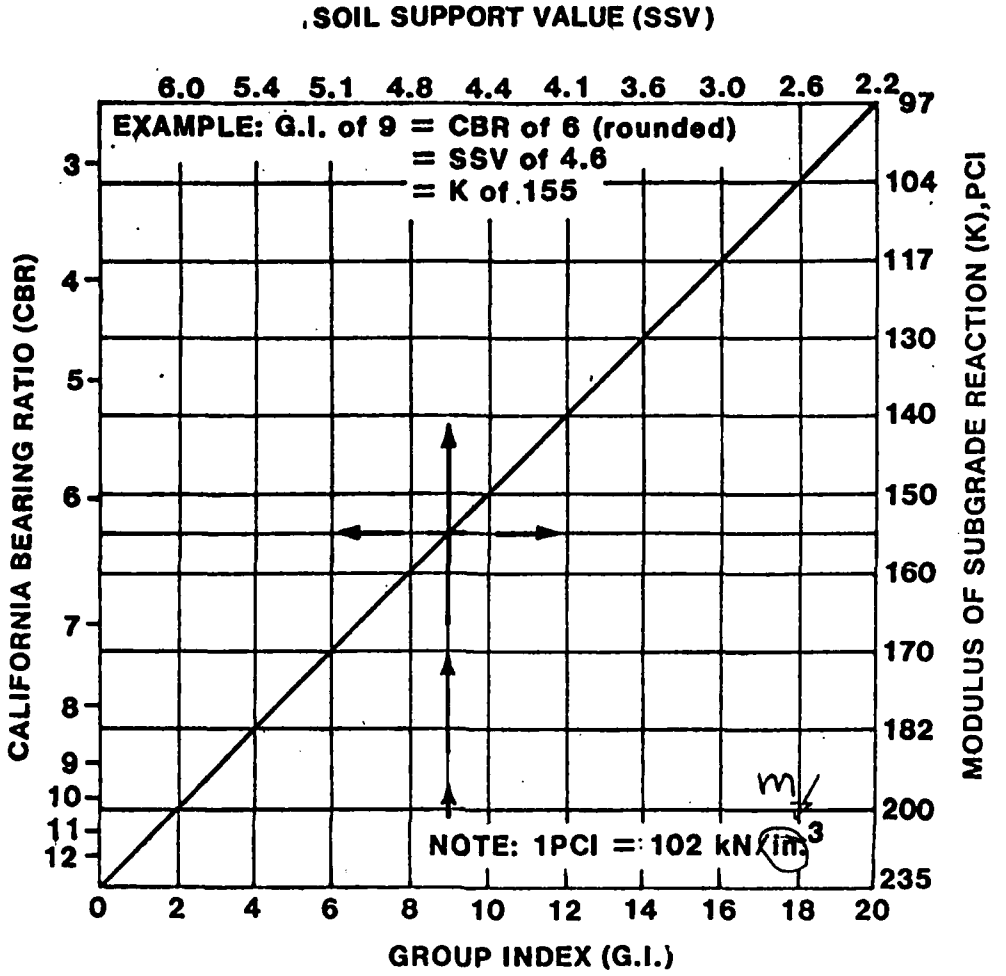

Figure 6. Relation between soil properties and CBl2.

where

EN = modulus of the nth layer above it.
EN-1 = modulus of the layer

This equation is a compromise between the Shell COE, and Kentucky models and recognizes the fact that the degree of compaction of granular materials depends on the modulus of the underlying layer. If both a subbase and a base layer is used, Equation 4 should be applied twice, first to determine the subbase modulus from subgrade, then the base modulus from subbase modulus. Sensitivity analyses using both elastic layer theory as well as the RISC program show that the critical stress in concrete is only slightly dependent of the value of the base/subbase modulus; therefore, exact values for these layers are not required.

(f) The modulus of asphalt bases is temperature dependent and should be estimated at mean annual temperature. This mean temperature depends on the slab thickness and the base thickness as well as on the mean annual air temperature, but using mean annual air temperature will be adequate in most cases. Figure 7 may be used in absence of test data.

(g) The moduli of cement-treated bases are quite variable, depending on aggregate type and the cement contents; therefore, the use of laboratory test data is recommended.

The above discussion should provide the user some guidelines in the selecton of imput parameters required for this design program. However, since the program has the capability of analyzing a wide variety of programs, some planning and forethought is recommended.

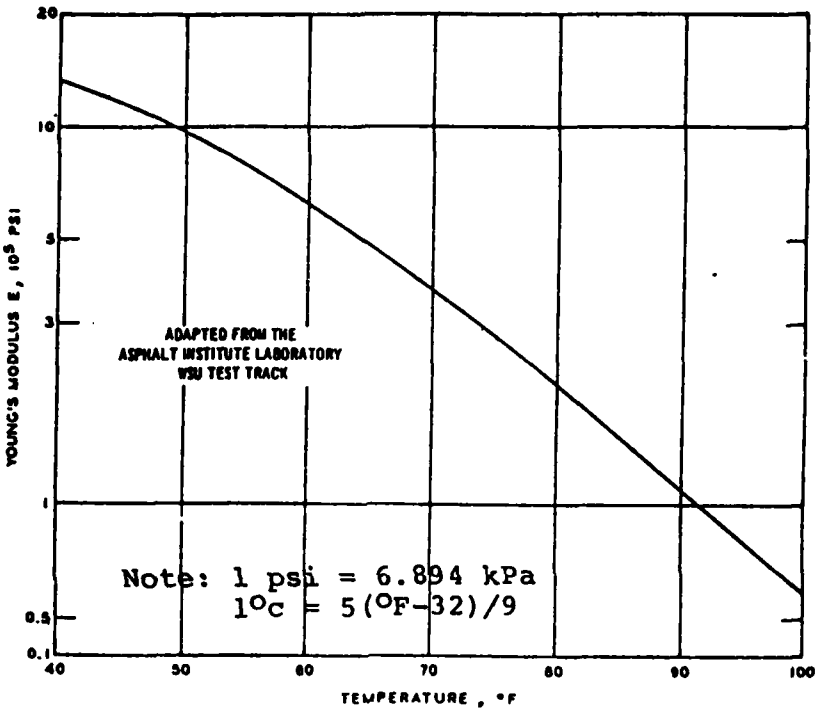

Figure 7. Assumed temperature dependence of Young's modulus of AC pavements and AC base materials

DESIGN EXAMPLE USING EFRON

*** PAVEMENT DESIGN ***

FEDERAL AVIATION ADMINISTRATION

PAVEMENT DESIGN PROGRAM

(MECHANISTIC APPROACH)

Version 1 February 1983

Developed by Resource International Inc.
130 E. Wilson Bridge Rd.
Worthington, Ohio 43085
Tel. (614) 885-1959

```
FAA 10043 40@ VERTICAL LOAD =200 LB
0
     1     0     0    00     0     1     1     0     0     0    -1     1     2     0
     1    01     1     0   000     1
12.          12.          .125          1.              .2
2.00         1112000.     .35           .0000056                3.
24.
.025         1112000.     .35           .0000056
1.5          4400000.     .15           .0000056
6.           300.         .47           .0000056
0.0          0.00
4400000.     .001         .000006    1.5          10.
     1
11.0625      200.         -33.333333
```

PROJECT TITLE : FAA 10043 40@ VERTICAL LOAD =200 LB

OVERLAY DESIGN

THE DESIGN PARAMETERS

I. APPLIED LOAD

MECHANICAL + GRAVITY

II. SUPPORT TYPE AND BOUNDARY CONDITIONS

BASE
RIGID SUBGRADE
SIDE BOUNDARY CONDITIONS: FREE

III. REINFORCEMENT TYPE

1-LAYERED FABRIC

IV. STRESS ANALYSIS TYPE

PLANE STRESS ANALYSIS
NO ITERATION SCHEME IS USED DUE TO PARTIAL CONTACT
AND/OR ELASTIC-PLASTIC SHEAR BOND CONDITIONS BETWEEN SLAB AND FOUNDATION

V. INPUT/OUTPUT OPTIONS

FULL OUTPUT
NO STIFFNESS MATRIX INFORMATION
F.E.M. MESH WILL BE CREATED BY THE PROGRAM
MESH TYPE IS REGULAR
GRAPHICAL OUTPUT WILL BE GENERATED AS A RESULT OF AN INTERACTIVE PROCEDURE
HARDWARE REQUIREMENT - TEKTRONIX 4025
LOAD VECTOR WILL BE CALCULATED BY GIVEN DISTRIBUTED LOAD

MATERIAL AND GEOMETRIC PROPERTIES

SLAB #1 LENGTH = 12.0000 SLAB #2 LENGTH = 12.0000

LAYER #1 (TOP LAYER) :
THICKNESS = 2.0000 MODULUS EXX=EYY= 1112000.0 MODULUS EXY= 0.0 POISSONS RATIO =0.350
ALFA = 0.0000056 SLAB WIDTH = 3.00000

FABRIC-LAYER #1 :
THICKNESS = 0.0250 MODULUS EXX= 1112000.0 MODULUS EXY= 0.0 POISSONS RATIO =0.350
ALFA = 0.0000056 FABRIC WIDTH = 24.00000

MODULUS EYY FOR EACH FABRIC LAYER IS EQUAL OF THE MODULUS OF THE TOP LAYER

FABRIC PLACED AT THE BOTTOM OF LAYER # 1

LAYER #2 :
THICKNESS = 1.5000 MODULUS EXX=EYY= 4400000.0 MODULUS EXY= 0.0 POISSONS RATIO =0.150
ALFA = 0.0000056

LAYER #3 :
THICKNESS = 6.0000 MODULUS EXX=EYY= 300.0 POISSONS RATIO =0.470

CONTACT CONDITIONS

NORMAL STIFFNESS =.44000E 07 SHEAR STIFFNESS =.10000E-02
COEFFICIENT OF FRICTION =1.5000 COHESION =10.000

MECHANICAL LOAD

DISTRIBUTED LOAD # 1 :
BEGINING = 11.0625 END = 13.0625 PRESSURE = -33.3333

*** STRESS-STRAIN INFORMATION ***

*** EXTREME INFORMATION ***

EMENT NO.	COORDINATES X	Y	STRESSES/STRAIN SXX/EXX	SYY/EYY	SXY/EXY	S11	S22	TETA
13	12.063	7.512	+ 0.9953E 03	0.3461E 03	0.3392E-05	0.9953E 03	0.3461E 03	0.2994E-06
17	12.063	9.225	*-0.1445E 03	-0.3255E 02	-0.8522E-06	-0.3255E 02	-0.1445E 03	-0.9000E 02
13	12.063	7.512	0.9953E 03	+ 0.3461E 03	0.3392E-05	0.9953E 03	0.3461E 03	0.2994E-06
96	10.500	7.625	-0.2003E 02	*-0.4171E 02	-0.1091E 02	-0.1549E 02	-0.4625E 02	-0.2259E 02
04	11.500	7.512	0.7467E 02	0.9224E 01	+ 0.8505E 02	0.1331E 03	-0.4918E 02	0.3448E 02
22	12.625	7.512	0.7467E 02	0.9224E 01	*-0.8505E 02	0.1331E 03	-0.4918E 02	-0.3448E 02
13	12.063	7.512	0.9953E 03	0.3461E 03	0.3392E-05	+ 0.9953E 03	0.3461E 03	0.2994E-06
17	12.063	9.225	-0.1445E 03	-0.3255E 02	-0.8522E-06	-0.3255E 02	*-0.1445E 03	-0.9000E 02

*** DISPLACEMENT INFORMATION ***

*** EXTREME INFORMATION ***

NODAL POINT #	COORDINATES		DISPLACEMENTS	
	X	Y	U	V
78	24.125	6.000	+ 0.034954	-0.047262
53	0.000	6.000	* -0.034954	-0.047262
117	12.000	6.750	-0.000231	* -0.049931

*** CONTACT STRESS INFORMATION ***

*** EXTREME INFORMATION ***

ELEMENT NO.	COORDINATES		CONTACT STRESSES			
	X	Y		SYY		SXY
13	12.000	0.000	*	-3.102		0.000
1	0.000	0.000		-1.898	+	0.000
25	23.125	0.000		-1.898	*	-0.000

+ — MAXIMUM
* — MINIMUM

REFERENCES

1. McCullagh, F.R., "Reflection Cracking of Bituminous Overlays on Rigid Pavements", Special Report 16, Engineering Research and Development Bureau, New York Department of Transportation, 1973.

2. Vicelja, J.L., "Methhods to Eliminate Reflection Cracking in Asphalt Concrete Resurfacing Over Portland Cement Concrete Pavements:, Proceedings of the Association of Asphalt Paving Technologists, Vol. 32. 1963.

3. Luther, M.S., Majidzadeh, K., and Chang, C.W. "Mechanistic Investigation of Reflection Cracking of Asphalt Overlays", Transportation Research Record 572, 1976.

4. McLaughlin, Aston, "Reflection Cracking of Bituminous Overlays for Airport Pavements, A State of Art", Final Report FAA-RD-79-57, U.S. DOT Federal Aviation Administration, May 1979.

5. Jackson, Ralph D., Preventive Measures for Reflective Cracking of Asphalt Concrete State of the Art, Preliminary Report, U.S. Army Corps of Engineers, Vicksburg, MI, March 1979.

6. Way, George B. "Prevention of Reflective Cracking in Arizona", TRB, Transportation Research Record 756, 1980.

7. Majidzadeh, K., and Sucharieh, G. "The Study of Pavement Overlay Design: Final Report", Ohio State University, Columbus, Ohio 1977.

8. Treybig, H.J., et. al., "Overlay Design and Reflection Cracking Analysis for Rigid Pavements - Volume 1", Final Report FHWA-RD-77-66, U.S. DOT, Federal Highway Administration, August, 1977.

9. Luther, M.S., "The Fracture Mechanics Approach to Reflection Cracking", M.S. Thesis, The Ohio State University, 1974.

10. Shi, G.C., "Strain-Energy-Density Factor Applied to Mixed Mode Crack Extension Problems", Institute of Fracture and Solid Mechanics Technical Report, Lehigh University, 1972.

11. Majidzadeh, K., et. al., "Application of Fracture of Mechanics for Improved Design of Bituminous Concrete", Final Report, FHWA-RD-76-91, U.S. DOT, Federal Highway Administration, June 1976.

12. Germann, F.P., and Lytton, R.L., "Methodology for Predicting the Reflection Cracking Life of Asphalt Concrete Overlays", Research Report 207-5 Texas Transportation Institute, March, 1979.

13. Majidzadeh, K., Ilves, G.J., and Luther, M.S., "Reflection Cracking Models - Review and Laboratory Evaluation of Engineering Fabrics", TRB Paper, September 1982.

14. Ahlborn, G., "Elastic Layered Systems with Normal Loads," Institute of Transportation and Traffic Engineering, University of California at Berkeley, 1972.

15. Henkelom, W., and Klomp, A.J.G., "Road Design and Dynamic Loading", Proceeding Association of Asphalt Paving Technologist, Vol. 33,, 1964.

16. Majidzadeh, K., Ilves, G.J., and Sklyut, H., "Mechanistic Design of Rigid Pavements - Volume 1," Final Report, DTFH11-9568, November, 1983.

17. Wilson, Edward L., "Solid Sap: A Static Analysis Program for Three Dimensional Solid Structures," Report UC SESM 71-19 of September.

18. Goodman, Richard E., Taylor, Robert L., and Brekke, Tor L., "A Model for the Mechanics of Jointed Rock," Proc. ASCE J. of the Soil Mechanics and Foundations Div., 94, No. SM3, pp. 637-59, May, 1968.

19. Zienkiewicz, O.C., The Finite Element Method in Engineering Science. London: McGraw-Hill, 1971.

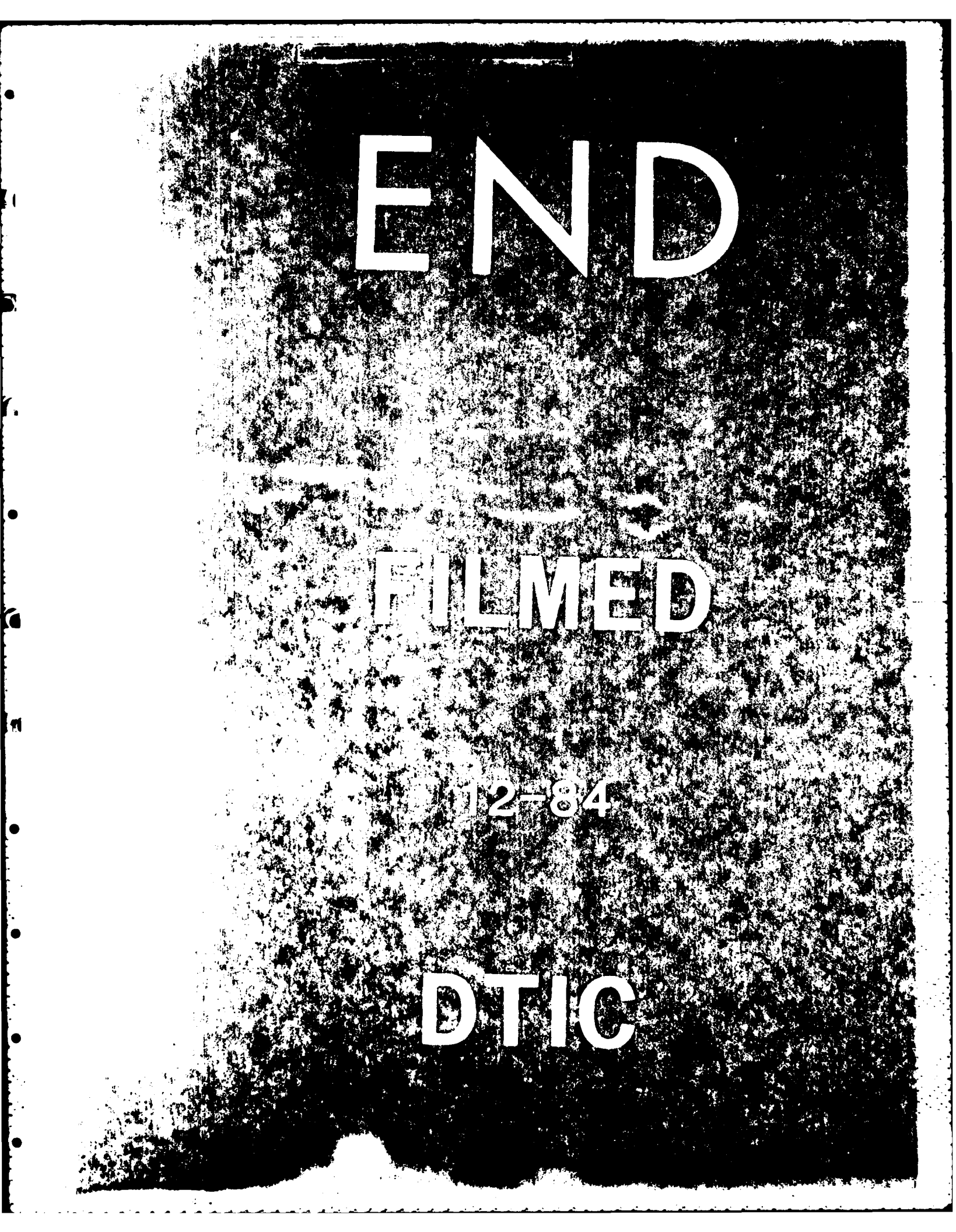
END
FILMED
12-84
DTIC